Insight on water remediation application using magnetic nanomaterials and biosorbents

M.I.A Abdel Maksoud [a], Ahmed M. Elgarahy [b], Charlie Farrell [c,d], Ala'a H. Al-Muhtaseb [e], David W. Rooney [f], Ahmed I. Osman [f*]

[a] Materials Science Laboratory, Radiation Physics Department, National Center for Radiation Research and Technology (NCRRT), Atomic Energy Authority, Cairo, Egypt.

[b] Zoology Department, Faculty of Science, Port-Said University, Port-Said, Egypt.

[c] South West College, Cookstown, Co. Tyrone, BT80 8DN, Northern Ireland, UK.

[d] School of Mechanical and Aerospace Engineering, Queen's University Belfast, Belfast BT9 5AH, Northern Ireland, UK.

[e] Department of Petroleum and Chemical Engineering, College of Engineering, Sultan Qaboos University, Muscat, Oman.

[f] School of Chemistry and Chemical Engineering, Queen's University Belfast, Belfast BT9 5AG, Northern Ireland, UK.

Corresponding Authors: Ahmed Osman, Ala'a H. Al-Muhtaseb

Email: aosmanahmed01@qub.ac.uk, muhtaseb@squ.edu.om

Address: School of Chemistry and Chemical Engineering, Queen's University Belfast, David Keir Building, Stranmillis Road, Belfast BT9 5AG, Northern Ireland, United Kingdom

Fax: +44 2890 97 4687

Tel.: +44 2890 97 4412

Abstract

Adsorption to date is the most effective and utilized technology globally to remove several pollutants in wastewater. In this approach, many adsorbents have been synthesized, tested and used for the elimination and separation of the contaminants such as radionuclides, heavy metals, dyes and pharmaceutical compounds both at lab and industrial scale. However, there are many challenges to adsorption processes such as reducing the high cost, through means of separation of suspending adsorbents to be used again, as well as the ease to synthesize. Two methods that have shown promising results and gained significant interest is that of magnetic nanomaterials and biosorbents due to their effective, safe, eco-friendly, low cost and low-energy intensive material properties. Magnetic nanomaterials act as efficient adsorbents due to their ease of removal of contaminants from wastewater using an applied magnetic field but also their advantageous surface charge and redox activity characteristics. On the other hand, biosorbents have a synergistic effect with their efficient adsorption capacity to remove contaminants, high abundance and participation in waste minimization, helping alleviate ecological and environmental problems. This review highlights, discusses and reports on the state-of-the-art of these two promising routes to adsorption and provides indications as to what are the optimum materials for utilization and insight into their efficiency, reusability and practicality for the removal of pollutants from wastewater streams. Some of the main material focuses are zero-valent iron, iron oxides, spinel ferrites, natural and waste-based biosorbents.

Keywords: Water treatment, Magnetic adsorbents, Zero-valent iron, Iron oxides, Spinel ferrites, Biosorbents

Abbreviations

Abbreviation and nomenclature			
Acetaminophen	*ACP*	**safranin O**	*SO*
Activated carbon	*AC*	**Direct Red 16**	*DR16*
Acid mine drainage	*AMD*	**Yellow 40**	*Y40*
Acid orange	*AO7*	**Point of zero charge**	PH_{PZC}
Amino-functionalized vermiculite	*AVT*	**Sorption capacity of biosorbent**	q_{eq}
Amoxicillin	*AMX*	**Removal percentage**	*R%*
Carbamazepine	*CBZ*	**Sorption capacity as a function of time t**	q_t
Carboxymethyl cellulose	*CMC*	**Reusability study**	*RE%*
Cobalt ferrite	*CFO*	**Reusability cycle number**	*N*
Congo-red	*CR*	**Sum of squared errors of prediction**	*SSE*
Escherichia coli	*E. coli*	**Chi-square statistic**	X^2
Eosin red	*ER*	**The composite fraction error function**	*CFEF*
Nanoparticles	*NPs*	**Average relative error**	*ARE*
2,4-Dichlorophenoxyacetic acid degradation	*2,4-D*	**Marquardt's percentage standard deviation**	*MPSD*
4-nitrophenol	*4-NP*	**Hybrid fractional error function**	*HYBRID*
Layered double hydroxide	*LDH*	**Experimental sorption capacity**	$q_{e,exp}$
Hematite	α-Fe_2O_3	**Model calculated (predicted) sorption capacity**	$q_{e,cal}$
Malachite green	*MG*	**Empty bed contact time**	*EBCT*
Magnetite	Fe_3O_4	**Number of bed volume**	*NBV*
Maghemite	γ- Fe_2O_3	**Mass transfer zone**	*MTZ*
Methylene blue	*MB*	**Biosorbent exhaustion rate**	*AER*
Methyl orange	*MO*	**Bed depth**	*Z*
Minocycline	*MC*	**The cross-sectional area of the adsorption bed**	*S*
Negative type	*n-type*	**Flow rate**	*Q*
Rhodamine B	*RhB*	**Breakthrough time**	t_b
Octahedral site	*B-site*	**Exhaustion time**	t_e
Pinewood biomass	*PB*	**Stoichiometric time**	t_{st}
Positive type	*p-type*	**Total flow time**	t_{total}
Porous carbonaceous materials	*PCMs*	**Influent concentration**	C_0
3-aminopropyl triethoxysilane	*APTS*	**Effluent concentration**	*C*
Schiff base complex	*SBC*	**Dry weight of biosorbent**	*M*
Staphylococcus aureus	*S. aureus*	**Total volume treated through the column**	V_e
sulfamethoxazole	*SMX*	**Total removal efficiency**	*TR%*
Trichloroethylene	*TCE*	**Total amount of sorbate passed through the bed**	m_{total}
Perchloroethene	*PCE*	**The column sorption capacity**	q_e
1,2-dichloroethene	*1,2-DCE*	**Kinetic coefficient**	K_{Th}
Rose Bengal	*RB*	**Kinetic rate constant**	K_Y
Solochrome Black-T	*SBT*	**The time required for 50% sorbate breakthrough**	τ_Y
Sulfapyridine	*SP*	**Sorption capacity**	N_0
Tetrahedral site	*A-site*	**Rate constant**	K_α
Zero-Valent Iron	*ZVI*		

1. Introduction to magnetic nanoparticles:

Nowadays, water treatment technologies have become a significant interest worldwide with the increasingly rapid development of industrialization, and environmental pollution [1-3]. This evolution of industries has led to the generation of massive amounts of pollutants such as heavy metals and dyes. When dyes seep into the environment, this is a severe problem, as it promotes surface and groundwater contamination [4]. Also, there is an increasing demand for water purification globally to meet the requirements of humankind and other living organisms due to the depletion of ground-water resources [5-9]. Therefore, advanced technologies have emerged to eliminate the contaminants from water such as membrane filtration [1, 10-12], ion exchange [13, 14], coagulation and flocculation [15-17], alternative chemical processes [18, 19], and adsorption technologies [20-23].

Among water treatment technologies, adsorption has shown to be an effective approach to remove several kinds of pollutants in water and as a result is the most widely used technology in water treatment processes [24-26]. Recently, carbon-rich materials have been used as adsorbents in water purification such as activated carbons [27-30], carbon nanotubes [25, 31-35], biochar [36-39], carbon fibers [40], and graphene oxides [41-43]. Furthermore, zeolites [44-46], silica [47-49] and clay-based nanocomposites [50-52] have also been employed as suitable materials in water treatment. In recent years, researchers have focused on waste biomass for the removal of dyes, and heavy metals for water treatment. This is due to their availability, renewable nature, and low cost [53-55]. Some examples of waste biomass sources used in such an application are: rice bran [56], wheat bran [57], sawdust[58], groundnut husk [59], walnut shell [60], switchgrass grass [61], Bacillus laterosporus [62], pine sawdust [63], oak shell [64], and pine cone [65]. The results have shown that these adsorbents have been highly efficient in water treatment. However, they are not

easy to separate from wastewater streams during treatment processes. Therefore, various investigations have been attempted to explore the application of magnetic adsorbents in water treatment as an effective, safe, and low-cost material to separate these suspended adsorbents in wastewater [53, 66, 67]. Various characteristics of magnetic substances are attributed to the variation in their response to outside magnetic fields, as some substances are significantly more magnetic than others [68]. Recently, magnetic nanomaterials have been considered as superior adsorbents for the elimination of the pathogenic and polluting composites found in water. However, magnetism is not the only considered characteristic for their use. The extraordinary surface charge and redox activity characteristics are prominent reasons for their qualification when considering other materials [69]. Herein, the first part of this review will give insight from recent studies on the utilization of magnetic nanomaterials such as zero-valent iron, iron oxides, and spinel ferrites, and their application in water remediation applications and wastewater problems.

2. Magnetic Absorbents:

2.1 Zero-Valent Iron Nanoparticles (ZVI NPs):

To date, numerous research has focused on the elimination of pollutants using zero-valent iron (ZVI) due to it is non-toxic nature, abundance, low-cost, ease to synthesize, and bioavailability [70]. The pollutant's removal mechanism using ZVI regards the electrons transport from ZVI to the pollutants, which convert the latter into non-toxic or less toxic species as shown in Figure 1. Furthermore, ZVI can be used in the degradation and oxidation of a range of organic compounds (as shown in Table 1) in the presence of dissolved oxygen to generate Hydrogen peroxide (H_2O_2) [71]. The generated H_2O_2 can be reduced to water by consecutive two-electron transportation from ZVI. Furthermore, the Fenton reaction occurs by the combination of H_2O_2 and Fe^{2+}, generating hydroxyl radicals ($^{\bullet}OH$) that possess potent oxidizing capability for the various organic compounds

[71]. As far as the authors' knowledge, metallic iron NPs show a high value of magnetization, and consequently, their use is assumed to promote the magnetic recovery step. Furthermore, nanoscale ZVI (E^0 = −0.44 V), exhibits remarkably large surface activity. So, ZVI NPs are extensively utilized for the elimination of toxic heavy metals and created a high oxidation state in water (Table 2). The generated hydrogen within the oxidation reaction on the surface of the ZVI NPs is more effective for pollutants removal in an aqueous solution. Moreover, the presence of numerous active sites on the ZVI surface is beneficial to eliminate the contamination. The oxidation reaction that occurs on the ZVI surface liberates an e^- and Fe ions in an aqueous media. Also, the reduction in the ZVI's reactivity is correlated with the metal hydroxides impregnation on the ZVI surface. These obstacles prevent the hydrogen generation and subsequently, decrease the ZVI reactivity. On the other hand, titanium dioxide has a small bandgap that can support electrons to reduce the oxide layer production (Fe^{2+} and Fe^{3+}) on the ZVI surface. Therefore, the degradation reactivity of ZVI is still stable. The generated electrons, that are associated with the exposure of TiO_2 to UV irradiation, are captured by the two half-reactions (Fe^{3+}/Fe^{2+} and Fe^{2+}/Fe^{o}) and prevent the recombination between the electrons and holes [72]. Lately, Shahrokh et al.,[73] prepared ZVI/titanium dioxide-based on activated carbon via the sol-gel method for 2,4-Dichlorophenoxyacetic acid degradation (2,4-D). The degradation efficiency is enhanced, and then slightly reduced by increasing the time of irradiation and the concentration ratio between $NaBH_4$ and the 2,4-D concentration. The adsorption and degradation efficiency were found to be 46.44 and 86.37%, respectively. The data of degradation matched well with the Pseudo-second-order kinetic model. The efficiency of degradation was stable up to 4-cycles and then decreased significantly.

The small particle size and the solid powder state of ZVI NPs can rapidly react with surrounding media and leads to agglomerates during the synthesis method. This subsequently decreases the reactivity of ZVI NPs and leads to low mobility of ZVI NPs into the pollutants, thus, restricting the wide application of ZVI NPs. For reduction of the aggregation of ZVI NPs, these NPs are conventionally deposited on a substrate such as graphite, silica, clay or a membrane [73]. Recently, Kallepally et al.,[74] reported the synthesis of bentonite/ZVI NPs for 4-nitrophenol reduction. The results revealed that the crystallite size and specific surface area of bentonite/ZVI NPs were observed around l50 nm and 62.47 $m^2.g^{-1}$, respectively. The green synthesized bentonite/ZVI NPs have a higher photodegradation for 4-NP in the presence of hydrogen peroxide. The synthesized bentonite/ZVI NPs were stable and possessed a high catalyst efficiency for the reduction of 4-NP after 5 cycles. Furthermore, bentonite/ZVI NPs were found to be magnetically separable and synthesized using a green synthetic approach. Dye contaminants in the human body can cause diseases, skin irritation, cancer, and genetic mutations. Due to their dangers, it is necessary to separate them from water streams before releasing into the environment [75]. Wei Wang et al., [76] have used porous 3D graphene (3DG) as a matrix to support ZVI NPs to degrade orange IV dye. The degradation efficiency of orange IV azo dye achieved was 94.5% within 1 hour using ZVI NPs immobilized 3DG, whilst only 70.9% was eliminated via ZVI NPs. The reaction rate between orange IV and 3DG-ZVI was found to be five times higher than the standard ZVI NPs sample. The results implied that reaction efficiency and rate are enhanced by decreasing pH and the increase in temperature.

Additionally, ZVI NPs as a reducing material has gained attention due to its notable advantages of large specific surface area, simplicity, low cost, and extraordinary reactivity with heavy metals. Zhao et al.,[77] have reported the enhancement of Cr (VI) removal using amino-functionalized

vermiculite-supported ZVI NPs (AVT-ZVI NPs). The results revealed that the removal efficiency of Cr (VI) achieved 100% for AVT-ZVI NPs, whereas the standard sample only reached 87.5%. The removal efficiency of Cr (VI) by AVT-ZVI NPs was shown to be still stable at above 70% after four cycles. Once discharged into the natural environment, radionuclides could pose severe health implications and environmental deterioration even at very low concentrations. Shujun et al., [78] prepared ZVI NPs supported on double-layered hydroxide (DLH) composites (DLH/ZVI NPs) for U (VI) removal. The observed data showed that the DLH/ZVI NPs had a higher efficiency for U (VI) removal than those of DLH adsorption or ZVI NPs reduction. The maximum adsorption capacity reached was 176 $mg.g^{-1}$, which indicated that DLH/ZVI NPs can be used as a suitable adsorbent for U (VI) removal from sewage water.

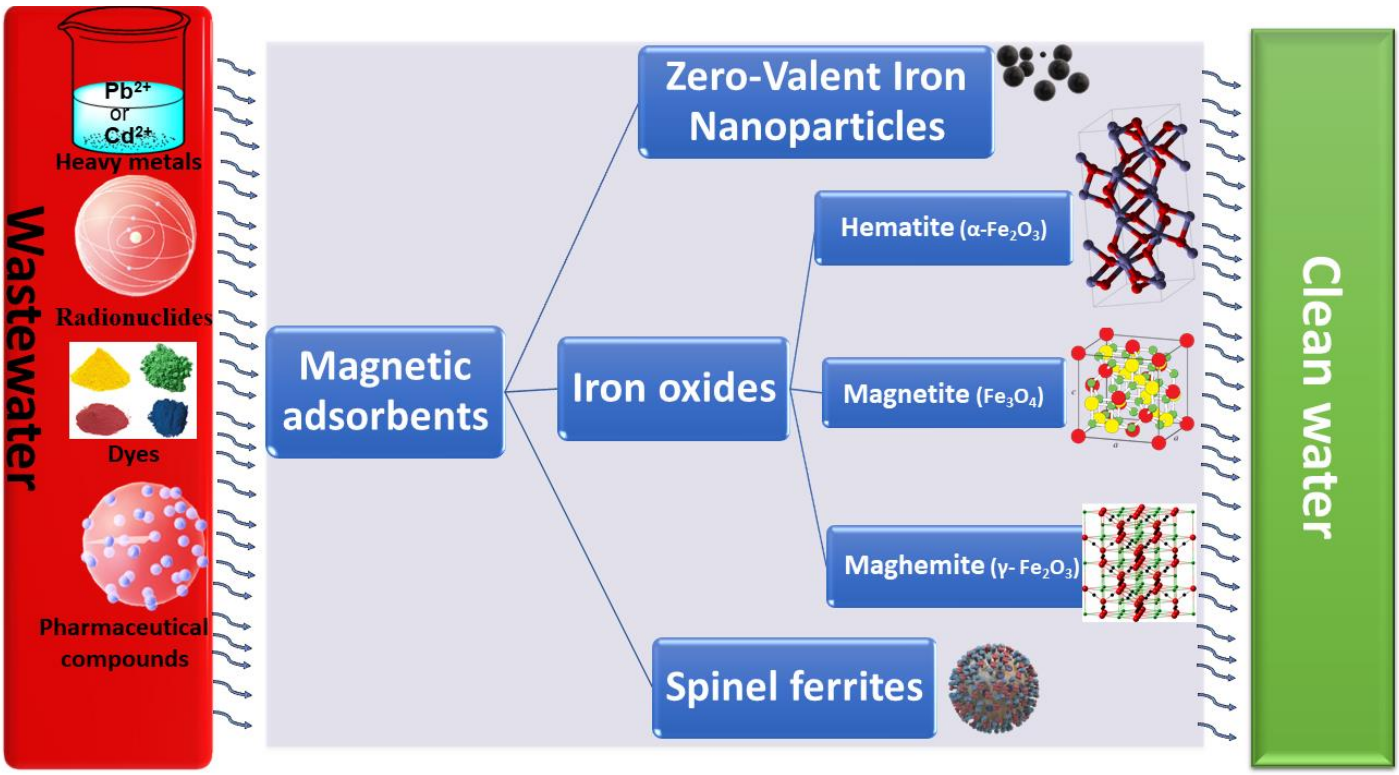

Figure 1: shows the utilization of different magnetic adsorbent materials in the wastewater treatment application.

Table 1: Degradation efficiency for adsorption of organic pollutants using magnetic adsorbents.

No.	**Magnetic Adsorbents**	**Pollutant/s**	**Degradation efficiency**	**Ref.**
1	ZVI/kaolinite	Acid Black 1	98% (120 min)	[79]
2	ZVI/Peroxymonosulfate	Tetracycline	88.5% (5 min)	[80]
3	ZVI/ sulfite	Propranolol	96.7 (60 min)	[81]
4	ZVI/polyethylene	Ponceau 4R	96% (30 min)	[82]
5	ZVI/Peroxymonosulfate	Bisphenol M	95.9% (90 min)	[83]
6	ZVI/organo-montmorillonite	Sulfamethazine	97% (10 min)	[84]
7	N-doped ZVI /Fe3C@C	Bisphenol A	-	[85]
8	ZVI/ peroxydisulfat	Carbamazepine, Acetaminophen And sulfamethoxazole	CBZ (85.4%) ACP (100%) SMX (73.1%) (10 min)	[86]
9	ZVI/ polyethylenimine	Trichloroethylene (TCE), Perchloroethene (PCE), and 1,2-dichloroethene (1,2-DCE)	TCE (97%), PCE(96%), and 1,2-DCE (96%), within (2h)	[87]
10	ZVI NPs	Amoxicillin (AMX)	86.5% (25 min)	[88]
11	α- Fe_2O_3/ MWCNT/RGO	rhodamine B (RhB)	98% (2h)	[89]
12	CuO-Fe_2O_3	RhB	100 % (60 min)	[90]
13	Fe_3O_4/TiO_2	Methyl orange (MO)	90.3% (60 min)	[91]
14	g-C_3N_4/α-Fe_2O_3	congo-red (CR) and malachite green (MG)	CR (87%) MG (95) 100min	[92]
15	Ni-doped α-Fe_2O_3	Methylene blue (MB)	86% (140 min)	[93]
16	Fe_3O_4@SiO_2@AgO	phenol red	89%	[94]
17	Fe_3O_4/Ag_3PO_4@WO_3	MB	90%, 6 min	[95]
18	ZnO/ γ-Fe_2O_3	MB, Rose Bengal (RB) and Solochrome Black-T (SBT)	MB (100%, 70 min) RB (100%, 90 min) SBT (100%, 100 min)	[96]

19	γ-Fe_2O_3/BiOI	MO and sulfapyridine (SP)	MO (67.6%), 120 min SP (64.1%), 120 min	[97]
20	α-Fe_2O_3/γ-Fe_2O_3	RhB	80%	[98]
21	CdS/ γ-Fe_2O_3	MB	90% (120 min)	[99]
22	Fe_2O_3/$BiVO_4$	MB and RhB	100% 20 min	[100]
23	α-Fe_2O_3/TiO_2	(CR), (MB), and eosin red (ER)	CR (95.1%, 30 min) ER (98.4%%, 90 min) and MB (67.6%%, 160 min)	[101]
24	Fe_3O_4/ZnO/ZnS	MB and MO	MO (79.5%), 4h MB (75.3%) (4 h)	[102]
25	Fe_3O_4/SiO_2/Cu_2O–Ag	MB and RhB	MB (96.4%) 90 min RhB (94.3%) 90 min	[103]
26	Fe_3O_4-graphene/ZnO@ SiO_2	MB, RhB, and MO	95%, 84%, and 87% for MB, RhB, and MO, respectively, (60 min)	[104]
27	rhombic Cu_2O-rGO/Fe_3O_4 @SiO_2	MO	100% (120 min)	[105]
28	Fe_3O_4/TiO_2/SiO_2	MB	98% (2h)	[106]
29	Ag–Cu/Fe_3O_4/Rgo	Malachite green (MG)	98% (60 min)	[107]
30	Fe_3O_4/$CoWO_4$	RhB	98% (180 min)	[108]
31	Fe_3O_4@ZnO@Au	RhB	99% (8h)	[109]
32	B-$NaYF_4$:Yb^{3+},Tm^{3+} /TiO_2/Fe_3O_4 @SiO_2	MB	86.69 % 24 h	[110]
33	γ-Fe_2O_3@TiO_2	MO	94% 120 min	[111]
34	γ-Fe_2O_3@SiO_2@TiO_2–Ag	MO	84% 1h	[112]
35	γ-Fe_2O_3@SiO_2@AgBr:Ag	acid orange (AO7)	93.1% (20 min)	[113]
36	$NiAl_xFe_{2-x}O_4$	MO	74.12% (140 min)	[114]
37	$CoxMg1-xFe_2O_4$	MB	98.55%	[115]
38	La-N-TiO_2/ $SrFe_2O_4$/diatomite	Oxytetracycline	95.5% (2.5 h)	[116]
39	$SrFe_2O_4$/ g-C_3N_4	RhB	100% (40 min)	[117]
40	Cu_2ZnSnS_4/$ZnFe_2O_4$	MO	91% (120 min)	[118]
41	TiO_2/$CoFe_2O_4$	4-nitrophenol (4-NP)	94% (35 min)	[119]

42	ZnO-$Zn_{1-x}M_xFe_2O_4$ (M=Sm, Eu, Ho)	MG	98% (60 min)	[120]
43	$MgFe_2O_4$-TiO_2@GO	MB	100% (300 min)	[121]
44	$ZnFe_2O_4$:CeO_2	MG	96% (180 min)	[122]
45	$ZnFe_2O_4$-Ag/Rgo	Microcystin-LR (MC-LR)	100% (120 min)	[123]
46	MoS_2/$MnFe_2O_4$	Acid Blue 113	99% (42 min)	[124]
	$ZnFe_2O_4$/AgI	*E. coli* and RhB	*E. coli* (100%, 80 min) RhB (98.5% ,40 min)	[125]
47	Ag_3PO_4-$CoFe_2O_4$-GO	MB	100% (30 min)	[126]
48	3,5-Dinitrosalicylic acid/Chitosan/$MnFe_2O_4$	MB	98.9% (30 min)	[127]
49	C_3N_4@$MnFe_2O_4$-G	Metronidazole, amoxicillin, tetracycline and ciprofloxacin	94.5% (60 min)	[128]
50	Fe^0@C@$MnFe_2O_4$	Tetrabromobisphenol A	90% (120 min)	[129]
51	Porphyrin/$ZnFe_2O_4$@polythiophene	MO	94% (180 min)	[130]
52	α-Fe_2O_3	MB	78% (6h)	[131]
53	$CuYb_{0.5}Fe_{1.5}O_4$	MO and safranin O (SO)	MO (99.44%) SO (95.65%)	[132]
55	magnetite/phenylenediamine /cellulose	MB	74.58 - 88.78% (10 - 80) min	[133]
56	MWCNTs/Fe_3O_4/PANI	MO and CR	MO (446.25 $mg.g^{-1}$) CR (417.38 $mg.g^{-1}$)	[134]
57	α-Fe_2O_3/graphene –NS	MO	545.48 $mg.g^{-1}$ at pH = 6	[135]
	$MnFe_2O_4$/MWCNT	Direct Red 16 (DR16) and Cationic Yellow 40 (Y40)	DR16(608 $mg.g^{-1}$ at pH=2) Y40 (280 $mg.g^{-1}$ at pH=6)	[136]
58	activated carbon/γ-Fe_2O_3	Alizarin red S	108.69 $mg.g^{-1}$	[137]
59	γ-Fe_2O_3/SiO_2	MB	116.09 $mg.g^{-1}$	[138]
60	$MgFe_2O_4$/γ-Fe_2O_3	CR and minocycline (MC)	CR (259.1 $mg.g^{-1}$) MC (200.8 $mg.g^{-1}$)	[139]
61	Fe_3O_4@MnO_2	CR	95%	[140]

The degradation efficiency for inorganic/organic pollutants depends on many factors such as contact time, source of irradiation, the adsorbent dosage, initial concentration for inorganic/organic pollutants, effect of pH and temperature, and the kind and nature of the catalyst. The degradation efficiency for RhB using CuO-Fe_2O_3 is 100% for 60 min (as shown in Table 1). Adak et al. [96] reported that about 80% of MB and 75% of RB was found to photodegrade after 50 min of irradiation, whereas, after the same time interval, only 42% SBT was photodegraded. In the presence of light and the ZnO/γ-Fe_2O_3 film, the characteristic absorption peak at 662 nm for MB was found to be quenched almost completely after 70 min, whereas, RB and SBT took 90 and 100 min of exposure, respectively, for complete degradation. The α-Fe_2O_3/TiO_2 material reveals the fastest degradation toward CR, with about 95.1% discolouration efficiency in 30 min as shown in Table 1 [101]. At the same time, about 76.7% ER and 15.3% MB were degraded, and after 90- and 160-min irradiation, the degradation percentages reached 98.4% and 67.6% for ER and MB, respectively. The γ-Fe_2O_3@SiO_2@AgBr: Ag-2 material shows much higher photocatalytic activity for AO7 degradation. After visible light irradiation for 20 min, the degradation rates of AO7 is 93.1% [113].

2.2. Iron oxides:

In recent years, iron oxides nanoparticles (FO NPs) have exhibited excellent properties in sorption activities due to their high specific surface area, porosity structure, and strong magnetic response resulting in an exceptional sorption capacity [141, 142] as shown in Figure 1. In nature, FO NPs have existed in various structures, among them: hematite (α-Fe_2O_3), magnetite (Fe_3O_4), and maghemite (γ- Fe_2O_3) are acceptable candidates as they possess polymorphism that includes temperature-induced phase transition [143].

2.2.1 Hematite (α-Fe_2O_3):

Hematite usually exists in rocks and soils and is characterized as highly stable under surrounding conditions and is environmentally friendly [144]. Hematite has a trigonal crystal structure and belongs to the space group (R-3c) and the unit cell parameters a = b = 4.9865 Å, c = 13.5016 Å assigned to JCPDS card No. 33-0664 [145]. In the same context, the crystal structure of α-Fe_2O_3 is based on the hexagonal close packing of oxygen ions and two thirds (2/3) of the octahedral sites (B-site) is occupied by ferric ions [146]. Also, it is extensively used in many applications such as environmental treatment, photocatalysis, pigments, drug delivery, and sensors due to its low cost, small dimensions, convenient operation and high resistance to corrosion [147, 148]. In the bulk form and at room temperature, hematite is weakly ferromagnetic and transforms at the Morin temperature (T_M = -13.15 °C) to antiferromagnetic phase. Additionally, at temperatures above its Curie temperature (T_C = 682.85 °C), hematite has a paramagnetic phase [149, 150]. The magnetic properties of hematite depend on numerous parameters like the crystallinity, subparticle structure, the size of the particle, exchange interactions, and cation doping [150]. Additionally to the size and shape of hematite crystallites, substituting with different metal ions is also a critical factor that can enhance the adsorption properties of hematite which are crucial for water purification [146]. Furthermore, hematite is a cheap negative (n-type) semiconductor which has a bandgap of (E_g = 2.1- 2.2eV). It has been reported to absorb around 43% of light in the visible light region, which makes it a promising candidate material for water treatment application under visible light [151]. Nevertheless, the photocatalytic activity of hematite is restricted because of its low efficiency of separation and poor conductivity. Hence, hematite is usually incorporated with different semiconductor materials to produce a heterostructure [152]. The incorporation of hematite with different materials to form composite photocatalysts is confirmed by several researchers (as shown

in Table 1). For instance, Myung Jong Kang et al.,[153] have synthesized hematite, graphitic carbon nitride-based Z-scheme heterojunction via simple solid-state reactions. The hematite and graphitic carbon nitride-based Z-scheme heterojunction photocatalyst improved the efficiency of rhodamine B photocatalytic degradation, which was doubled compared to the pristine hematite and graphitic carbon nitride heterojunction photocatalyst. Liwei Chen et al.,[154] have synthesized the novel AgBr/Ag_3PO_4@natural hematite heterojunction via a facile approach to degrade four typical antibiotics (ciprofloxacin (CIP), norfloxacin (NOR), sulfadiazine (SDZ), and tetracycline (TTC)). In this catalyst, the molar ratio of [Ag]: [Hematite] was 1.5:1 and thereby named as $Ag_{1.5}$BrPFe. Similarly, $Ag_{0.5}$BrPFe, Ag_1BrPFe, and Ag_2BrPFe were also formed by changing the dosage of $AgNO_3$ through the synthesis method. The silver deposition considerably decreased the band gap and hence, improved the photocatalytic activity of hematite. Subsequently, hematite enhanced the stability of AgBr/Ag_3PO_4 in turn. Sulfadiazine antibiotic showed the excellent degradation kinetic rate results under simulated solar light illumination. The photocatalytic degradation rate constants of antibiotics by $Ag_{1.5}$BrPFe are 0.16, 0.19, 0.34 and 0.10 min^{-1} for CIP, NOR, SDZ, and TTC, respectively, at solution pH= 3. While, at pH of 5, TTC is changed to its neutral form. The attraction force produced by electric conductivity is reduced. As a consequence, the degradation process is obviously restrained. On the other hand, though the degrees of protonation of CIP and NOR are decreased when the pH rises to 5, the surface of $Ag_{1.5}$BrPFe is much more negatively charged. Therefore, the degradation process is not significantly retarded.

Tungsten trioxide (WO_3) NPs have excellent properties such as biocompatibility, high photodegradation activity and low-cost. Nevertheless, because of its quick recombination of electron and hole pairs, the photocatalytic activity of tungsten trioxide is not satisfactory. Hence,

in order to enhance the photocatalytic activity of WO_3 NPs, it should be combined with iron oxides. Hanan H. Mohamed et al.[155] has fabricated hematite, graphene oxide and tungsten trioxide (Fe_2O_3/GO/WO_3) Z-scheme photocatalyst to degrade inorganic dyes. The photocatalytic activity was seen to substantially improve for the hematite, graphene oxide and tungsten trioxide nanocomposite compared to other nanomaterials. The electrons in the conduction band of tungsten trioxide were transported by the graphene oxide interface and then recombined with the holes of the valance band of hematite increasing the electron-hole pair separation and overcoming their recombination in both hematite and tungsten trioxide systems. Xiaojuan Li et al.[156], have reported synthesizing a novel ternary hematite/zinc oxide/zinc ferrite (ZFO) via hydrothermal reaction. The ZFO composites showed high photocatalytic degradation efficiency for rhodamine B, where it reached up to 95.7% within one hour and kept stable for at least 3 cycles.

Hematite is not only a superior photocatalyst for the elimination of organic contaminants but is also a low-cost adsorbent for organic dyes and heavy metal ions (as shown in Table 2). Lately, Bing Li et al.,[157] have reported the fabrication of activated carbon-coated hematite (αFe_2O_3@AC) via impregnation technique to promote the removal of Cr (VI) from water. The removal efficiency of Cr (VI) was found to be 94%, which is three times higher than the AC reported. The reduced Cr (VI), coupled with the oxidized AC ion and low soluble $(Cr_xFe_{1-x})(OH)_3$ precipitates were finally formed. Shengsen Wang et al.,[158] have fabricated pinewood biomass (PB) and natural hematite (H) admixtures at different temperatures. The Langmuir isotherms illustrated that the maximum sorption capacities of the mixture at 300 $^{\circ}$C were 173 and 359 mmol.kg^{-1} for Cd^{2+} and Cu^{2+}, respectively. The sorption of both Cd^{2+} and Cu^{2+} increased with an increase in the pH up to 5, whereas the higher ionic strength reduced sorption of Cd^{2+} ions. Rini Ravindranath et al.,[159] have synthesized hematite/aluminium oxide composites which have a

belonging cubic structure. The high specific area, adsorption properties and porous structure of Fe_2O_3/Al_2O_3 showed high efficiency towards the mercury (Hg^{2+}), cadmium (Cd^{2+}), copper (Cu^{2+}), and lead (Pb^{2+}) cations removal from real samples. The cumulative removal efficiencies for mercury ions increased from 83.2% to 98.3%, while that of cadmium, copper, and lead ions enhanced from 81.9% to 97.9%, 81.4% to 96.0%, and 80.7% to 97.3%, respectively, as the cycles increased from one to four. Also, hematite has been used for radionuclide removal from aqueous solutions. Currently, M. Hashemzadeh et al.,[160] have prepared hematite for cobalt-60 radiocations removal via the hydrothermal route. The hematite nanoparticles were synthesized in the existence of oleic acid. Adsorption of cobalt-60 over hematite nanoparticles resulted in the maximum adsorption capacity 143 $mg.g^{-1}$, while the actual maximum adsorption capacity was almost around 100 $mg.g^{-1}$. Furthermore, Xie Shuibo et al.[161], have used hematite for the removal of U (VI) from aqueous solutions. The adsorption capacities were considerably affected by the pH of the solution. The adsorption was influenced by temperature, where the maximum adsorption capacity was enhanced. Finally, hematite has good efficiency adsorption of uranium.

Table 2: Adsorption capacity of inorganic Pollutants using magnetic adsorbents (related to q_e is the equilibrium adsorption capacity ($mg.g^{-1}$); q_m is the maximum adsorption capacity ($mg.g^{-1}$); K_L is the adsorption equilibrium constant of Langmuir (Lmg^{-1}), K_F and n are Freundlich isotherm constants related to the adsorption capacity).

No.	Magnetic Adsorbents	Adsorbate	Adsorption capacity ($mg.g^{-1}$) or Removal Efficiency (%)	Ref.
1	ZVI NPs	Pb (II)	807.23 $mg.g^{-1}$, 90.11 % at pH=6, q_m= 854.70, K_L=0.03	[162]
2	ZVI/activated carbon nanotubes	Te	99%, 800 $mg.g^{-1}$ at pH 4.7, K_F= 352.1, n=6.73 at 59.85 °C	[163]

3	ZVI-Coffee ground	Pb(II), Cd(II), As(III), As(V)	Pb(II) 164.1 $mg.g^{-1}$ (1h), K_F=235.68, n= 4.62 at pH 6, Cd(II) 112.5 $mg.g^{-1}$ (24h), K_F=32.84, n= 3.11 at pH 6 As(III) 23.5 $mg.g^{-1}$ (1h), K_F=5.51, n= 1.79 at pH 7 As(V) 9.3 $mg.g^{-1}$ (1h), K_F=7.41, n= 3.99 at pH 7	[164]
4	ZVI/ chitosan	U(VI)	591.72 $mg.g^{-1}$ at pH=6, q_m= 591.72, K_L= 1.09 at 24.85 °C	[165]
5	ZVI NPs	Cu(II)	343$mg.g^{-1}$ at 21.85 °C	[166]
6	ZVI/alginate	Pb(II)	88% , 581.7 mg g^{-1} (15 min), Optimum pH range of 4.0–6.0	[167]
7	ZVI/biochar	Cr(VI)	96%, 35.30 $mg.g^{-1}$ at pH=4, q_m=46.73, K_L=0.155 at 34.85 °C	[168]
8	ZVI/ Polyaniline/Attapulgite	Cr(VI)	86.56 $mg.g^{-1}$, q_m=73.52, K_L=0.3676 at 49.85 °C	[169]
9	ZVI/ZVAl	Cr(VI), Cd^{2+},Ni^{2+}, Cu^{2+}, Zn^{2+}	99.5% (300 h) pH 5.4	[170]
10	ZVI NPs	Cd(II), Cu(II), Ni(II), Pb(II)	Cd(II) 71.4% (79.33–102.00) $mg.g^{-1}$ Cu(II) 100% (111.11-142.85) $mg.g^{-1}$ Ni(II) 99.9% (107.30–137.96) $mg.g^{-1}$ Pb(II) 96.6% (110.97–142.68) $mg.g^{-1}$, at 11.85 °C via 200mg of ZVI NPs	[171]
11	ZVI/ fly ash	Pb(II) Cr(VI)	96.94 $mg.g^{-1}$ for Pb(II), 14.03 $mg.g^{-1}$ for Cr(VI) at 39.85 °C	[172]
12	Bentonite/ZVI	Pb^{2+} Cu^{2+} Zn^{2+} Ni^{2+}	100%, at pH= 6.5	[173]
13	ZVI/ magnetite carbon	U(VI)	80% (30 min), 203.94 $mg.g^{-1}$, at 25 °C , q_e= 273.74, K_L= 0.07	[174]
14	ZVI/ polyaniline-graphene aerogel	U(VI)	350.47 $mg.g^{-1}$ at pH 5.5, q_e= 663.54, K_L= 5.08, 44.85 °C	[175]

15	ZVI/ activated carbon	As(V)	100% after 2 h, at pH 6 - 7	[176]
16	Fe_3O_4/bone char/chitosan	As(V)	69%, 112 μg.g^{-1}, q_m= 112.36, K_L= 0.036, 44.85 °C	[177]
17	Fe_2O_3–Al_2O_3	Cu^{2+},Pb^{2+} Ni^{2+},Hg^{2+}	Cu^{2+} (21%, 4.98 mg.g^{-1}, K_F=1.59, n= 3.81) Pb^{2+} (52%, 23.75 mg.g^{-1}, K_F= 4.52, n= 1.91) Ni^{2+}(67%, 32.36 mg.g^{-1}, K_F= 1.49, n= 1.307) Hg^{2+} (89%, 63.69 mg.g^{-1}, K_F= 4.58, n= 1.105)	[178]
18	ZVI/ zeolite	Cd^{2+} Pb^{2+}	Cd^{2+} (63.14 mg.g^{-1}, q_m=51.21) Pb^{2+} (154.61 mg.g^{-1} , q_m=114.4)	[179]
19	Fe_2O_3@GO	Pb(II)	81.07% (60 min), 303.0 mg.g^{-1}, q_m=125,K_L= 14.69	[180]
20	γ-Fe_2O_3@ chitosan	Cd^{2+}	61.5%,15.2 mg.g^{-1},q_m=15.2,K_L= 2.95, 49.85 °C	[181]
21	Polyacrylonitrile/α-Fe_2O_3	As(V)	q_m=82.2 (2h), K_L= 8.4, 24.85 °C	[182]
22	chitosan/PVA/ZVI	As(V) As(III)	As(V)(q_m=200 mg.g^{-1} , K_L= 0.135, pH= 7) As(III)(q_m=142.9 mg.g^{-1}, K_L=0.556 pH=7)	[183]
23	ZVI/ MnO_2	As(V) As(III)	As(V)) 100%, 35.7 mg.g^{-1} As(III) 70% at 4th cycle, 29.4 mg g^{-1}	[184]
24	γ-AlOOH/α-Fe_2O_3	Cr(VI)	q_m=4.17, K_L=30	[185]
25	Fe_3O_4/GO/ beads	Cr(VI), As(V)	Cr(VI) (80%, K_F=0.511, n=1.559) As(V) (99%, K_F=2.394, n=4.24)	[186]
26	Chitosan/clay/ Fe_3O_4	Cu(II) As(V)	Cu(II) (17.2 mg.g^{-1}, K_F = 5.8277, n=6.08) As(V) (5.9 mg.g^{-1}, K_F = 0.2816, n=1.79)	[187]
27	Diethylenetriamine/GO/ Fe_3O_4	Cr(VI)	123.4 mg.g^{-1} at pH=2, K_L=0.58, 24.85 °C	[188]

28	ZVI/Diethylenetriamine/2-pyridinecarboxaldehyde	Co(II) Cu(II) Zn(II) Cd(II) Hg(II) Pb(II)	Co(II) 2600 μmol.g^{-1} Cu(II) 4750 μmol.g^{-1} Zn(II) 5600 μmol.g^{-1} Cd(II) 4000 μmol.g^{-1} Hg(II) 5200 μmol.g^{-1} Pb(II) 5050 μmol.g^{-1} At pH 7	[189]
29	Fe_3O_4/MgAl layered double hydroxide	Co(II)	95.8% at pH=8	[190]
30	Fe_3O_4@cyclodextrin	Eu(III)	95% (q_m= 8.35 × 10^{-5},K_L= 8.83 × 10^4, at pH=5.5)	[191]
31	γ-Fe_2O_3/TiO_2/ PVA/ beads	Ba(II)	99% in 150 min at pH 8	[192]
32	Fe_3O_4/PANI	Cr(VI)	q_m=200 mg.g^{-1}, K_L=0.4	[193]
33	γ-Fe_2O_3	Pb(II) Zn(II) Cd(II)	Pb(II)(92.47% at pH=7.5, 10.55 mg.g^{-1}) Zn(II) (39.1% at pH=7.5, 4.79 mg.g^{-1}) Cd(II) (14.26% at pH= 7.5, 1.75 mg.g^{-1})	[194]
34	γ-Fe_2O_3	Cd(II), Ni(II) Co(II)	Cd(II)(q_m=94.33, K_L= 0.0228) Ni(II) (q_m=86.206 , K_L= 0.0014)) Co(II)(q_m=60.60, K_L= 0.0105))	[195]
35	α-Fe_2O_3	Hg(II)	q_m=12.75 mg.g^{-1}, K_L= 6.676 at pH 6 and 39.85 °C	[196]
36	$CoFe_2O_4$–G & $NiFe_2O_4$–G	Pb(II) Cd(II)	Pb(II) is 142.8 and 111.1 mg.g^{-1} at pH of 5 and 310 K for $CoFe_2O_4$–G & $NiFe_2O_4$–G; while for Cd(II) it was 105.26 and 74.62 mg.g^{-1} at pH of 7 and 36.85 °C.	[197]
37	GO/ $NiFe_2O_4$	Pb(II) Cr(III)	Pb(II) (q_m=46.08, K_L= 1.74 , 328 K) Cr(III) (q_m=64.10, K_L= 3.75 , 328 K)	[198]
38	bacterial cells/Sawdust/$MnFe_2O_4$	As(III) As(V)	As(III) (66.34%, 87.573 mg.g^{-1}) As(V) (67.417%, 88.990 mg.g^{-1})	[199]

39	$Ni_{0.5}Zn_{0.5}Fe_2O_4$	Ag(I)	(q_m=243.90, KL=1.46, 30 min, pH=5	[200]
40	$NiFe_2O_4$-Nitrogen-doped mesoporous carbon	Hg^{2+}	87% at pH 6, q_m=476.2, K_L= 0.017, 298 K	[201]
41	$NiFe_2O_4$/Poly(m-phenylenediamine) /GO	Cr(VI)	(q_m=502.5 at pH = 3, K_L= 0.41)	[202]
42	$MgFe_2O_4$/biochar	PO_4^{3-}	163.02 $mg.g^{-1}$ (80.4%) at pH 3.0	[203]
43	$NiFe_2O_4/MnO_2$	Pb(II)	92.2% at pH=6, q_m= 85.78, K_L=1.3123	[204]
44	$Ni_{0.6}Fe_{2.4}O_4$	U(VI)	(95% at pH=7, q_m=189.04, K_L= 0.0434, 318.15 K)	[205]
45	Hydroxyapatite/$NiFe_2O_4$	$^{152+154}Eu$ ^{160}Tb	Eu(III) (95.51% , 137.35 $mg.g^{-1}$) Tb(III) (93.53%, , 130.43 $mg.g^{-1}$) at pH = 3.5	[206]
46	$MnFe_2O_4$	U(VI) Eu(III)	U(VI) (q_m=119.90 $mg{\cdot}g^{-1}$, pH=5) Eu(III) (q_m= 473.93 $mg{\cdot}g^{-1}$, pH=7) at 25 °C.	[207]
47	clinoptilolite/$CoFe_2O_4$	Sr^{2+}	(qm=20.58, K_L= 0.068)	[208]
48	Ammonium-pillared montmorillonite/ $CoFe_2O_4$ /calcium alginate	Cs^+	(qm=86.46 , K_L=0.0144)	[209]
49	$ZnFe_2O_4@NH_2$-SiO_2@ polydiphenylmethane diisocyanate @ dithizone	Pb(II)	(q_m=80 $mg.g^{-1}$ with pH = 7)	[210]
50	$MgFe_2O_4$	Co^{2+} Mn^{2+} Ni^{2+} Cu^{2+}	Co^{2+} (qm=13.90, K_L=0.25) Mn^{2+} (qm= 11.15, K_L= 0.04) Ni^{2+} (qm= 2.5, K_L= 0.06) Cu^{2+} (qm= 0.49, K_L= 3.35)	[211]

Ramin et al.,[212] showed that increasing the pH and magnetic chitosan-functionalized 3D graphene nanocomposite decorated with $NiFe_2O_4$ nanoparticles MCF3DG dosage value leads to an increase in the removal of the Pb(II) ions. The adsorption efficiency changes when the pH changes. Such

behavior may be due to the change of the charged group of MCF3DG and its reversal in acidic and basic mediums. At higher pH, the nanocomposite surface is mostly negatively charged with deprotonated surface sites. Due to these results, there are different electrostatic interactions between Pb(II) ions and nanocomposite in different pH values, which cause rise and fall in lead ions removal efficiency. Similar observations are available in the literature [213]. Shou et al., also reported that Co(II) is mainly present as the positively charged Co^{2+} species at pH= 2.0–8.0 [190]. The surfaces of Fe_3O_4/MgAl-LDH are positively charged in this pH range. So, the electrostatic repulsion between Co^{2+} and the protonated sites on Fe_3O_4/MgAl-LDH surfaces results in the low Co(II) adsorption at low pH. In contrast, the surfaces of Fe_3O_4/MgAl-LDH become negatively charged at high pH. The electrostatic attraction between the negatively charged binding sites on Fe_3O_4/MgAl-LDH and the positively charged Co^{2+} enhances the formation of surface complexes. In addition, the deprotonated sites can improve the dispersion of Fe_3O_4/MgAl-LDH in solution, which will increase the contact area between Co^{2+} and the binding sites on Fe_3O_4/MgAl-LDH, consequently enhancing the adsorption of Co(II). Nevertheless, at pH=8.0, Co(II) is mainly present as $Co(OH)_2$ with a proportion of $CoCO_3$ and $Co(OH)^+$. So, the high adsorption of Co(II) on Fe_3O_4/MgAl-LDH at pH =8.0 is attributed to the formation of $Co(OH)_2$ and $CoCO_3$ surface precipitates as well as some surface complexes. Majidnia et al. [192] used γ-Fe_2O_3/TiO_2/ PVA/ beads for removal of barium ions from aqueous solution under sunlight. It was noticed that as the pH increased the Ba(II) sorption capacity increased steadily until it reached pH 8. Increasing the pH of the solution beyond 8 did not improve the Ba(II) removal. It was assumed that the competition between hydronium ions (H_3O^+) and Ba(II) occurred towards the adsorbent in pH lesser than 8. A high concentration of H_3O^+ present near to the surface of adsorbent can produce a repulsive force that hinders the approach of Ba ions. Then the Ba sorption efficiency was found to be significantly low at a lower pH region.

2.2.2 Magnetite (Fe_3O4):

Magnetite includes both ferrous (Fe^{2+}) and ferric (Fe^{3+}) ions, contrary to all other iron oxides [9]. Also, magnetite has a cubic inverse spinel phase structure which belongs to the space group Fd3m assigned to JCPDS card No. 19‑0629 [214]. Furthermore, the structure of magnetite illustrated that the tetrahedral (A-site) and octahedral (B-site) produce two magnetic sublattices with the spin moments on the A and B sublattices which are antiparallel to each other [215]. In inverse spinel magnetite, the B- sites were filled by equal numbers of Fe^{2+} and Fe^{3+} ions, while the A-sites were filled only by Fe^{3+} ions. The ions of B-sites become ordered state at the point of Verwey transition (-153.15 °C). The crystal symmetry converted to orthorhombic phase [215, 216]. The density of magnetite is 5.18 $g.cm^{-3}$, which is insignificantly lighter than hematite (5.26 $g.cm^{-3}$). Furthermore, magnetite reveals both negative type (n-type) and positive type (p-type) semiconductor behavior and possesses a low band gap energy (0.1 eV) which shows the lowest resistivity of any mineral oxide (5 $x10^{-5}$ Ω.m) [144].

Recently, the surface modification of magnetite NPs by biocompatible shells or surfactants have been investigated. The adsorbent properties for magnetite depend on effective surfaces and morphological characteristics. Therefore, by utilizing the effective shell, which hasn't any notable magnetism effect for enhancing the surface effectiveness of magnetite, can greatly affect its use as an adsorbent [217]. Bi-functional materials that display both magnetic and photocatalytic activity are intelligent materials for the improvement of the environmentally favorable catalytic approach. Shanmugam and Young [218] have reported the usage of hybrid nanocomposites of the reduced graphene oxide/magnetite/nickel oxide (rGO-Fe_3O_4-NiO) as a proper photocatalyst compound. The results proved that the high degradation efficiency of inorganic dyes is achieved by using 2 wt.% of the synthesized catalyst within 15 min. The yield of photodegradation for the effluent dye

was 28 and 39% using Fe_3O_4 and NiO NPs, respectively. Also, Shashi et al.,[219] have reported the synthesis of magnetite and zinc oxide core-shell (Fe_3O_4/ZnO) for the methylene blue (MB) degradation using sunlight. Three core-shell have been synthesized (i) Fe_3O_4 NPs coated by zinc oxide, (ii) Fe_3O_4 core coated with SiO_2 and deposited by ZnO, (iii) magnetite core coated with SiO_2 and (3-aminopropyl) triethoxysilane (APTS) and ZnO deposition. The coating using SiO_2 in the last two samples exhibited better kinetics and higher activity. The coating with silica on magnetite in samples enhanced the transport efficiency of MB dye. The notable improvement in photoactivity could be ascribed to the synergistic effect of adsorption by SiO_2 and zinc oxide catalysis. Nemanja et al.,[220] have reported the photocatalytic activity of tungsten trioxide and magnetite (WO_3/Fe_3O_4) catalysts against thiacloprid using UV light and sunlight irradiation synthesized via co-precipitation technique. It was reported that the degradation efficiency decreased with enhancing the tungsten trioxide concentration. Also, the efficiency of degradation increased with enhancing the catalyst dosage due to of the increase of the surface area of the catalyst, which improves the absorption of photons. Moreover, the increase of the calcination temperature did not promote any notable changes in the degradation efficiency of thiacloprid. Additionally, the efficiency of separation was significantly enhanced by using an external magnetic field. Also, the efficiency of magnetic separation increased with increasing the tungsten trioxide content in the synthesized catalysts.

Compared with common adsorbents, magnetite could be utilized to eliminate heavy metals from water (as shown in Table 2). Honglei et al., [221] reported the synthesis of the carboxymethyl cellulose-immobilized magnetite NPs (CMC-Fe_3O_4). The carboxymethyl cellulose-immobilized magnetite NPs showed greater adsorption capacity for lead ions than those of pure magnetite NPs, and the maximum adsorption capacity of lead ions achieved was 152 $mg.g^{-1}$. The results indicated

that carboxymethyl cellulose-immobilized magnetite NPs displayed increased adsorption for lead ions. Guorui et al., [222] synthesized magnetite-chitosan@ bentonite (Fe_3O_4-CS@BT) composites to remediate acid mine drainage (AMD) for heavy metal removal. The supreme adsorption capacity of Cr (VI) elimination was reported to be 62 $mg.g^{-1}$. Actual AMD containing contaminants such as cadmium, copper, iron, zinc, and nickel was also treated. The heavy metal removal of copper, nickel, zinc, cadmium and lead were more than 89%, whilst iron was 84%. These results confirm (Fe_3O_4-CS@BT) would be an efficient adsorbent in the removal of heavy metals.

Additionally, magnetite NPs have been widely used for radionuclide removal due to its enhanced properties. Han Guo et al.,[223] reported Fe_3O_4/porous carbonaceous materials (Fe_3O_4/PCMs) synthesized via the hydrothermal technique. The maximum adsorption capacity of U(VI) using (Fe_3O_4/PCMs) NPs was reported as 123 $mg.g^{-1}$ at 55 ^oC. Furthermore, the regeneration experiment showed that the (Fe_3O_4/PCMs) NPs presented high stability and recoverability for U(VI) adsorption. These results indicated that (Fe_3O_4/PCMs) NPs can be accepted as suitable adsorbents to remove uranium for wastewater treatment applications. Ayub Khan et al., [224] have synthesized magnetite nanorod-decorated silicon Schiff base complex (M/SiO_2-Si-SBC) for the removal of U(VI) and Pb(II) from water solutions. The maximum adsorption capacities of magnetite nanorod-decorated silicon Schiff base complex were $6.45x10^{-4}$ $mol.g^{-1}$ for lead ions Pb(II), and $4.82x10^{-4}$ $mol.g^{-1}$ for U(VI) at 25 ^oC and were higher than those of silicon Schiff base complex ($5.18x10^{-4}$ $mol.g^{-1}$ for Pb(II), and $3.70x10^{-4}$ $mol.g^{-1}$ for U(VI)). The results showed that the magnetite nanorod-decorated silicon Schiff base complex could be used as suitable adsorbents for removal of U(VI) and Pb(II) from polluted wastewater. Also, Congcong et al.,[225] have synthesized fungus-magnetite nanocomposites as adsorbents for the elimination of radionuclides.

The sorption ability of Sr(II), Th(IV) and U(VI) using fungus-magnetite was examined with a batch-based method. The maximum removal capacities of fungus-magnetite were 280.8, 100.9, and 223.9 $mg.g^{-1}$ for Th(IV) at pH 3.0 and Sr(II) and U(VI) at pH 5.0, respectively.

2.2.3 Maghemite (γ- Fe_2O_3):

Maghemite (γ-Fe_2O_3) has a very similar crystal arrangement to magnetite [69]. Maghemite (γ-Fe_2O_3) has a cubic structure where the Fe^{3+} ions are distributed over A-sites (8 Fe^{3+} ions per unit cell) and B-sites. Hence, the γ-Fe_2O_3 can be attributed as the fully oxidized Fe_3O_4 (JCPDS card No. 39‑1346) [144]. The private occupation of Fe^{3+} in maghemite NPs signifies high chemical stability without any reducing activity [69]. γ-Fe_2O_3 is widely used as a suitable adsorbent due to the high value of its magnetization saturation, which facilitates the efficiency of separation from wastewater through the application of water treatment for additional use (as shown in Tables 1&2). Additionally, it is used due to its non-toxicity, and low-cost synthesizing compared to other materials [226]. Nadia Boukhalfa et al.,[227] used the magnetic alginate functionalized multiwalled carbon beads to coat the maghemite NPs. The synthesized beads revealed a greater adsorption removal for MB elimination. The maximum adsorption capacity of 905.5 $mg.g^{-1}$ and the adsorption experiments were well matched via the Freundlich model. The results showed that the synthesized beads can be used as an excellent and low-cost adsorbent for MB dye degradation and enhanced the separation after treatment.

Huiwang et al.,[228] improved the degradation of orange II by magnetite @maghemite by utilizing the oxalate. The results revealed that iron ions must be filtered from the catalyst to enhance the Fenton reaction. Also, the results revealed that increasing the pH of the solution leads to increased Fenton reaction.

At the same time, the conducting polymers can be used as promising materials for the functionalization of magnetic materials where they show activity as chelating agents ascribed to the existence of electrons on the chains of the polymers. As a result of the process of doping, these polymers can get a positive charge on the amine nitrogen atoms, to keep neutrality. This is significant because several pollutants can be removed with the assistance of these polymers by electrostatic interactions. Alicia et al.,[229] used polypyrrole/maghemite (PPY/γ-Fe_2O_3) and polyaniline/maghemite (PANI/γ-Fe_2O_3) for the removal of chromium (VI) and copper (II) ions from aqueous media. The polypyrrole/maghemite presented higher and quicker adsorption potential than polyaniline/maghemite for both the heavy metals. Polypyrrole/maghemite had a maximum adsorption capacity of 209 $mg.g^{-1}$ and 171 $mg.g^{-1}$ for removal the chromium (VI) and copper (II) ions, respectively. While the maximum adsorption capacity for the polyaniline/maghemite were 196 $mg.g^{-1}$ and 107 $mg.g^{-1}$, respectively. Shalini et al., [230] reported Pb^{2+} and Cu^{2+} removal from water using synthesized maghemite NPs. The specific surface area of mesoporous maghemite NPs is 79 $m^2.g^{-1}$ and the saturation magnetization is 45 $emu.g^{-1}$ at 27 °C. The removal of lead and copper ions occurred at a low pH and enhanced as pH increased, while it decreased as temperature increased. The maximum adsorption capacity was 68.9 and 34.0 $mg.g^{-1}$ for lead and copper ions, respectively.

The production of new and effective magnetic adsorbents, especially from TiO_2 nanotubes are more suitable for photodegradation applications. The Fenton reaction and photocatalysis are confronted with significant restrictions such as reducing the activation of the catalyst, which is attributed to the increase of organic aggregates on the catalyst surface. This restriction can be reduced by using ultrasound irradiation, which gives high-speed microjets of liquid, which consequently continuously wash/renew the surface of the catalyst [231]. Furthermore, the studies

to confirm the catalytic activity and stability of the catalyst are significant for photodegradation in water treatment processes. Lately, Yean Ling et al.,[232] developed new sonocatalytic activities of maghemite and TiO_2 magnetic catalysts to degrade the orange G dye. The sonocatalytic efficiency was exceptionally enhanced with the addition of titanium dioxide nanotubes. The higher specific surface area allowed major dye reactants to adsorb over the surface of the catalyst, whilst higher pore volume appeared in the further rapid diffusion of several compounds throughout the sonocatalytic reaction. Titanium dioxide nanotubes/maghemite with suitable composition and specific structural characteristics have synergetic effects such as charge carriers and hydroxyl radicals' separation which are generated via Fenton reactions. This improved the sonocatalytic activity to degrade the Orange G under ultrasonic irradiation.

Maghemite NPs are viewed as more superior adsorbents for As (V) than magnetite. Their capacity to adhere with As (V) oxy-ions is ascribed both to the adsorption on the structure of maghemite or on the hydrolyzed surface created after the connection with water. Additionally, maghemite NPs may have smaller crystallite sizes and, hence, offer high specific surface area [69]. Homero et al.,[233] reported using the concrete/maghemite nanocomposite (CM nano) as a suitable adsorbent for remediation of As(V). The adsorbent was synthesized by aging a mixture of magnetite NPs, sand and Portland cement. It was revealed that the columns of CM nano can reduce the concentration of As (V) in water from 10 ppm-10 ppb. For concrete/maghemite adsorbent, the remediation of As (V) reached 85% at pH= 5. While, at pH = 3 and 7, the remediation of As (V) was 75 and 80%, respectively. Hosik et al.,[234] reported the synthesis of maghemite NPs for As (V) removal from aqueous solution. The average size and surface area of the maghemite NPs were observed in the range (11–23) nm and (41–49) $m^2.g^{-1}$, respectively. Based on the particle size of γ-Fe_2O_3 NPs, the adsorption removal for γ-Fe_2O_3 NPs (11 ± 6 nm), is roughly 1.6 times higher

than that of those γ-Fe_2O_3 NPs (23 ± 5 nm). The maximum adsorption capacity of As (V) for γ-Fe_2O_3 NPs was 4.643 $mg.g^{-1}$ at pH = 7. The adsorption capacity constants increase with an increase in temperature (i.e. endothermic nature).

2.3 Spinel ferrites and their composites:

Spinel ferrites are still being investigated broadly in nanostructures, where they have numerous exceptional properties, particularly, their magnetic properties. The spinel ferrites are also magnetic semiconductors, which is used in broad and distinct technological areas such as high density information storage materials, phase shifters, converters, inductors, low and high-frequency transformer cores, catalysts, electronic devices, ferrofluids, humidity sensors, magnetic resonance imaging, drug delivery, antenna materials and microwave absorption [235-252].

Spinel ferrites are characterized by the formula MFe_2O_4, where M stands for divalent metal ions with an ionic radius between 0.6 and 1Å; such as Cu, Ni, Mg, Mn, Co, Zn, and Cd etc. M can be replaced by other divalent metal ions. Fe^{3+} can be replaced by other trivalent ions such as Al, Cr, Ga, In etc. The spinel structure is derived from the mineral $MgAl_2O_4$ which crystallizes in the cubic system. This crystal structure was first determined by Bragg and by Nishikawa [253]. The smallest cell of the spinel lattice that has cubic symmetry contains 8 molecules of MFe_2O_4, assigned to the Fd3m space group (JCPDS: 22-1086). The relatively large oxygen ions form an f.c.c (face centred cubic) lattice, in which two types of interstitial sites are present; namely tetrahedral sites surrounded by 4 oxygen ions (A site) and octahedral sites surrounded by 6 oxygen ions (B site) [254, 255]. The properties and applications of spinel ferrites strongly depend on the nature and distribution of the cations and the methods of synthesis. Various methods have been used for synthesizing the spinel ferrites such as the sol-gel [256], oil-in-water microemulsion

reaction method [257], sonochemical approach [258], hydrothermal method [259], surfactant-assisted coprecipitation method [260], and micro-emulsion method [261]. The spinel ferrites have an interesting bandgap (as shown in Table 1) which makes them an excellent choice in enhancing the photodegradation efficiency and heavy metals removal applications illustrated in Tables 2&3.

Recently, there has been a notably increased interest in using spinel ferrites and their composites for water treatment applications due to their magnetic behavior, chemical stability, and biocompatibility. Furthermore, the catalytic activity of the spinel ferrite NPs catalyst remarkably depends on their synthetic method, where the crystalline, crystallite size, and specific surface areas of the spinel ferrite can be adjusted using various calcining temperatures and different pH values. Meijuan et al.,[262] synthesized a series of Co ferrite (CFO) via a microwave technique. XRD data revealed that the CFO NPs calcined at 500 ℃ has a high level of crystallization. Also, the specific surface area of CFO NPs reduces with the rising sintering temperature. The photodegradation activity of Congo red and methyl orange are higher than of those for MB, RhB, 4-nitrophenol and 4-chlorophenol using the CFO NPs photocatalyst due to the CFO NPs preferential degradation of the nitrogen bonds in the dye molecule. The photodegradation rate of the CFO NPs enhanced with the increasing specific surface area and in the presence of hydrogen peroxide. The hydrogen peroxide easy dissolves to hydroxyl radicals to create the peroxide radical.

Among the hazardous pollutants, the aromatic nitro compounds, particularly nitrophenols, are the significant pollutants present in industrial and agricultural wastewaters due to their solubility and stability in water. The spinel ferrites have been used as photocatalysts for the removal of the aromatic nitro compounds in water, due to their easy and simplistic synthesis method, in addition to their higher resistance to critical acidic and basic conditions. Ibrahim et al.,[263] have studied the stability and magnetic recovery nature of MFe_2O_4 (M = Zn, Co, Mn) spinel ferrite NPs. These

were manufactured utilizing sol gel-hydrothermal method and using PVA as a surfactant for the degradation of nitroarenes. The results revealed that Mn ferrite is more efficient for the degradation of nitroarenes compounds due to its large pore radius and high pore volume values compared to the other ferrites NPs. On the other hand, the reducing of the activity of Zn ferrite is ascribed to the increase in the size of Zn^{2+}ions, which lead to a rise in values of lattice constant. The Mn-ferrite NPs showed the largest saturation magnetization and extraordinary reduction efficiency for nitroarene compounds in the existence of sodium borohydride. The data of photodegradation obeyed the Pseudo-first-order model.

Zinc oxide (ZnO) is used as an efficient photocatalyst due to its wide direct bandgap (3.2–3.4 eV), which allows it to act as an efficient low-cost photocatalyst at UV range. Nevertheless, the ineffective performance of ZnO under sunlight and the fast recombination of its photogenerated electron-holes, make that ZnO cannot achieve good efficiency. Several efforts have been made to defeat this problem, such as the substitution by metal and nonmetal elements, dye sensitization and coupling with other semiconductors [264, 265]. Furthermore, the combination of ZnO with a magnetic catalyst such as spinel ferrite (with bandgap about 1.6 eV) is more efficient, due to the ability of separation and the recovery of the catalyst [266, 267]. Recently, Raheleh et al. [268] have synthesized Zn-ferrite, and zinc oxide nanocomposites as a photocatalyst to degrade the MB and 4-nitrophenol (4-NP) under visible LED light radiation. The results revealed that the maximum photocatalytic efficiency reached 97 % and 67% of MB and 4-NP within 150 min, respectively. The high photocatalytic activity of this composite was attributed to the efficiency of separation of photoinduced electrons and holes. Furthermore, it has an easy separation by a magnetic field and can be used reused twice more, resulting in three cycles.

Fenton reaction is a high-efficiency process for the elimination of the contaminants based on the creation of •OH, which is created by stimulating the hydrogen peroxide with ferrous ions, but the recovery of ferrous ions is extremely low. To increase the ratio between ferrous/ferric ions recycle, UV irradiation has been utilized through the Fenton process [269]. Lately, Yang Li et al.,[270], have synthesized metals substituted $ZnFe_2O_4$ NPs, for the removal of organic contaminants under UV irradiation. The results indicated that photodegradation efficiency of CR dye reached 94.6% within 3h due to the production of more •OH, which was created during the photo-generated holes and the oxidation of the hydrogen peroxide by metal ions on the surface of the catalyst. Additionally, the decomposition efficiency of CR was still stable at 75.5% at the end of the third cycle. Therefore, metal-substituted Zn ferrite can be used as a suitable photocatalyst for the removal of organic chemicals in the practical application of wastewater treatment.

Also, Abdel Maksoud et al.,[271] have studied the photocatalytic activity of metals-substituted spinel CFO NPs synthesized using a facile sol-gel technique for the degradation of MB dye. The photocatalytic efficiency of Mn substituted CFO NPs enhanced with increasing the Mn content. Furthermore, the results revealed that the maximum photodecomposition efficiency reached 96.0% within 100 min under UV irradiation using $Mn_{0.75}Co_{0.25}Fe_2O_4$ NPs. Also, the data of photodegradation exhibits that, the efficiency of photodegradation increases as pH and concentration of $Mn_{0.75}Co_{0.25}Fe_2O_4$ NPs increases.

Several materials show highly efficient photocatalytic effects, nevertheless, the expensive cost of these materials and the high energy needed for the separation of NPs restricts its large-scale implementation or application [272]. An efficient procedure to achieve the above-mentioned criteria is by loading these materials on a magnetic carrier. Among these materials, Ag_2O has a high photocatalytic activity for degradation of MO dye and phenol and is an ideal candidate for a

diverse number of applications. However, a reduction in the cost of the Ag_2O photocatalyst and enhancement of its separation efficiency is needed to satisfy practical demands. Recently, Fujin et al.,[273] have synthesized the construct Ag_2O/MFe_2O_4 (M = Co, Zn, Ni) composites to reduce the cost of Ag consumption and enhance the recovery rate. The three obtained composites show high photodegradation efficiency towards the organic pollutants (MO, MB, RhB, and phenol). The data of photodegradation confirms that Ag_2O/CFO has the worst recovery due to the low recovery rate and Ag concentration. This behaviour may be attributed to the relatively slow separation of the CFO carrier and the weak adhesion of Ag_2O. The $Ag_2O/NiFe_2O_4$ is higher than $Ag_2O/ZnFe_2O_4$ in the recovery, but in contrast, the photocatalytic performance of $Ag_2O/ZnFe_2O_4$ is better. Hence, the performance stability of $Ag_2O/ZnFe_2O_4$ is the highest through renewed use and semi-continuous procedure.

Among the ferrites, $ZnFe_2O_4$ (ZFO) incorporated with carbonaceous materials exhibits extraordinary photocatalytic activity due to their ease of electron migration, high light absorption efficiency, and the excellent separation performance. Arjun et al.,[274] have synthesized ZFO modified by (CNT, GO, Fullerene) carbonaceous materials via the hydrothermal method for the degradation of norfloxacin and Cr (VI) under sunlight irradiation. The adsorption capacity and excitation separation efficiency enhanced by the incorporation of carbonaceous materials with ZFO NPs. ZFO@CNT shows better activity than of those for the other nanocomposites. The photodegradation efficiency of ZFO@CNT was reported to be 91.36% of norfloxacin and 82% of Cr (VI) in 90 and 60 min, respectively, under sunlight illumination.

Microbial pollution has increasingly become the main way of transmission of infectious diseases. Usually, these pollutants have excellent solubility in water and can permeate to deep soil strata and transfer to groundwater. Rapid economic losses and death occur due to these dangerous

diseases arising from microbial pollutants, which contaminated water has been a significant problem preventing social development, particularly for those in underdeveloped areas. In traditional sterilization approaches, chlorine gas, chlorine dioxide gas, and ozone gas are the usual effective disinfectants for eliminating the microorganisms. But these approaches have restrictions due to the unwanted property of being toxic gases, which therefore have potential risks to operation workers and other environmental hazards as well [275, 276]. Usually, the photocatalytic inactivation includes many parallel oxidation processes, containing oxidative destruction of cell wall components, oxidation of coenzyme A and oxidation of nucleic acids. While the vital factors in deactivating cells are the quantity and quality of photocatalytic produced reactive oxygen species (ROS). Therefore, exposing materials which could generate enough, and effective ROS is the critical issue. The spinel structure ferrite exhibits superior ferromagnetism, nontoxic properties, and extraordinary photochemical stability. Hence, it has been used as a catalyst to eliminate microorganisms and environmental contamination [277, 278]. Xue-Gang et al.,[279] have studied the photocatalytic inactivation performance of AgI/$CuFe_2O_4$ against typical bacteria *Escherichia coli* (*E. coli*) and *Staphylococcus aureus* (*S. aureus*). The results showed that the AgI/$CuFe_2O_4$ composite could effectively inactivate both *E. coli* and *S. aureus* cells in 50 and 40 min, respectively, under visible light irradiation. The results of catalysts showed that the optimum concentration of AgI/$CuFe_2O_4$ (18.75% of AgI) composite is 0.4 $mg.mL^{-1}$ at reaction pH = 7. Additionally, the results of magnetization and cycling performance revealed that the AgI/$CuFe_2O_4$ (18.75% of AgI) composite was separated from the mixture due to its unique magnetic property, stability, and reusability.

Silver phosphate (Ag_3PO_4) has high photocatalytic efficiency due to its narrow bandgap of 2.42 eV. One of the advantages of using Ag_3PO_4 photo-catalytically is the inductive nature of PO_4^{3-}

which improves the separation of electrons and holes. However, the functional applications of Ag_3PO_4 are sincerely limited by some drawbacks. The Ag^+ produced from Ag_3PO_4 can be transformed to Ag^0 via the electrons generated during the photocatalysis process, resulting in the Ag_3PO_4 photo corrosion, which would reduce the light absorption efficiency and the stability of Ag_3PO_4. Therefore, the construction of magnetically recyclable heterojunction composites by incorporation of the magnetic spinel ferrites with photocatalyst possessing high photocatalytic efficiency is a promising way. Yanjun et al.,[280] synthesized the magnetic PANI/Ag_3PO_4/$NiFe_2O_4$ ternary composite to decrease the photo corrosion of Ag_3PO_4 and improve the reusability. The PANI/Ag_3PO_4/$NiFe_2O_4$ composites with various PANI concentrations exhibited improved photocatalytic activity for RhB and MO dyes degradation correlated to Ag_3PO_4, Ag_3PO_4/$NiFe_2O_4$, and PANI/Ag_3PO_4 composites. The maximum degradation efficiency achieved for RhB and MO for PANI/Ag_3PO_4/$NiFe_2O_4$ was 100 and 94.97%, respectively. The rate of degradations was found to be 12.1 and 15.4 times faster than those of pure Ag_3PO_4, respectively. In recent years, carbon materials like 3D Graphene, chitosan, and multi-walled carbon nanotubes (MWCNTs) have gained significant interest and attention due to their unique structure and properties. Recently, MWCNTs have been utilized in heavy metals and radionuclides removal. Nevertheless, MWCNTs are highly hydrophobic and suffer from rapid aggregation in aqueous solution due to great van der Waals interaction forces within MWCNTs, which may limit the effective adsorption performances and decrease the adsorption potential [281]. Hence, to enhance the adsorption performance of MWCNTs, incorporation with magnetic adsorbents such as the spinel ferrites should occur. Lichao et al.,[282] have synthesized (CFO/MWCNTs) via hydrothermal technique for U(VI) removal from water. The adsorption potential enhances as the pH increases from 2.0-6.0 and then reduces with a further increase in pH. Furthermore,

CFO/MWCNTs shows a high adsorption capacity which reached 212.7 $mg.g^{-1}$. After 3 cycles, the adsorption capacity of the CFO/MWCNTs reduces from 116.0-104.4 $mg.g^{-1}$, indicating that CFO/MWCNTs can be used as an efficient adsorbent for radionuclide removal in wastewater treatment. Also, 3D graphene incorporated with chitosan, not only improves its high surface area, but also enhance sits heavy metal removal potential and limits the defects of chitosan, like its weak mechanical strength, low acid stability, inadequate thermal stability, and suffering from agglomeration. Furthermore, obstacles correlated to the separation of 3D graphene can be resolved by incorporation of magnetic NPs into the 3D graphene [283, 284]. Ramin et al.,[212] have synthesized 3D graphene/chitosan/$NiFe_2O_4$ via hydrothermal process for the removal of Pb(II) from wastewater. The maximum removal efficiency of Pb(II) achieved was 100% at pH = 8.5, within 18 min. These results reveal that 3D graphene/chitosan/$NiFe_2O_4$ can be used as an ideal candidate adsorbent for Pb(II) removal.

Table 3: Optical band of spinel ferrites.

Cations substituted Spinel Ferrite	Optical band gap (Ev)	Ref.
$CoTm_xFe_{2-x}O_4$	1.33 - 1.64	[258]
$NiAl_xFe_{2-x}O_4$	1.60 - 1.89	[114]
$Ni_{0.3}Zn_{0.5}Co_{0.2}Gd/La_xFe_{1.98-x}O_4$	1.69 - 1.85	[285]
$Ni_{0.3}Cu_{0.3}Zn_{0.4}Tm_xFe_{2-x}O_4$	1.78 - 1.94	[286]
$Co_xMg_{1-x}Fe_2O_4$	2.14 - 2.59	[115]
$NiCr_xFe_{2-x}O_4$	1.39 - 2.00	[287]
$Zn_{1-x}Mn_xFe_2O_4$	1.90 – 1.99	[288]
$Co_{0.5}Mn_{0.5}Nb_xFe_{2-x}O_4$	0.37 – 0.54	[289]
$Li_{2x}Cu_{1-x}Al_yFe_{2-y}O_4$	1.89 – 2.10	[290]
$Zn_xCo_{1-x}Fe_2O_4$	1.50 – 1.67	[291]
$Ni_{1-x}Cu_xFe_2O_4$	1.57 – 2.62	[292]
$Ni_xCo_{1-x}Fe_2O_4$	1.15 – 1.62	[293]

3. Biosorbent in water remediation applications:

This part attempts to investigate a broad range of magnetic adsorbents such as zero-valent iron, iron oxides, and spinel ferrites for the elimination of several types of contaminants such as radionuclides, heavy metals, dyes and pharmaceutical compounds from wastewater streams. The use of these magnetic adsorbents for water purification gives a significant advantage over other adsorbents, such as their low-cost and ease of separation of suspending adsorbents to be used again to reduce cost, as well as the ease to synthesize. It is illustrated from this review that the incorporation of the recent magnetic materials with the superior adsorbents such as WO_3, TiO_2, ZnO, and GO reduces the rapid recombination of photoinduced electron-holes and therefore, enhances the photocatalysis potential of these materials besides the ease of separation of suspending adsorbents. Furthermore, the mechanism and kinetics of the sorption approach depend

on many factors such as surface morphology, magnetic behavior of the adsorbent and the experimental conditions like pH, adsorbent concentration, irradiation time, temperature and the initial dosage of pollutant. Nevertheless, magnetic adsorbents face many obstacles that require discussion and dissemination in the form of research and development, such as the commercialization of these adsorbents to estimate their utility on a wider scale as well as a complete evaluation of the possibility of using these adsorbents to eliminate the multipollutant solutions.

Recently, the over-utilization of water resources as well as water pollution, in different demographics simultaneously occur as a consequence of uncontrolled greed associated with human civilization, urbanization and rapid industrialization. Unfortunately, where people live and work, wastewater is inevitably found. Several industries such as metallurgy, machinery, textile, printing, machinery manufacturing, mining operations, rubber, paper and pharmaceutical industries are strong producers of wastewater, laden with a great diversity of pollutants including heavy metals, dyes, pesticides, phenols, pharmaceutical compounds and insecticides [294-298]. Seepage of these contaminated effluents into aquatic environments above their statutory limits without proper management provokes tremendous ecological and health problems on our biosphere (including flora, fauna and human), as they exhibit immunogenic, teratogenic, mutagenic and carcinogenic characteristics [299, 300]. It is well known that about 70-80% of diseases in developing countries are attributed to water pollution [301].

The global enhancement in pollution of water sources has increased awareness among the world and hence, more efforts have been directed to combat this problem. Therefore, elimination of various water pollutants from water bodies is becoming a critical issue. Numerous obsolete scenarios including physical, chemical and biological approaches are implemented to capture

water pollutants from water systems. Photooxidation [302], phytoextraction [303], electrocoagulation [304], electrodialysis [305] (Nemati et al., 2017), irradiation [306], membrane separation [307], ultrafiltration [308], forward osmosis [309], ion exchange [310], precipitation [311], coagulation/flocculation [312, 313], microorganisms and plants [314-316] are applied to tackle different water pollutants from aquatic systems. However, most of these sophisticated processes have many certain limitations and restrictions such as high costs, inefficiency in low pollutants concentrations, long cycle times, reagents and energy consumption and chemical sewage sludge formation [317, 318].

3.1 Biological approach for wastewater treatment

In general, bioremediation-based terminologies are categorized into five main processes including biotransformation, biomineralization, bioaccumulation, biosorption, whereas the phytoremediation process is mainly performed on the basis of fractional or whole plant sectors. A large extent of susceptibility and productivity of each specialist strategy significantly depends on the quality of procedures employed.

3.1.1 Phytoremediation

The algae and/or plant-based technology is an emerging approach (commonly known as phytotechnology), applied to detect, tackle, immobilize and biodegrade different pollutants from the environment. Phytoremediation (agro-remediation) is a sustainable and green in-situ bioremediation aspect, mostly used by employing natural organisms (algae and plants) to clean up different pollutants from the contaminated environment [319]. It is an aesthetical, eco-friendly mechanism in which naturally abundant and cheap plants, macro and/or micro-algae can successfully uptake, accumulate and store high concentrations of contaminants from highly contaminated areas into their organism. The selected species have the abilities to remove a range

of water pollutants. After organic and/or inorganic pollutants absorption, they are converted from toxic to non-toxic forms in different ways and hence, detoxification of the polluted environment occurs [320]. Its main advantages are the superior efficiencies of biomaterials to tackle and accumulate chemicals from the environment via adsorption mechanisms and they are also low-cost compared with other conventional scenarios. Generally, phytoremediation has been utilized in the three environmental matrices including: water, air and soil pollution. Phytoremediation is grouped into seven sub classes including phytostabilization, rhizodegradation, rhizofiltration, phytodegradation, phytoextraction, phytoaccumlation and phytovolatilization. Inorganic contaminants are removed by phytostabilization, phytoextraction, phytovolatilization, phytoaccumlation and rhizofiltration, whilst organic contaminants are removed by phytodegradation, rhizodegradation and rhizofiltration [321]. Numerous invasive aquatic plants or aquatic macrophytes are widely adapted for pollutants remediation from aquatic systems or water resources. Aquatic macrophytes are classified into three main subclasses including floating, emergent and submerged. They have been effectively used at lab scale, field trials, in addition to aquatic ecosystems for removal of multiple pollutants including agrochemicals, heavy metals, dyes, organic pollutants, petrochemicals, personal care products and pharmaceuticals byproducts. They also have been utilized to decline algal population and enteric pathogen in polluted water. Their applicability to remove pollutants from different real wastewater streams using electroplating, mine tailing, domestic, stormwater, textile dyes, paper and pulp effluents were evaluated [322].

3.1.2 Biotransformation

Biotransformation acts as another potential pathway for pollutant levels decline at a contaminated area by converting higher toxic compounds into less toxic compounds using biological systems [323]. Generally, it is classified into two main categories: xenobiotic and biogenetically directed [324]. Its conception in wastewater treatment plants is based on inducing chemical reactions due to the presence of microbial communities such as bacteria which have the ability to biotransform numerous pollutants such as micropollutants [325]. For instance, the biotransformation mechanism of a set of amine and amide contained micropollutants has been investigated. Outlined valuable insights related to biotransformation analyses such as microbial community structure, microbial community characterization (i.e., metatranscriptomics and metagenomics) and gene expression patterns elucidate the biotransformation process of definite micropollutants. Other studies explored the enzymes (intracellular and extracellular) extraction from microbial communities of wastewater as well as their activities in terms of linking the observed biotransformation to specific enzymes [326].

3.1. 3 Biomineralization

Biomineralization is a set of processes by which organisms form minerals [327]. It is known as a process mediated by different microorganisms, (i.e. bacteria) for minerals formation based on numerous ions present in the surrounding environment [328]. Numerous minerals such as calcite, jarosite, dolomite, siderite, vaterite and kaolinite can precipitate due to the microbial activities [329]. Mainly, it is classified into three main fundamental categories: biologically induced mineralization, biologically influenced mineralization and biologically controlled mineralization.

i) Biologically induced mineralization: it is described as an environmental chemical modification performed by the biological activities and hence, producing oversaturation in addition to minerals precipitation [330].

ii) Biologically influenced mineralization: it consists of passive precipitation of minerals as a result of the interaction between the environment and compound changes found at the cellular surface because of bacterial metabolic activities. Due to the microorganism's metabolism, biominerals are secreted with low system control ability over the minerals that have been deposited [331].

iii) Biologically controlled mineralization: specifically, it is represented by numerous cellular activities for the purpose of minerals formation. Under certain conditions, organisms direct the minerals synthesis in specific parts of their cells, for example, magnetite synthesis by magnetotactic bacteria.

3.1.4 Bioaccumulation

Bioaccumulation is defined as a metabolically active process at which microorganisms have the ability to uptake water polluters inside their intracellular space structures through an establishment of importer complexes creating a translocation pathway in the lipids bilayer. Once pollutant molecules reach the inside of the mentioned space, they can be eliminated by peptides and proteins ligands. The bioaccumulative capacity of the as-used biomass for the target pollutants is considered to be the real measurement of its performance [332]. The main requirement of the engineered bioaccumulation process related to the host cell is to be alive. This imposes some necessary challenges such as nutrient provision for sustaining the biomass and supplementary aeration to accommodate with aerobic/anaerobic needs. As well, attributing to the process nature of proteins involvement in the cytosol and their embedment in the lipid membranes, additional

unique challenges such as decline cell viability, phenotype loss because of native microorganism's competition and immoderate proteins aggregation should be imposed [333].

3.2 Biosorption

3.2.1 Fundamentals of Biosorption

Biosorption as a practical application branch of sustainable development (biotechnological approach) is counted upon as an ecofriendly, economic and efficient technique for minimizing different contaminant concentrations in different water resources (i.e. drinking water), to the acceptable limits recommended by different federal regulations globally [334-336]. This green protocol is in accordance with the basics of green chemistry. The involved fundamentals of biosorption processes related to its different ingredients should be clearly comprehended. Briefly, it is defined as a passive uptake (metabolism-independent process), built on the usage of non-living biomass for elimination of different water pollutants. Generally, numerous benefits are achieved due to the recycling of these biomass sources (biowastes). Their utilization in their native and/or modified forms directly participates in wastes minimization, which can help rectify many ecological and environmental problems [337]. It also characterizes, by remarkable merits such as low operating and manufacturing cost, flexibility, wide availability, low energy requirements, ease of operation and high efficiency.

3.2.2 Biosorption strategy

In recent years, the biosorption conception as a multidimensional, effective process has been evolving. It is perceived as an alternate admirable scenario, compared with other traditional technologies used for the wastewater manipulation purpose. Sorption is mainly described as a physicochemical phenomenon by which gas or liquid molecules (sorbate) concentrate on the surface of another substance (sorbent). Sorbate is defined as a material that accumulates at the

sorbent surface, whereas sorbent is a substance upon whose surface the sorption was carried out and hence, providing purified effluents with high quality. In spite of denoting a biological entity involvement by using "bio" prefix, the biosorption term is also simply known as a physicochemical process in which the capturing of target sorbate molecules from aqueous solution using a biological matrix occurs. Both bioabsorption and bioadsorption dimensions are involved in terms of sorption mechanism. Absorption is the incorporation (integration) of a material in one state into a material with another state (i.e. gases absorbed by water or liquids absorbed by a solid). While adsorption is a physical bonding in which sorbate (i.e. molecules and/or ions) interacts with a surface of a sorbent resulting in sorbent-sorbate interface [338]. Briefly, the adequate description of the biosorption process is a passive, metabolically independent process covering all interaction aspects between any sorbate and biological matrix (biosorbent). It plays a crucial part in many processes naturally occurring in different scientific disciplines such as life sciences, biotechnology and medicine approaches.

3.2.3 Selection of biosorbents

Suitability of biosorbents is known to be the foremost, important step controlling the selection as well as preparation of the biosorbent itself. Taking into account the cost-effectiveness, as well as the biomass origin as one of the most important requirements, they represent a vital criterion to be considered during biosorbent selection. The waste biomass has the priority over the non-waste alternatives and seems to be a preferred technology used for the tackling of different water pollutants. Employing waste biomass has many merits summarized as: (1) absence of the need of growth requirements (i.e. media, nutrients) to be contained in the feed solution; (2) absence of toxicity limitations; (3) possible reusability and recovery of saturated biosorbent and sorbed pollutants, respectively; (4) easier mathematical and statistical modelling of pollutants uptake.

Additionally, for ensuring enormous potential capacity of biosorbent to detoxify different water polluters, the selected biosorbent should be characterized by numerous requisite aspects such as eco-friendliness, availability, biocompatibility and feasibility. Other diverse, admirable features are characterized to the biosorbent, such as high sorptive performance towards target pollutants under variable physicochemical operational parameters (i.e. pH, salinity, temperature, etc.) and good stability under acidic/alkaline conditions with the ability of sequential sorption of multiple pollutants. From both an economic and environmental perspective, recyclability, in addition to easy adaptability to different designs (i.e. batch, fixed bed systems) is significantly necessary features required for the established biosorbents. Figure 2 presents different categories and subcategories of available low-cost adsorbents ranging from natural adsorbents to highly stable composites [339]. On the basis of wastes as wealth, utmost attention should be given for these available wastes. Utilization of these promising cheap wastes offers multiple benefits because of their environmentally benign nature. Their reuse is economically beneficial because it overcomes disposal problems and generates revenue for different industries. In reality, the plentiful biological materials are substantially different in structure with the presence of variety of ligands like alcohols, amino acids, aldehydes, carboxylic acids, hydroxyl, phosphate, thiol, ketones, phenolic and ether groups at varying degrees capable to interact with target pollutants via different mechanisms and hence, enhance their sorption activities. Biosorption capacities of various biosorbents towards multiple pollutants have been investigated and reported in numerous research articles.

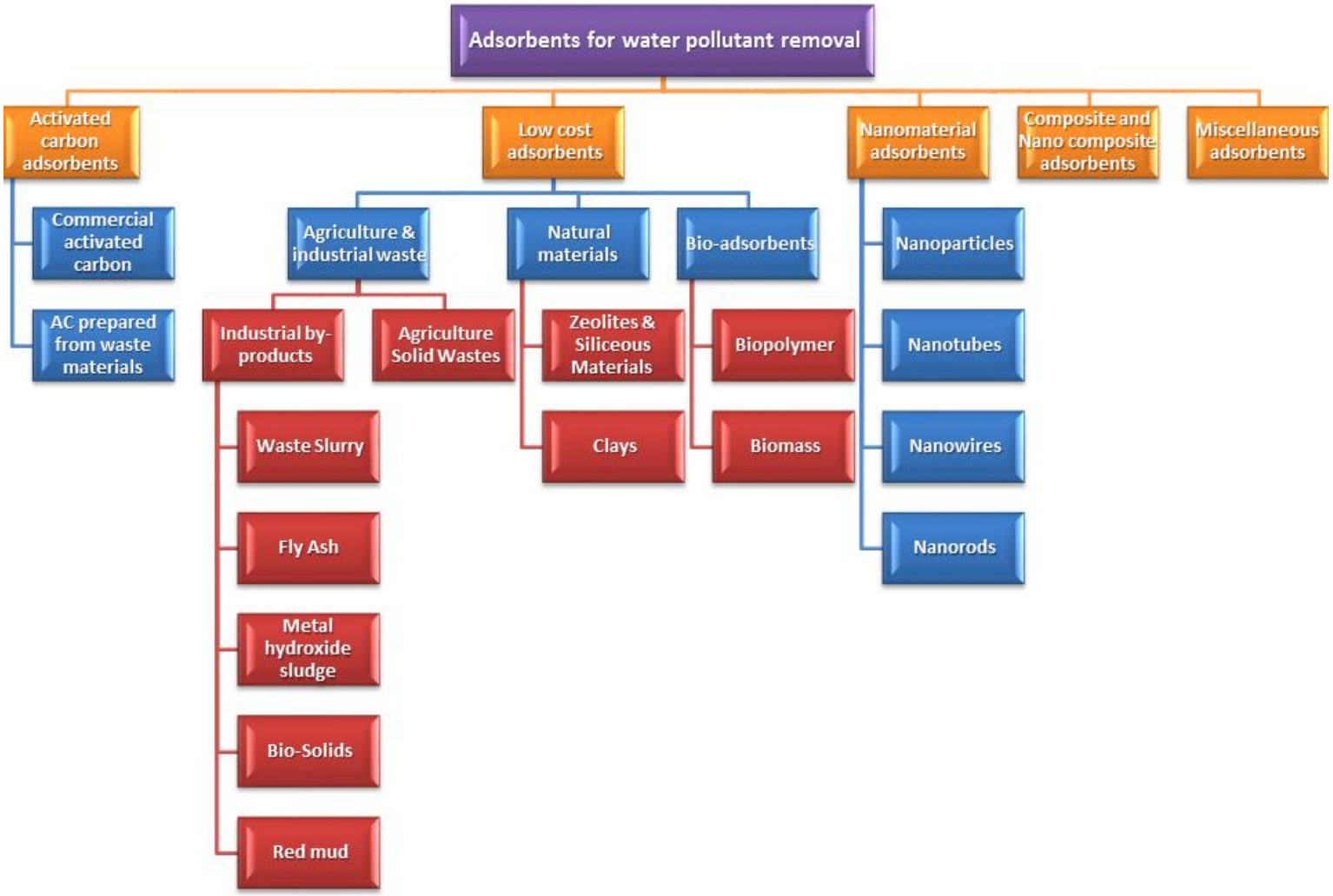

Figure 2: Different types of water pollutants adsorbents.

3.2.4 Examples of some biosorbents for water purification

3.2.4.1 Natural adsorbents

Numerous naturally occurring materials are considered to be promising and ideal sorbents because of the unique features such as low cost, readily abundant and great sorption capacities. Among them, chitin, chitosan, cellulose, zeolite, clay (i.e. montmorillonite, kaolinite and bentonite), wood, peatmoss and coal have successfully been employed for wastewater remediation. The aforementioned substances possess excellent structures that represent a convenient basis for biosorbent production to be further used in biosorption applications.

Two important natural promising biopolymers namely chitin and chitosan are majorly obtained from the exoskeleton of most invertebrates and cell wall of fungi. Chitin is frequently extracted from commercial and marine sources like crab, shrimp shells, oyster, squids, crayfish, cuttlefish and fungi [340]. Approximately 10^{12} kg of chitin is produced per year. Additionally, other estimates reported that above 80,000 tons of chitin is synthesized based on marine by-products [341]. Chitin is the precursor of chitosan. After cellulose chitosan is considered as the second most copious natural biopolymer on the earth. It is commonly known that chitin can be processed to chitosan via alkali treatment (Deacetylation process). They are industrially attractive because of their diversified admirable characteristics such as non-toxicity, biocompatibility, biodegradability, bioactivity and high hydrophilicity [342]. It is worth noting that possessing remarkable mechanical, physical and chemical features, in addition to presence of numerous functional groups on their backbones ($-NH_2$, - OH), makes them strong candidates to be exploited for sequestering different pollutants from water systems [343, 344].

Renewable cellulose is the most available polysaccharide on the earth. It is a linear homopolymer, which comprises of numerous hydro-β-D- glucopyranose units linked by (1→4) glycosidic bonds.

Widely, this sustainable biopolymer is known to be a promising alternative to synthetic plastics [345]. It has attracted significant attention because of endowing ingrained robust properties such as nontoxicity, durability, biodegradability, availability, mechanical, chemical and thermal stabilities [346]. Original and/or modified cellulose-based biosorbents are produced by various functionalization methods and introduced for multiple environmental applications in comparison with other natural polysaccharides like starch and proteins. Proper utilization of this natural polymer is widely performed for wastewater treatment from toxic, undesirable substances such as heavy metals and dyes [347, 348]. Furthermore, cellulosic nanomaterials are synthesized based on cellulose biopolymer into the following categories: cellulose nanocrystals, cellulose nanofibrils, bacterial cellulose and electrospun cellulose [349]. They have gained extensive credibility to be used as effective alternates to replace petroleum-based polymer (synthetic resins) for use in the removal or recovery of metals due to their abundance and low cost.

Zeolites are aluminosilicates materials (metal alumino orthosilicate) with the chemical formula ($M_2/nO.Al_2O_3.xSiO_2.yH_2O$), where M refers to metal (i.e. lithium, sodium, potassium, magnesium and calcium). The "n" variable represents the metal cation valence and "y" indicates the number of water molecules in the zeolite structure. There is also a possibility that alumina could be prepared from waste materials such as aluminium foil waste [350, 351]. Zeolite materials are characterized by microporous structures and crystalline nature. Aluminium and silicon are combined with each other by a shared oxygen atom (tetrahedral coordination). In particular, many research articles have shown that zeolites are upgraded to a promising commodity of great importance in a variety of application fields such as building, agronomy & horticulture and wastewater treatment [352]. Zeolites are characterized by their low cost, eco-friendliness, thermal stability, recyclability, high sorption capacity, selectivity and easy modification. Therefore, they

are widely employed at industrial scale as molecular sieves in air purification units [353]. Many studies extensively investigated the ability of zeolites as a natural material to be used in pure or modified forms of water pollutants elimination because of their unique three-dimensional network structures associated with interconnected pores, microporous structure and negative surface charge with high ion exchange capability [46].

3.2.4.2 Agriculture wastes

In general, agricultural wastes refer to organic by-products discarded by humans during agricultural production processes. Mainly, it includes different materials such as agricultural wastes, plant wastes, rural wastes generated from household activities and livestock & poultry manure. Also, animal manure and crop stalks as agriculture wastes originate from our daily life activities [354]. Various merits such as large quantities, vast sources range, environmental friendliness, biodegradability and reproducibility are characterized to these worthless wastes. They are lignocellulosic materials in nature comprising of main components lignin, cellulose and hemicellulose. These chemical components contents are different between various types of agriculture crops. For example, lignin, cellulose and hemicellulose in crops residues are 20-30%, 35-50% and 15-30%, respectively [355]. Chemically, lignin is an aromatic polymer comprised of numerous functional groups including carboxyl, hydroxyl, methyl and other functional groups. While, cellulose and hemicellulose possess different oxygen-containing functional groups like carbonyl, ether and hydroxyl groups. Due to their diversity in chemical composition and renewability, they are presently exploited in five main aspects of agriculture wastes resources utilization. Fertilizer, feed, industry, energy and wastewater treatment are broadly considered to be the most important applications for recycling of agriculture wastes in our practical life. In recent years, with the increasingly severe environmental issues related to water pollution, numerous

studies have shown the continuous contribution of agriculture wastes to be utilized as promising biosorbents for different water pollutants including aromatic compounds, dyes, drugs, heavy metals, pesticides, and oily substances [356]. Due to its loose surface, high porosity, mechanical and chemical stability, agriculture wastes are considered as natural, effective and economic biosorbents for the elimination of different contaminants from water bodies. Existence of numerous functional groups and some elements facilitate the removal of different pollutants for water systems through a variety of supposed mechanisms in terms of ion exchange, chelation, surface complexation, coordination and hydrogen bonding [357]. This presents the significance and advantages obtained from agriculture wastes based biosorbents to be used as suitable and effective alternatives, instead of the expensive and commercial adsorbents extensively used in water contamination control (i.e. silica gel, activated alumina and activated carbon). Figure 3 portrays numerous functional groups (active sites), naturally present in biosorbents prepared from variable sources.

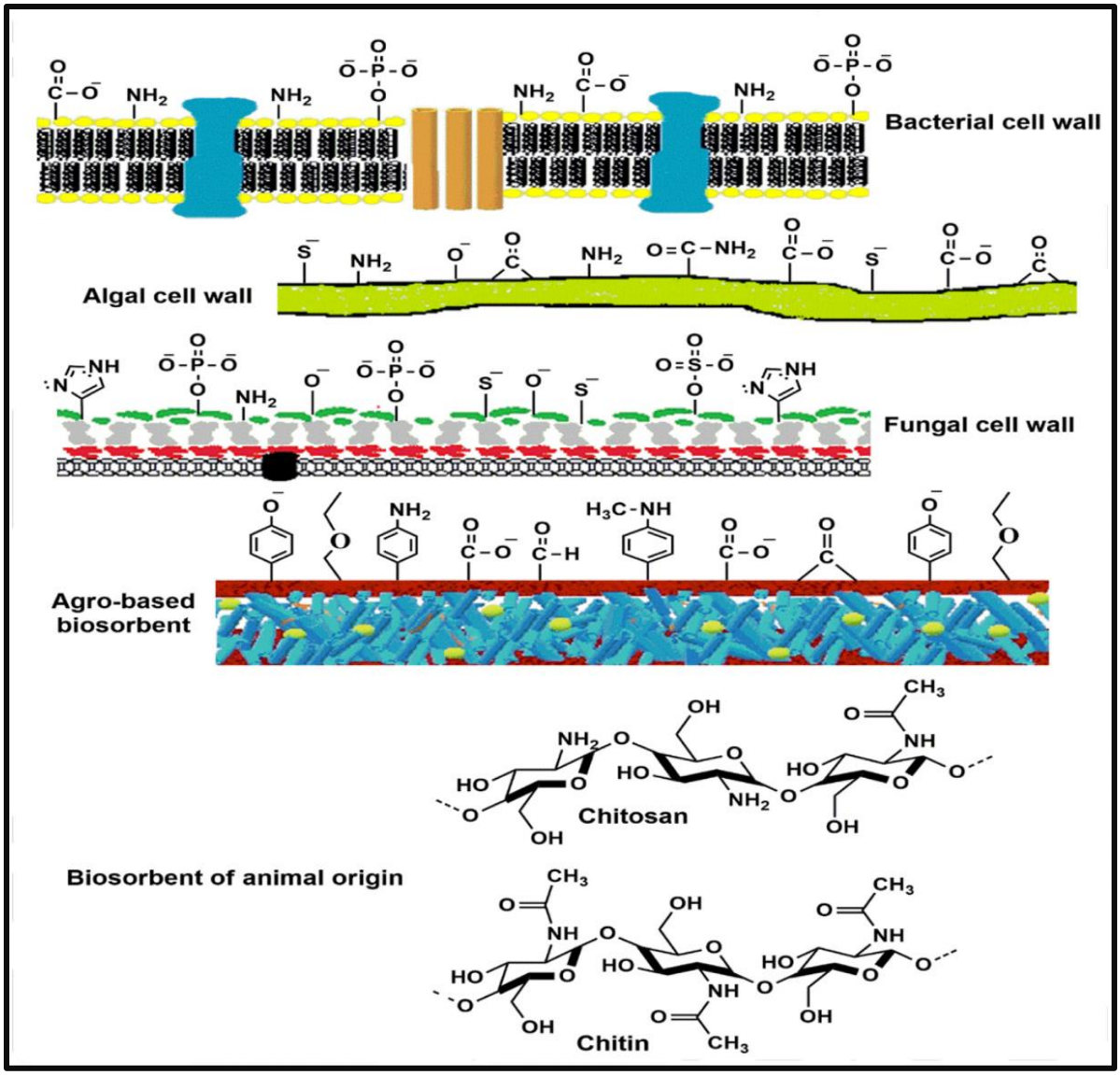

Figure 3: Functional groups characterized to biosorbents from different origins [337].

3.2.3 Biosorption Scenarios

Fundamentally, biosorption of sorbate onto a biosorbent surface is based on numerous physicochemical factors influencing on the overall process. Experimental evolution of biosorption performance, as well as biosorbent feasibility, can be illustrated in term of batch and fixed-bed methodologies.

3.2.3.1 Batch experiments scenario

Conventionally, batch scenario is used as a primitive step to evaluate biosorbent capability to eliminate pollutants from their matrices. Influence of several operational parameters can be estimated during this strategy (Figure 4).

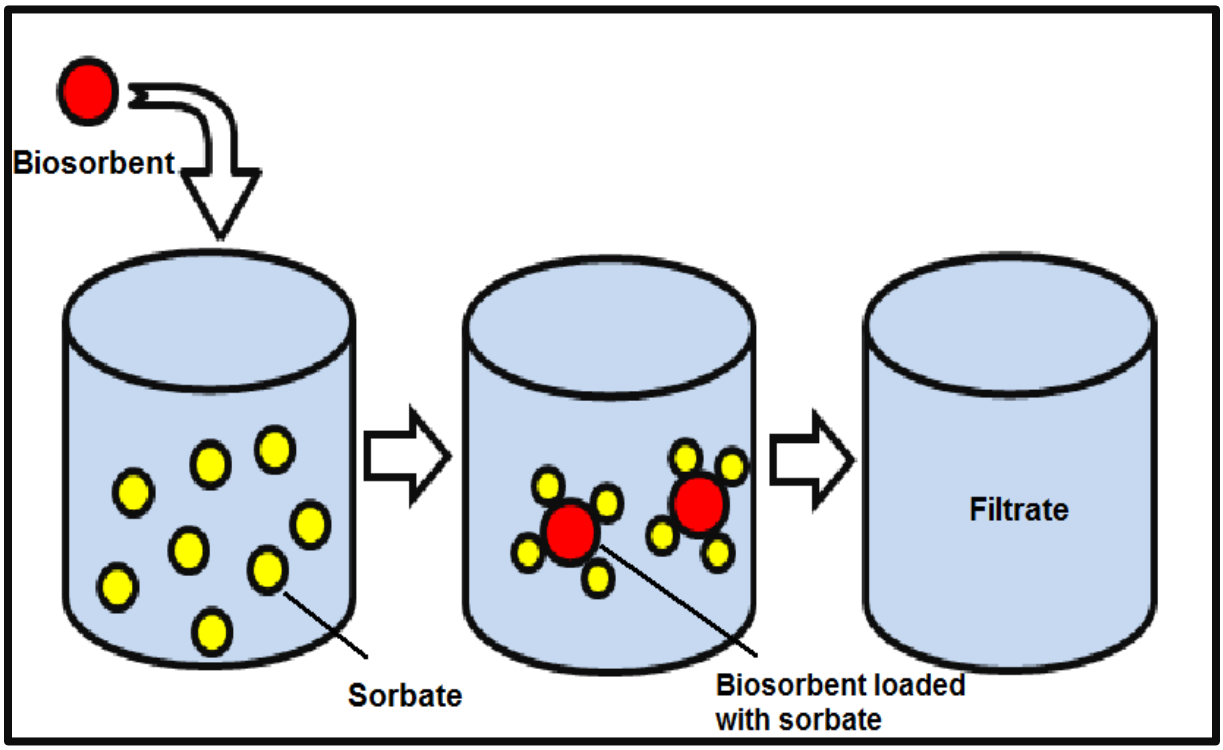

Figure 4: Schematic diagram of batch sorption.

Factors affecting the batch sorption

Influence of pH

The pH of the solution is a significant and critical parameter, playing a great role in the biosorption process. In particular, it has a drastic effect on the biosorbent surface charge density, ionization of functional groups (active sites) present on the surface of biosorbent and chemical species of sorbate in aqueous solutions [358]. Irrespectively, the nature of most biosorbents is strongly influenced by solution pH. More H^+ ions are present at very acidic conditions, whereas, in the alkaline domain,

OH^- are found in excess and thus, affect the sorption process performance. For instance, at acidic conditions, biosorption of negatively charged pollutants (i.e. metal anions) is favourable, due to protonation of binding functional groups and not competing with OH^- and hence, an enhancement of biosorption process performance. Additionally, solution chemistry (speciation) of sorbate is drastically affected by the medium pH. Sorption, as well as precipitation reactions, are mainly dependent on the environmental pH [359]. For example, at lower solution pH, metal cations are almost found in stable states and therefore easy to be sorbed on biosorbent surface. Whereas, at higher pH values, their solubility decreases with the possibility of the precipitation phenomenon occurrence, which complicates the biosorption process. It was reported that the maximum sorption capacity of Ca_2-Al EDTA LDH_S sorbent towards Cu^{2+} metal ion from $CuSO_4.5H_2O$ tested solution reached 568 $mg.g^{-1}$ [360]. Physico-chemical characteristics of biosorbent greatly influence the point of zero charge (pH_{PZC}). This is commonly defined as the pH value at which the surface net charge of biosorbent is zero. The biosorbent surface will be negatively charged when the solution pH is greater than pH_{PZC}, contrarily; if the pH of a solution is less than pH_{PZC}, it will carry a positive charge. Obviously, the value of pH_{PZC} clarifies the electrokinetic behaviour of biosorbent. The maximum experimentally achieved removal percent of 99.5 ± 0.4 was obtained under optimum conditions (pH of 10.10, the temperature of 55.92 °C, time of 21.10 min, the initial dye concentration of 16.35 $mg.L^{-1}$, and biosorbent amount of 48.64 mg) [361].

Influence of biosorbent dosage

Biosorbent dose is a vital factor to determine the optimum amount or saturation point, at which any further enhancement in the biosorbent amount does not present any significant improvement in the biosorption process. Generally, introducing a larger amount of biosorbent greatly increases the biosorption performance. This is interpreted to the available larger surface area with more

vacant biosorption sites and hence, easier access of sorbate molecules to these active sites occurs. It was elucidated that with an enhancement of ECCSB@Fe_3O_4 sorbent dose from (0.1-0.4 g), the removal percentage towards Pb(II) reached to 97.64%. Slight rise in the removal percentage with an increase in the sorbent dosage to 0.5-0.6 g [362]. Meanwhile, any additional increment of biosorbent amount above the optimized biosorbent dosage does not provide any increase in the biosorption process because of unsaturation state of biosorbent vacant active sites. Decline in overall biosorption capacity because of equilibrium imbalance between the huge biosorbent active sites and constant number of target sorbate molecules is attributed to the blocking of biosorbent active sites. This has resulted from overlapping or agglomeration of higher biosorbent particles at higher biosorbent doses which are commonly known as screen effect phenomena. This was confirmed with the decrement of removal percentage characterized to serpentine towards methylene blue dye from 64 to 63.4% with an increasing the mentioned sorbent applied dose from 0.15 to 0.35 g [363].

Influence of starting pollutant concentration

Undoubtedly, initial pollutant concentration in the aqueous phase has a significant influence on the biosorption process, as it clears the correlation between the mentioned parameter and the binding capacity of biosorbent. For a specific amount of biosorbent, higher pollutant quantity in terms of starting pollutant concentration provides a greater driving force required to outstrip the mass transfer resistance and transport the pollutant (molecules and/or ions) from the aqueous solution to the surface of biosorbent (solid phase). This leads to an increase in the motivating gradient force and therefore facilitating the sorbate migration to the biosorbent surface. It was reported that with an increase in the initial concentrations of both Cr(VI) and MB dye contaminants from 100 to 200 $mg.L^{-1}$, the sorption capacities of as-prepared COSs-AC sorbent enhanced from

231.0 and 391.93 to 282.1 and 462.67 $mg.g^{-1}$, respectively, for Cr(VI) and MB, respectively [364]. In fact, an enhancement in initial pollutant concentration gradually enhances the biosorption quantity and contrarily decreases the biosorption rate. An enhancement of CG-SH sorption capacities for Pb(II), Cd(II) and Hg(II) pollutants was observed with an increase in their initial concentrations. The maximum theoretical sorption capacities characterized to the mentioned sorbent were achieved as 332.8, 110.4 and 179.2 $mg.g^{-1}$ for Pb(II), Cd(II) and Hg(II), respectively [365]. This is explained by the competition between extra or higher solute concentration and fewer number of available biosorbent active sites.

Influence of contact (immersion) time

Irrefutably, contact time is one of the most influential factors among various parameters involved in biosorption experiments. Obviously, it provides the equilibrium time for the biosorption process. At the earlier stages, remarkably accelerated sorption rate is attributed to the large availability of functional groups (active sites) on the surface of the biosorbent that can be easily accessed by sorbate (molecules and/or ions). As the active sites are occupied by target sorbate, sorption process rate declines until reaching to equilibrium (plateau) stage, because of the concentration gradient decrease because of biosorbent active sites saturation. A competition between the retained sorbate in the solution takes place to occupy the remaining sites. Therefore, enough time for solid-liquid equilibrium establishment should be ensured [366]. Studying the sorption performance of St: DB18C6 adsorbent against (Cd^{2+}, Zn^{2+}, Ni^{2+} and Cu^{2+}) metal ions for different duration ranging from 30 to 240 min revealed that removal percentage were raised with rising adsorption time up to 120 min and after 120 min, no important variation on the adsorption percentage was observed.

Influence of temperature

The sensitivity of sorption process to the environmental temperature is a vital parameter that significantly influences the sorbate molecules diffusion rate through the external boundary layer surrounding the biosorbent and therefore, investigating its effect on elimination of water pollutants is very important. The garnered information obtained from effect of temperature change can reveal the biosorption process whether its nature is temperature-dependent or not [367]. Favorability of sorption processes at elevated temperatures may be related to reduction in liquid viscosity, inducing sorbate particles mobility (more kinetic energy) or an increase in the collision frequency between biosorbent and sorbate and that can diffuse from the aqueous phase to the biosorbent. Another explanation is attributed to an enhancement of biosorbent active sites due to bonds rupturing. Furthermore, the high affinity of biosorbent under these conditions, suggests an endothermic nature of the sorption process. Tassist et al. [368] reported the sorption of Al (III) onto *S. rimosus* biomass in batch experiments. The Gibbs free energy of adsorption (ΔG°) was determined to be between 1.07 and - 3.62 $kJ.mol^{-1}$ at a temperature between 10 and 80 °C. The decrease in the ΔG° value with an increase in temperature favors the removal process of aluminium at a high temperature. On the other hand, in other research articles, an increase in the environmental temperature can lead to decline in the binding force between biosorbent and sorbate and thus, resulting in decrease in biosorbent sorption capacity at elevated temperatures. This indicates that the nature of biosorption process is exothermic. Inyinbor et al. [369] elucidated that the sorption capacities of CCDNc and DNc sorbents towards Rhodamine B dye declined from 80.00 to 26.57 $mg.g^{-1}$ and from 66.50 to 19.58 $mg.g^{-1}$ as temperature increased from 27 to 60 °C.

Influence of agitation rate

Generally, in a batch mode, adequate contact between the biosorbent and sorbate is heavily dependent on the agitation speed. Providing the suitable stirring rate has a greater impact on the biosorption process, as it overcomes the external mass transfer resistance (decreasing the thickness of boundary layer) surrounding the biosorbent particle by enhancing the mixing degree). Various parameters related to agitation influence the process such as agitator type and agitation time, which can also be investigated. Gupta et al. [370] concluded that the adsorption of Cr (III) using activated carbon prepared from waste rubber tires increased from 10% to nearly 80% with gradual increase in agitation speed from without or low agitation speed up to 150 rpm, respectively.

Influence of ionic strength (co-existing ions)

Estimation of biosorbent capturing performance towards target pollutants in the subsistence of other coexisting species (mixed solution) is necessary to be accomplished. Organic, inorganic materials (i.e. acids, alkalis and salts) and other co-existing (competitive) ions; cations and anions in the form of suspended or dissolved compounds are major constituents of different aquatic systems including natural (i.e. river, estuaries and oceans) or industrial wastewater. Optimization of the biosorption process can be established when the influence of interfering species existence is well studied. Significantly, biosorption efficiency is heavily dependent on the contribution of these interfering species present in the tested solution as they may hinder the sorption of the target pollutant of interest. The attenuation of the biosorption process with increasing in the ionic strength content may be attributed to the restraining phenomenon between electrolytes (Na^+/Cl^-) and the sorbate species. Wierzba and Kłos observed a considerable reduction in the sorption efficiency of BSG for copper metal ion in the presence of other cations in the examined solution. The existence of sodium cations with concentrations of 15 $mmol.L^{-1}$ declined copper sorption by nearly 60%,

whereas the presence of calcium and manganese cations with concentrations of 7.5 mmol.L^{-1}, decreased it by nearly 80% [371]. For example, the existence of NaCl salt in the tested aqueous phase may have shielded the electrostatic interaction between the biosorbent surface and sorbate molecules because of the salting-out effect. The hydratability of the examined pollutants can be influenced as a result of other ions presence and finally, affecting the whole biosorption process [372].

Reusability

In practice, in addition to the excellent biosorption capacity characterized to the biosorbent, other aspects such as stability and recyclability are of great significance for the as-used biosorbent from the economic perspective. The renewability of exhausted biosorbent is considered as a true criterion for judging the reusability, as well as biosorbent quality and hence, assessing its potential to eliminate target pollutants from wastewater. A desirable desorption process is not limited to reduce the overall cost of the process, but it extends to include recovery of pollutants (i.e. metals) extracted from aqueous solutions by effective methods such as electrolysis process. The extracted pollutants can be exploited as a feedstock in other industrial sectors. Reusability of chitosan/MWCNT's-COOH composite to desorb chromium (VI) was successfully investigated by using 0.10 M NaOH. It is evident that the sorption behavior of the composite remained essentially unchanged up to the 4th cycle (~98–100%), although its sorption capacity slightly declined to ~91% on the 5th cycle [373]. Feasibility of recovery process depends mainly on biosorbent type, biosorption mechanism and desorbing agent. Selection of suitable eluent is critical for maintaining the biosorbent quality and hence, achieving the desired degree of reusability. It is preferable for desorbing agents to be available, low cost, effective and harmless.

Real application (actual wastewater)

Additional pieces of evidence for judging the beneficial suitability and validity of the biosorbent can be potentially confirmed by evaluating its sorptive evacuation towards the examined pollutants in real spiked wastewater matrices. The outcomes derived from the biosorbent implementation may show its superiority and environmental adaptability for wastewater treatment.

3.2.4 Biosorption calculations

Usually, Biosorption outlined data collected from the mono-pollutant system are subjected to appraise the biosorption kinetics, isotherms and thermodynamics. The biosorbed amount of pollutant (q_{eq}) and the percentage of removal ($R\,\%$) can be determined, respectively, by the decline in concentration after equilibrating time using the given equations:

$$q_{eq} = \frac{(C_o - C_e)\,V}{m} \qquad (1)$$

Where, q_{eq} is the sorption capacity of biosorbent; C_0 and C_e refer to the initial and equilibrium pollutant concentrations, respectively. V is the equilibrium solution volume in litres and m is the biosorbent dry mass in grams.

$$\text{Removal}\ (\%) = \frac{(C_o - C_e)}{C_o} \times 100 \qquad (2)$$

Where, $R\%$ is the percentage of removal; C_0 and C_e indicate the initial and equilibrium pollutant concentrations.

Influence of contact time parameter on the biosorption process can be investigated by determining the sorbed amount of pollutant per unit mass of the biosorbent (q_t) as a function of time t, which can be investigated from the following equation:

$$q(t) = \sum_{i=1}^{n} \frac{(C(t)_{(i-1)} - C(t)_{(i)}) \times V(t)_{(i-1)}}{m} \qquad (3)$$

where C(t)(i) is the concentration of the pollutant withdrawn sample number i at time t and $C_{(t)(0)}$ = C_0, $V_{(t)(i)}$ (mL) is the volume of the solution in the flask at sample number i and time t, and m is the mass of the biosorbent in the flask. Here $V_{(t)(i)}$-$V(t)_{(i-1)}$ equals (the sample volume).

Reusability of biosorbent can be investigated by using the following equation:

$$RE\% = \frac{Amount\ sorbed\ pollutant\ at\ run\ (N+1)}{Amount\ sorbed\ pollutantat\ run(1)} \times 100 \qquad (4)$$

Where N is the reusability cycle number.

3.2.5 Modeling of Isotherm studies

Sorption isotherm consideration provides the graphical representation of the biosorbent-sorbate relationship in terms of the amount of sorbate biosorbed by the as-used biosorbent (unit weight), and the remaining sorbate amount in an aqueous solution at equilibrium conditions under constant temperature. It provides information related to adsorbable sorbate distribution between solid and liquid phases at variable equilibrium (final) concentrations. Widely, they portray the nature of sorption form (monolayer or multilayer), nature of biosorbent (homogenous or heterogeneous) and allow the distinguishing between physisorption and chemisorption [374]. Derived data obtained from equilibrium distribution of sorbate between the biosorbent and sorbate are specific and separate characteristics for each system. An assessment of suitable isotherm model is crucial to be carried out for every application. Numerous equilibrium isotherm models including Langmuir, Freundlich, Temkin, Dubinin-Radushkevich, Fowler- Guggenheim, Flory-Huggins, Jovanovic, Halsey, Harkin–Jura, Frumkin and others have been put together by taking into consideration three fundamental approaches including kinetic consideration, thermodynamics and potential theory. Figure 5 represents the availability of various models on the basis of parameter number whether two, three, four and five parameters. These isotherm models are continuously subjected to

investigation of wastewater pollutants removal by various biosorbents. Table 4 shows linearized and non-linearized forms of commonly used isotherm models [339].

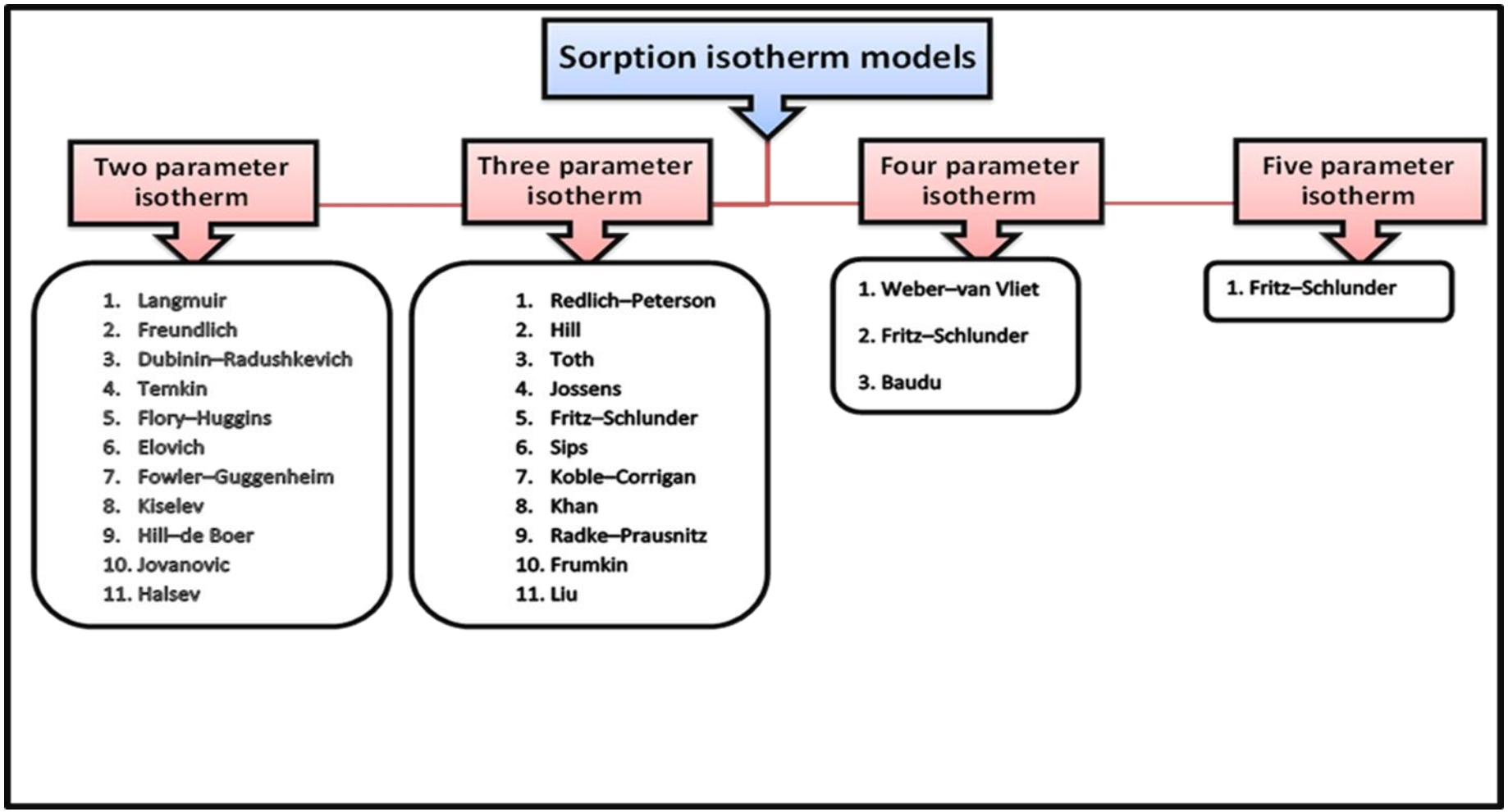

Figure 5: Different isotherm models based on the number of parameters used.

Table 4: Linearized and non-Linearized forms of different isotherm models.

Isotherm	Non-Linear form	Linear form	Plot
Langmuir	$q_e = \frac{q_{m,L}\ K_L\ C_e}{1 + K_L\ C_e}$	$\frac{C_e}{q_e} = \frac{C_e}{q_{m,L}} + \frac{1}{K_L\ q_{m,L}}$	$\frac{C_e}{q_e}$ *vs.* C_e
Freundlich	$q_e = K_F\ C_e^{1/n}$	$\ln q_e = \ln K_f + \frac{1}{n} \ln C_e$	$\ln q_e$ *vs.* $\ln C_e$
Dubinin–Radushkevich	$q_e = Q_{DR} e^{-K_{DR}\varepsilon^2}$	$\ln q_q = \ln Q_{DR} - K_{DR}\varepsilon^2$	$\ln q_e$ *vs.* ε^2
Temkin	$q_e = \frac{RT}{b_T}[\ln(A_T C_e)]$	$q_e = (\frac{RT}{b_T})\ln A_T + (\frac{RT}{b_T})\ln C_e$	q_e vs. $\ln C_e$
Flory - Huggins	$\frac{\theta}{C_0} = K_{FH} - (1-\theta)^{n_{FH}}$	$\log\ (\frac{\theta}{C_0}) = \log\ K_{FH} - n_{FH} \log(1-\theta)$	$\log \frac{\theta}{C_0}$ *vs* $\log\ (1-\theta)$
Hill	$q_e = \frac{q^s H C_e^n H}{K_D + C_e^n H}$	$\log\left(\frac{q_e}{q^s H - q_e}\right) = nH \log(C_e) - \log K_D$	$\log\ (\frac{q_e}{q^s H - q_e})$ *vs* $\log(C_e$
Redlich - Peterson	$q_e = \frac{K_R C_e}{1 + a_R C_e^g}$	$\ln(K_R \frac{C_e}{Q_e} - 1) = g \ln(C_e) + \ln(a_g)$	$\ln\left(K_R \frac{C_e}{Q_e} - 1\right)$ *vs* $\ln(C_e)$
Sips	$q_e = \frac{K_S C_e^{\beta s}}{1 + a_S C_e^{\beta S}}$	$\beta_S \ln C_e = -\ln\left(\frac{K_S}{q_e}\right) + \ln(a_s)$	$\ln\left(\frac{K_S}{q_e}\right)$ *vs* $\ln(C_e)$
Toth	$q_e = \frac{K_T C_e}{(a_T + C_e)^{1/t}}$	$\ln(\frac{q_e}{K_T}) = \ln(C_e) - \frac{1}{t}\ln(a_r + C_e)$	$\ln\ (\frac{q_e}{K_T})$ *vs* $\ln(C_e)$

Koble Corrigan	-	$q_e = \frac{A\,C_e^n}{1 + BC_e^n}$		$\frac{1}{q_e} = \frac{1}{AC_e^n} + \frac{B}{A}$	-
Khan		$q_e = \frac{q_s b_k C_e}{(1 + b_k C_e) a_k}$	-		-
Radke Prausnitz	-	$q_e = \frac{a_{RP}\, r_e\, C_e^{\beta R}}{a_{RP} + r_R C_e^{\beta R - 1}}$	-		-
Frenkel Halsey - Hill	–	$\ln\left(\frac{C_e}{C_s}\right) = -\frac{\alpha}{RT}\left(\frac{q_s}{q_e\, d}\right)^r$	-		-
MacMilla Teller	-	$q_e = q_s \left(\frac{k}{\ln\left(C_s/C_e\right)}\right)^{1/3}$	-		-

C_0 sorbate initial concentration ($mg.L^{-1}$), Ce the equilibrium concentration ($mg.L^{-1}$), q_e the amount of sorbate sorbed in the absorbent at equilibrium ($mg.g^{-1}$), $q_{m,L}$ the capacity of maximum monolayer ($mg.g^{-1}$), K_L Langmuir isotherm constant ($dm^3.mg^{-1}$), K_F Freundlich isotherm constant ($mg.g^{-1}$), n adsorption intensity, R universal gas constant (8.314 $J.mol^{-1}.K^{-1}$), T temperature (K), A_T Temkin isotherm equilibrium binding constant ($L.g^{-1}$), b_T Temkin isotherm constant, ε Dubinin–Radushkevich isotherm constant, q_s theoretical isotherm saturation capacity ($mg.g^{-1}$), β Dubinin–Radushkevich isotherm constant ($mol^2.kJ^{-2}$), θ degree of surface coverage, K_{FH} Flory–Huggins isotherm equilibrium constant ($L.g^{-1}$), n_{FH} Flory–Huggins isotherm model exponent, K_D Hill constant, n_H Hill cooperativity coefficient of the binding interaction, q_{sH} Hill isotherm maximum uptake saturation ($mg.L^{-1}$), K_R Redlich–Peterson isotherm constant ($L.g^{-1}$), a_R Redlich– Peterson isotherm constant ($1.mg^{-1}$), g Redlich–Peterson isotherm exponent, Sips isotherm model constant ($L.mg^{-1}$), β_S Sips isotherm model exponent, K_S Slips isotherm model constant ($L.g^{-1}$), K_T Toth isotherm constant ($mg.g^{-1}$), B Koble–Corrigan isotherm constant $(L.mg^{-1})^n$, A Koble–Corrigan isotherm constant ($L^n\ mg^{1-n}.g^{-1}$), b_k Khan isotherm model constant, α_k Khan isotherm model exponent, α_{RP} Radke–Prausnitz isotherm model constant, βR Radke–Prausnitz isotherm model exponent, γR Radke–Prausnitz isotherm model constant, α Frenkel–Halsey–Hill isotherm constant ($Jmr.mole^{-1}$), r sign of inverse power of distance from the surface, d Interlayer spacing (m), k MacMillan–Teller (MET) isotherm constant.

3.2.6 Modelling of Kinetic studies

During the solid-liquid phase extraction process, kinetic interpretation is vital because it is useful to define equilibrium time, reaction order, reaction pathway and therefore determining the mechanism and the rate-controlling step of pollutant capturing from the solution onto the biosorbent. Theoretically, in any solid-liquid sorption based water treatment system, the process can be categorized into three consecutive steps including 1) the external mass transfer of sorbate from bulk solution to biosorbent surface, 2) inward diffusion stage and 3) bisorption onto biosorbent surface binding sites [375]. Once biosorbent comes in contact with sorbate solution, migration of sorbate (molecules and/or ions) from the bulk solution to the boundary layer around biosorbent particle occurs. Once, surpassing the external mass – transfer resistance (boundary layer surrounding biosorbent surface), the sorbate concentration decreases in the bulk solution due to the sorbate (molecules and/or ions) diffusion onto the internal surface of the biosorbent. Finally, the intense interaction between sorbate and biosorbent active sites takes place [376].

Kinetics studies provide insight with outcome data necessary for modelling and designing an efficient biosorption operation system. Commonly, the time-dependent biosorption data are evaluated by several kinetic models such as pseudo-first-order rate equation (PFORE) [377], pseudo-second-order rate equation (PSORE) [378], Weber and Morris model (W&M) [379], Boyd model [380] (Okewale et al., 2013), Bingham's model [381] and Elovich model [382] (Zeldowitsch, 1934). Usually, Linearized forms of different aforementioned models are used for explaining the sorption process, which is shown in table 5.

Table 5: Linearized forms of different kinetic models.

Kinetic model	**Linear form**	**Plot**
Pseudo-First order	$\log (q_e - q_t) = \log q_e - (\frac{k_1}{2.303}) t$	$\log (q_e - q_t)$ *vs.* t
Pseudo-Second order	$\frac{t}{q_t} = \frac{1}{k_2 q_e^2} + (\frac{1}{q_e}) t$	(t/q_t) *vs.* t
Intraparticle diffusion	$q_t = k_i t^{0.5} + X$	q_t *vs.* $t^{0.5}$
Elovich equation	$q_t = \frac{1}{\beta} \ln \alpha\beta + \frac{1}{\beta} \ln t$	q_t *vs.* lnt
Boyd model	$B_t = -0.4977 - \ln(1 - \frac{q_t}{q_0})$	B_t vs. t
Bingham's model	$\log(\log \frac{C_t}{C_0} - q_t m) = \log K_0 + q_t \log t$	$\log(\frac{C_t}{C_0} - q_t m)$ *vs.* log t

The goodness of model fitting

The goodness of fit of the used mathematical models to the experimental data can be determined by using various statistical functions errors as presented in Table 6. The following equations are normally applied to estimate the difference between the predicted and experimental data. The smaller values of SSE, X^2 and CFEF, ARE, MPSD and HYBRID, the more similar the experimental data is to the calculated one.

Table 6: Statistical functions used to investigate error deviation between experimental and calculated values.

Functions	Equation
An error analysis of sum of squared errors of prediction (SSE)	$SSE = \sum_{n=1}^{n} (q_{cal} - q_{exp})^2$
Chi-square statistic (X^2)	$X^2 = \sum_{n=1}^{n} \left[\frac{(q_{e,exp} - q_{e,cal})^2}{q_{e,cal}} \right]$
The composite fraction error function (CFEF)	$CFEF = \sum_{n=1}^{n} \left[\frac{(q_{e,exp} - q_{e,cal})^2}{q_{e,exp}} \right]$
Average relative error (ARE)	$ARE = \frac{1}{n} \sum \left(\frac{q_{e,cal} - q_{e,exp}}{q_{,exp}} \right) 100$
Marquardt's percentage standard deviation (MPSD)	$MPSD = \sqrt{\frac{\sum (\frac{q_{e,exp} - q_{e,cal}}{q_{e,exp}})^2}{n - P}}$
Hybrid fractional error function (HYBRID)	$HYBRID = \frac{1}{n-p} \sum \left(\frac{q_{e,exp} - q_{e,cal}}{q_{e,exp}} \right) 100$

Where, $q_{e,exp}$ and $q_{e,cal}$ are the experimental and model calculated (predicted) sorption capacity values, respectively. *n* is the experimental samples number. P is the number of the parameters in each isotherm model.

3.2.7 Thermodynamic studies

Detailed insights of any pollutants biosorption process, including nature, whether it is exothermic or endothermic, spontaneity and feasibility can be accurately simulated by taking into consideration the calculated thermodynamic parameters values. Valuable information in term of Gibb's free energy change (ΔG^o), enthalpy change (ΔH^o) and entropy change (ΔS^o) can be estimated at different temperatures using the following equations:

$$K_c = \frac{C_S}{C_e} \quad (5)$$

C_s and C_e refer to the equilibrium concentrations of pollutant on the biosorbent surface and in aqueous solution, respectively, while the ratio of sorbate concentration on solid biosorbent to the dissolved in liquid aqueous solution is expressed by equilibrium constant, K_c. Classic Van't Hoff reaction isotherm equation correlates between free energy change (ΔG), standard free energy change (ΔG^o) and equilibrium constant (K_c) at constant temperature (T) as:

$$\Delta G = \Delta G^o + RT\ln K_c \quad (6)$$

At equilibrium, free energy change (ΔG) is zero; hence the Eq. 6 reduces as:

$$\Delta G^o = - RT\ln K_c \quad (7)$$

Commonly, it is the most used equation in sorption thermodynamics to investigate the sorption process feasibility. To estimate standard entropy change (ΔS^o) and standard enthalpy change (ΔH^o), Eq. 7 is rearranged in the form of equilibrium constant (Kc) as:

$$\ln K_c = \frac{\Delta G^\circ}{- RT} \quad (8)$$

Standard free energy change (ΔG^o) refers to standard entropy change (ΔS^o) and enthalpy change (ΔH^o) at constant temperature by the equation:

$$\Delta G^o = \Delta H^o - T\Delta S^o \quad (9)$$

Therefore, the van't Hoff equation becomes as:

$$\ln K_C = \frac{-\Delta H^\circ}{RT} + \frac{\Delta S^\circ}{R} \quad (10)$$

The main findings of ΔG^o, ΔS^o, ΔH^o and $T\Delta S^o$ for sorbate sorption on biosorbent surface are investigated by plotting ln K_c versus 1/T. If the predicted ΔH^o and ΔS^o exhibit positive magnitudes values, this seriously refers to endothermic nature of bisorption process in addition to an enhancement in randomness degree between solid-solution interfaces during bisorption process pattern and vice versa [383]. ΔG^o consideration value is a helpful tool to expect the biosorption process type. Considering its value, If it is located in the range -20 - 0 KJ.mol^{-1}, this indicates physisorption, while in the range -400 - 80 KJ.mol^{-1} indicates chemisorption [384].

3.2.7.1 Fixed bed experiments scenario

Most of the considerable progress and research regarding sorption processes can be performed through lab-scale with batch mode or fixed bed mode. All the equilibrium data derived from batch mode do not directly agree with wastewater treatment plants, where most ion exchange and adsorption processes operate through fixed bed columns [385, 386]. Fixed bed scale can provide more useful insights about sorption equilibrium and dynamics necessary for predicting column behaviour in large scale operations [387]. Fixed bed column efficiency is usually appraised through two important concepts, which are breakthrough and exhaustion points calculated from exit concentration versus time. Determination of mentioned points is required for providing the fundamental data necessary for successful design of a continuous adsorption system. A breakthrough occurred when concentration of effluent typically reaches about 5% of influent concentration, while bed exhaustion occurs when effluent concentration typically reaches 95% of influent concentration. Complete (total) exhaustion occurs when the concentration of effluent equals the concentration of influent [388]. Breakthrough time, curve shape, exhaustion time and

ion exchange properties strongly depend on variable operational parameters such as bed height, flow rate, influent concentration and chemical composition of biosorbent. Many important definitions are derived from mathematical calculations of fixed-bed column performance like Empty bed contact time (EBCT), Number of bed volume (NBV), Mass transfer zone (MTZ) and biosorbent exhaustion rate (AER) [389].

Empty bed contact time (EBCT) is defined as a measurement of the interaction between sorbate and biosorbent and expressed as:

$$EBCT = \frac{Z \times S}{Q} \tag{11}$$

Where, *Z* relates to the bed depth, *S* represents the cross-sectional area of the adsorption bed and *Q* indicates the flow rate.

Mass transfer zone (MTZ) represents the hydraulic loading rate and described as the fixed bed length, where sorption of sorbate takes place and it is calculated as:

$$MTZ = Z \times \left(1 - \frac{t_b}{t_e}\right) \tag{12}$$

Where *Z* is the length of the column, t_b and t_e are breakthrough and exhaustion times, respectively. The number of bed volume (NBV) is defined as the ratio of volume of water treated until breakthrough point to the packed bed volume. It can be expressed as:

$$NBV = \frac{Volume\ of\ water\ treated\ till\ break\ through\ point}{Volume\ of\ the\ biosorbent\ bed} \tag{13}$$

Better and efficient sorption can be monitored and determined by a lower value of biosorbent exhaustion rate (AER) which is denoted as:

$$AER = \frac{Mass\ of\ biosorbent}{Volume\ of\ water\ treated\ tillexhaustion\ point} \tag{14}$$

Fixed bed mode (dynamic) studies

Design of continuous fixed-bed column can be employed at lab-scale through design of a plastic column with known diameter and height as shown in Figure 6. Biosorbent particles were packed into the column between upper and lower supporting layers (i.e. glass wool) to prevent biosorbent particles outflow. Various operational parameters including effect of different bed height and influent, (flow rate and initial concentration) are crucial to be investigated. In the mentioned process scenario, each pollutant (molecule/ion) is rapidly sorbed on the biosorbent due to great availability of numerous vacant sorption sites. Consequently, the target pollutant is eliminated by the as-used biosorbent; meanwhile the discharged effluent from the bed bottom is free of sorbate. As the pollutant solution continues to flow through the bed column, the uptake becomes less effective, because of the gradual occupation of the free available sorption sites and accordingly, the effluent outlet concentration starts to increase until it reaches to the saturation state.

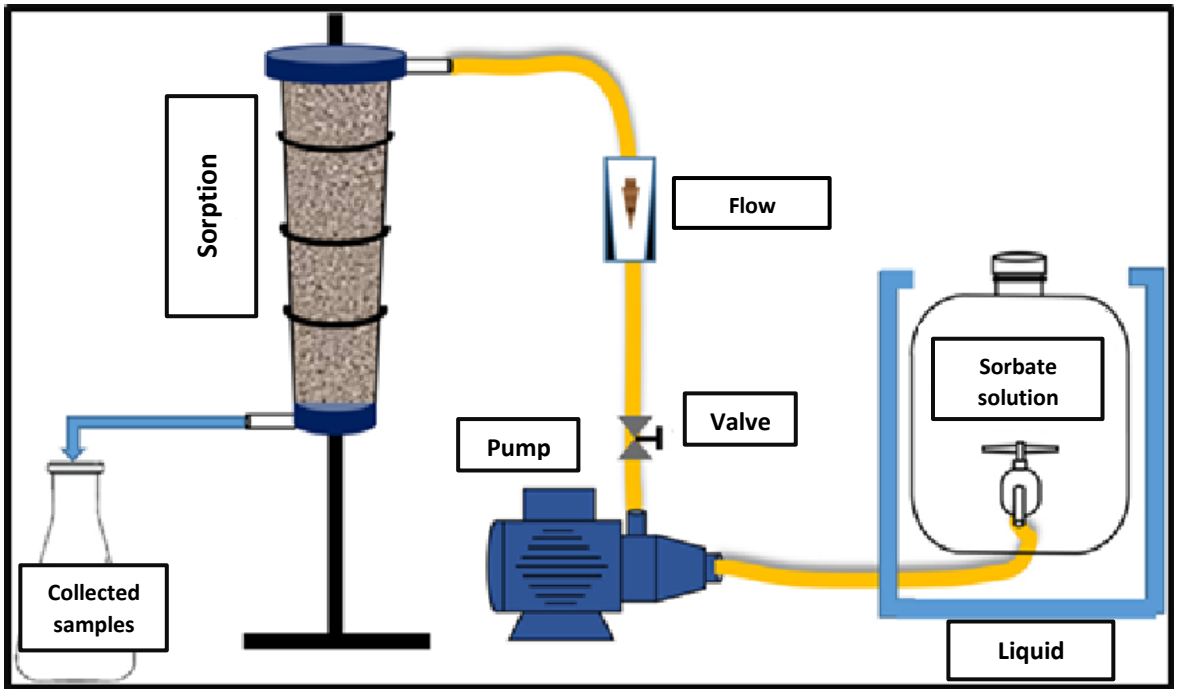

Figure 6: Schematic diagram of dynamic (continuous) fixed-bed column system[390].

Influence of environmental conditions

Influence of bed height (depth)

One of the important parameters in the fixed bed operation process is the working bed height (depth), in terms of the solid amount used of the prepared biosorbent packed in the column. To investigate the influence of bed height on sorption processes, different bed heights are chosen with a constant flow rate and fixed pollutant concentration. Taking into consideration the pressure drop through the column and the handling problems, selection of the suitable biosorbent particle size is necessary. Generally, the removal capacity of the column enhances by an enhancement in the bed height. This is since more present biosorbent particles, in case of higher bed provide larger surface area and hence, more vacant binding sites will be available for attachment with pollutant (molecules and/or ions). Broadening in the mass transfer zone (MTZ) as well as the later breakthrough time and exhaustion time with an enhancement in the column height can be observed because the pollutant (molecules and/or ions) have enough time to diffuse deeper into the biosorbent pores and sorbed onto the biosorbent active sites. The influence of increasing the bed height on the breakthrough curve related to sorption of thallium (TI^{+3}) ion using rice husk was evaluated. The results illustrated that with an increase in the bed height (from 1 to 7 cm), better efficiency of TI^{+3} removal is achieved. Specifically, an enhancement in the bed height from 1 to 7 cm raises the breakthrough and saturation points from 5 and 100 min to 52 and 700 min, respectively [390].

Influence of flow rate (fluid superficial velocity)

To evaluate the influence of flow rate on water pollutant removal in the adsorption column, different flow rates were pumped into constant bed height and a fixed pollutant concentration. Basically, when the sorption system is controlled at a lower flow rate, the sorbate (molecules and/or ions) have more time (residence time) to contact with biosorbent active sites, resulting in greater sorption efficiency towards the examined sorbate from their aqueous solutions. While the reduction of sorption efficiency at greater flow rate is probably due to short retention time for sorbate to interact with biosorbent during sorbent-sorbate interface as well as the sorbate limited diffusivity into the pores or sorptive sites of biosorbent. The decline in residence time at greater flow rates leads to fast leave of sorbate before complete equilibrium occurs. In addition to that, decline in the surface film thickness, which is considered as resistance for mass transfer zone, increase the mentioned zone. Under enhanced flow rate, marginal enhancement in MTZ associated with faster breakthrough time and exhaustion time can be noticed due to the higher sorbate loading rate onto the biosorbent and fast movement of the primary sorption zone under the mentioned operating conditions. It is widely known the favorability of sorption process to be performed at slower flow rates by the intraparticle mass transfer control. Effect of different flow rates on the breakthrough curve in term of Al^{+3} sorption using by non-living *P. putida* was appraised. Higher breakthrough time and exhausting time were obtained at lower flow rates. At 0.5 $mL.min^{-1}$ t_b and t_e were 60 and 153 min, respectively, whereas these times were 35 and 134 min when the flow rate was 1 $mL.min^{-1}$ [391].

Influence of influent concentration

Analyzing the influence of initial pollutant concentration is an important operational factor greatly affecting the sorption process performance and is very necessary. To evaluate the effectiveness of initial metal concentration on the column performance, different initial pollutant concentrations are used with keeping the other factors of flow rate equal and bed height constant. Sorption capacity increases with an enhancement in the concentration of influent, because the biosorbent sorption sites become saturated more quickly as a result of higher concentration gradient between sorbate and specific biosorbent active sites. The (MTZ) becomes smaller because of the higher pollutant loading rate. Increase in influent concentration results in accelerated breakthrough time and exhaustion because of the fast bed saturation. Influence of variable feed concentrations on the breakthrough curve through the Cr(III) sorption process using MPB sorbent was analyzed. Results showed that both t_b and t_e had lower values when higher feed concentrations are introduced. A reduction of 62.1% of stoichiometric time (t_{st}) was observed when C_E was tripled [385].

Influence of particle size

Normally, the decrement in the biosorbent particle size results in an enhancement in the time required for reaching the breakpoint, which is attributed to the greater surface area with higher vacant binding sites and is associated with a decline in the particle size of biosorbent, and this leads to an enhancement in saturation time. Contrarily, the larger particle size, the higher thickness characterized to the stagnant film surrounding the biosorbent, as well as a higher total path length inside the biosorbent pores. Under the mentioned operation circumstances, the overall kinetics of the biosorption process decreases due to the larger diffusion path along the pores leads to longer timer for sorbate molecules to reach the sorption sites. A rapid increase in the breakthrough values was observed with an enhancement in particle size from $0.25<x<0.5$ to $1<x<2$ mm [392].

Analysis of column data

The breakthrough curve gives insights about the fixed bed column performance by plotting (C_t/C_0) on the Y-axis against time (min) on the X-axis. Generally, the breakthrough curve shape is controlled by the equilibrium isotherm shape [393]. The total amount of adsorbed pollutant (molecules and/or ions) through a fixed-bed column can be estimated through the given equation:

$$q_{total=\frac{Q}{1000}} \int_{0}^{t_{total}} c_{ad}\, d_t \qquad (15)$$

Where Q indicates the flow rate ($mL.min^{-1}$), t_{total} relates to total is the total flow time (min) and C_{ad} = C_0-C_t, C_0 and C are the concentrations of influent and effluent, respectively.

The biosorption capacity of the column represents the amount of pollutant (molecules and/or ions) sorbed per unit dry weight of biosorbent (g) can be investigated through the given equation:

$$q_{eq=\frac{q_{total}}{M}} \qquad (16)$$

Where *M* (g) refers to the total dry weight of biosorbent in the column.

Also, the total volume treated through the column V_e (mL) is calculated by the following equation:

$$V_{e=Q\times t_{total}} \qquad (17)$$

The total removal efficiency (TR%) of biosorbent toward pollutant can be expressed through the following equation

$$TR(\%) = \frac{q_{total}}{m_{total}}\times 100 \qquad (18)$$

Where m $_{total}$ (mg) relates to the total amount of sorbate passed through the bed which can be derived by using the given expression:

$$m_{total} = \frac{C_0 \times V_e}{1000} \quad (19)$$

3.2.8 Mathematical dynamic models

Numerous kinetic models are usually applied to portray the dynamic process of a sorption system. An accurate evaluation of pollutant concentration as a function of time profile, in terms of effluent breakthrough curve, is necessary for optimized successful design on the sorption column. Three of the most used kinetic models are utilized to clarify the obtained outcome data. Their general expression and linearized forms are shown in Table 7:

Table 7: Mathematical dynamic models of fixed bed (continuous) sorption system.

Kinetic model	General expression	Linear form	Plot
Thomas model	$\frac{C}{C_0} = \frac{1}{1 + \exp(\frac{K_{Th} q_e m}{Q} - K_{Th} C_0 t)}$	$\ln[\left(\frac{C_0}{C}\right) - 1] = \frac{K_{Th} q_e\, m}{Q} - K_{Th} C_0 t$	C/C_0 vs. t
Yoon-Nekson model	$\frac{C}{C_0 - C} = \exp(K_Y t - K_Y \tau_Y)$	$\ln\left[\left(\frac{C_0}{C}\right) - 1\right] = K_Y \tau_Y - K_Y t$	ln $((C_0/C)-1)$ vs. t
Bed-depth/service time analysis (BDST) model	$\frac{C}{C_0} = \frac{\exp(K_\alpha C_0 t)}{\exp(K_\alpha C_0 t) + \exp\left(\frac{K_\alpha N_0 HA}{Q}\right) - 1}$	$\ln\left[\left(\frac{C_0}{C}\right) - 1\right] = \ln[\exp\left(\frac{K_\alpha N_0 HA}{Q}\right) - 1] - K_\alpha C_0 t$	ln $((C_0/C)-1)$ vs. t

q_e the column sorption capacity, K_{Th} kinetic coefficient, C_0 and C are the influent and effluent concentration of sorbate, K_Y kinetic rate constant, τ_Y the time required for 50% sorbate breakthrough, N_0 sorption capacity, K_α rate constant.

3.2.9 Modification (activation) of biosorbents

Several parameters including particle size, surface area, pore size and pore volume influence functional groups existence on manipulation abilities of different biosorbents. Utilization of native biosorbents may have some drawbacks, including low sorption capacities in addition to relatively small particle size, low density, low surface area, weak mechanical strength and less rigidity. Consequently, many operational disturbances can be generated during scaling up of biosorption processes in term of columns (fixed bed) strategy including biosorbent swelling, difficult separation between biosorbent (solid) and sorbate (liquid), column clogging and poor reusability. In order to minimize or overcome these disadvantages, most of the biosorbents need to undergo some modifications (in the form of a pretreatment step) to improve their physicochemical attributes, and consequently, enhance their affinities toward different pollutants from aqueous solutions. In general, different expected desirable aspects are obtained as a result of adequate choice of pretreatment procedures, such as removal of impurities from the surface of native biosorbents, activating biosorption sites, introducing more binding sites and removing interfering sorption sites. Modification techniques can be classified into main broad categories including immobilization, magnetic, chemical, physical, biological, and combining with other minerals.

Immobilization technology is considered as a paramount methodology for biosorption scale up to industrial scale. Usually, it is performed to overcome some limitations associated with utilization of biosorbent free particulate (powder form) in continuous systems (fixed-bed column) such as low particle size, poor mechanical strength, strong densification and weak distribution in the bed [394, 395]. These shortcomings cause problems during column operation including decline of the process efficiency, poor regeneration (reusability) and difficulties in separation process after biosorption process. The free *Sargassum sp*. achieved an uptake of 1.23 mmol of Ni^{2+} g^{-1} and 1.51

mmol of Cu^{2+} g^{-1}, whereas the immobilized biosorbent reached a removal of 1.69 mmol of Ni^{2+} g^{-1} and 2.06 mmol of Cu^{2+} g^{-1}[394, 395]. The pretreatment step is done by adhering (mixing) biosorbent to the external surfaces of polymeric matrices of natural biopolymers like alginate, chitin, chitosan and cellulose derivatives [396]. These supporting materials act as biological carriers which can enhance the economic feasibility of the biosorbent, through improving its structural features including particle size, mechanical strength, porosity, density and enhancing its ability for repeated (continuous) utilization through allowing it to undergo with numerous sorption-desorption cycles without any performance loss. Fortunately, these mentioned benefits will increase the biosorbent capacity and hence, support its suitability to be used in columns and reactors. Ding et al. [397] reported that AAMs sorbent possesses a rapid and superior sorption capacity towards thorium Th(IV) ions reached to 303.95 $mg.g^{-1}$ n less than 100 min.

Magnetic modification (magnetization) represents a viable and promising approach to overcome the drawbacks related to the application of conventional separation techniques (i.e. centrifugation, sedimentation and filtration) for biosorbent loaded pollutants at the end of biosorption; in particular for large industrial scale elimination of different pollutants [398]. The mentioned methods are considerably cumbersome, time-consuming, difficult to handle and non-cost effective, especially when dealing with a large volume of wastewater effluents. During their application, the possible loss or filters blockage by the biosorbents particles can occur. In addition, presence of residual biosorbents particles may implicate in secondary water pollution. In the recent years, magnetic solid-phase extraction (MSPE) has been increasingly employed as an effective methodology for preconcentration as well as fast separation of different contaminants (i.e. inorganic, organic and radionuclides) species from aqueous matrices [399]. It is based on introducing Ferro-, Ferri- or superparamagnetic materials to biosorbents, to improve their separation/ recovery. Ostensibly, the

constructed magnetized biosorbents are potentially, more efficient and easily separated from the treated matrix by using an external magnetic field. Their utilization leads to discharge of a huge amount of purified effluents in a short time with less energy consumption as well as no extra pollutants. Various magnetically modified biosorbents have been designed using numerous modification procedures and subsequently, applied as strong candidates for different pollutants removal [400, 401]. MPC-50 sorbent has high affinities to eliminate different types of dyes from their aqueous solutions. Its sorption capacities reached to 175.66, 109.11, 227.05, 196.21, 287.62 and 247.23 $mg.g^{-1}$ for MB, MO, TB, CV, SO and MG dyes, respectively [402]. They are characterized by several characteristics such as low cost, low toxicity, ease of synthesis, superparamagnetism features, high magnetic stability, ease of fast isolation from solution and reusability for multiple biosorption cycles.

Usually, natural biosorbents in their native (non-activate) form exhibit poor mechanical properties, weak physical stability, in addition to low exchange and non-selective biosorption capacities. Therefore, the chemical functionalization process is considered as a reliable protocol, that can greatly improve the biosorbent performance through increasing surface area, developing new pores, introducing more binding sites well as prohibiting the elution of biosorbents native (original) compounds to the treated solution through different aspects [403]. Grafting of new binding groups on the biosorbent surface in terms of amination, carboxylation, phosphorylation, sulfonation, xanthanation, oxidation, halogenation and thiolation. Successful modification for *Cystoseira indica* brown algae in term of sulfur functionalization based on xanthation strategy was performed. The chemically modified algae had high sorption capacities reached 168.06 and 179.43 $mg.g^{-1}$ for Ce(III) and La(III), respectively [404]. The as-prepared Pb–ITMCB sorbent was successfully introduced to adsorb Pb(II) with maximum sorption capacity reached to 259.68 $mg.g^{-}$

^{1} at pH 6 and 40 °C [405]. The synthesis of FMH sorbent using 0.2% formaldehyde solution was achieved and the produced sorbent had sorption capacities reached to 15.22 and 19.83 $mg.g^{-1}$for Mn^{2+} and Fe^{3+}, respectively. These values are high compared with the sorption capacities of other modified biosorbents (i.e. Black carrot residues (acetic acid-ethanol modified) had 3.87 $mg.g^{-1}$for Mn^{2+}/ Chitin (HCl and NaOH modified) had 1.37 $mg.g^{-1}$ for Fe^{3+} [406]. 1-methyl-3-decahexyl imidazolium ionic liquid (IL) was utilized to modify peanut shell (NS) and activated carbon (AC), to produce IL modified peanut shell (ILNS) and IL modified AC (ILAC), respectively. Results showed that sorption capacities of ILNS for RB and CR dyes reached to 290.00 and 136.41 $mg.g^{-1}$ compared with the values characterized to the native sorbent (4.8 and 3.55 $mg.g^{-1}$ for RB and CR, respectively). Whereas, sorption capacities of ILAC for RB and CR dyes reached to 364.14 and 150.0 $mg.g^{-1}$ compared with the values characterized to the unmodified sorbent (65.58 and 29.27 $mg.g^{-1}$ for RB and CR, respectively) [407]. Novel and low-cost chemical modification strategy was introduced to masau stone by using NaOH, epichlorohydrin and diethylenetriamine (DETA) through different consecutive procedures. Sorption character of the obtained CMMS sorbent towards Orange II and Cr(VI), individually, simultaneously and consecutively was appraised. Maximum Orange II sorption capacity was calculated as 136.8 $mg.g^{-1}$ for the dye onto the Cr(VI)-loaded CMMS consecutive system at C_o = 100 $mg.dm^{-3}$, while the sorption capacity for the Cr(VI) system was found to be 87.32 $mg.g^{-1}$ at the same C_o max [408]. Activated carbon biosorbent prepared based on *Lantana camara* had higher sorption capacity towards tartrazine dye (90.90 $mg.g^{-1}$) compared with other sorbents (i.e. 2.47, 4.484 and 30 $mg.g^{-1}$ for Polyaniline nanolayer composite, commercial activated carbon and chitin, respectively) [409]. Fabricated biofilm of *Corynebacterium glutamicum* MTCC 2745 supported on granular activated carbon/$MnFe_2O_4$ composite (MGAC) was successfully tested to eliminate As(III) and As(V) with

maximum sorption capacities of 2584.668 mg.g^{-1} and 2651.675 mg.g^{-1}, respectively [410]. The as-prepared UiO-66 and activated carbon composite was impressively evaluated to eliminate Hg^{2+} and SeO_3^{2-} with maximum sorption capacities of 205 mg.g^{-1} and 168 mg.g^{-1}, respectively [411]**.** A friendly and inexpensive BCTD sorbent was fabricated by ultrasonic biochar and nanoscale TiO_2, can simultaneously tackle Cd(II) and As(V) from their aqueous solutions with maximum sorption capacities of 72.62 and 118.06 mg.g^{-1} for Cd and As, respectively [412].

A novel mesoporous biochar was facilely prepared from *Medulla tetrapanacis* and exhibited high efficiency for the sorption of Cu^{2+} (458.72 mg g^{-1}) and Pb^{2+} (1031.23 mg g^{-1}) metal ions [413]. The as-synthesized biochar had higher sorption capacities of 20.23 mg g^{-1}, 23.26 mg g^{-1}, 24.95 mg g^{-1}, 33.90 mg g^{-1} and 37.80 mg g^{-1} for Co(II), Zn(II), Cu(II), Cd(II) and Pb(II), respectively comparable with commercial active carbon [414]. A new tannin resin with carbon nanotubes and coconut fibers was developed and achieved a capacity of Pb(II) adsorption higher than 13.8 mg g^{-1} [415]. The as-designed CNFs-CNTs adsorption materials based on growing carbon nanotubes (CNTs) vertically and uniformly on the surface of carbon nanofibers (CNFs) via plasma-enhanced chemical vapor deposition showed remarkable adsorption capacity toward of 227 mg g^{-1} for Cr(VI) [416].

Contrarily, removing or eliminating of inhibiting groups from the biosorbent surface in terms of carboxyl groups elimination (decarboxylation), amine groups elimination (deamination). Graft polymerization can be performed with different scenarios. Simply, it can be carried out by putting an amount of biosorbent in contact with a definite volume of modifying agent solution followed by heating and stirring for a pre-determined time. The modified biosorbent samples are separated and rinsed with deionized water to remove the excess of modifiers solutions [417]. Numerous activation methods based on several modifying agents have been used in the biosorbent

modification. Commonly, it can be performed by using different modifiers solutions including; acidic solutions (i.e. hydrochloric, phosphoric, sulfuric, citric, nitric, etc.), alkali solutions (i.e. sodium hydroxide, calcium hydroxide), oxidizing agents (i.e. hydrogen peroxide), organic solvents (acetone, ethanol, methanol, epichlorohydrin, etc.) and organic acids (acetic acid, formic acid). Other modifying agents such as ethylenediaminetetraacetic acid (EDTA), pyromellitic dianhydride, sodium carbonate and sodium bicarbonate have been used for pretreatment purposes. Rice bran was introduced for different chemical modifications and tested for biosorption of Ni(II). Obtained results showed that maximum sorption capacities of NaRB, HARB, CaRB and SARB for Ni(II) was found to be 153.6, 149.4, 144.0 and 140.0 $mg.g^{-1}$, respectively [402].

Compared with chemical activation, physical activation can be considered as an environmentally friendly methodology to produce effective biosorbents for further utilization in wastewater treatment, because it doesn't involve the utilization of any harmful chemicals. In principle, the activation route can be applied only through one-step methodology instead of complex procedures (no additional steps) [418]. Generally, it is known as a process at which both carbonization, as well as activation, occurs, referring to the dry oxidation resulting from the reaction of precursor with an oxidizing gas (i.e. steam) in a temperature higher than 700 °C. The precursors can be physically activated by different ways such as H_2O steam or under CO_2 flow at an elevated temperature range (800-1000 °C), air activation and thermal activation (radiation, torrefaction, pyrolysis and gasification) [419]. This method is characterized by some unique properties including short activation time, no chemical reagents consumption, and no need of large amount of deionized water for rinsing stage at the end of activation step, compared with the chemical one. Different operational parameters such as heating methodology, heating rate, heating temperature and residence (activation) time can strongly influence the physicochemical features of the produced

modified biosorbents such as its porosity, surface area and surface chemistry. Trubetskaya et al. [420] reported that steam activation of biomass soot and tire carbon black leads to significantly higher filter efficiencies compared to untreated materials for the removal of phenol and chlorine - with filter efficiencies as high as 95% (both phenol and chlorine) for steam activated pinewood soot and tire carbon black compared to 81.6% (chlorine) and 73% (phenol) for the untreated material.

Despite the fact that the implementation of chemical or physical methods can improve the properties of the as-used biosorbents, the energy consumption in addition to reagents costs cannot be ignored. Recently, biological activation is forwarded as a promising strategy to develop effective biosorbents. In the pretreatment step, the biosorbent feedstocks undergo with aerobic/anaerobic digestion or bacterial conversion process [421]. Both aerobically and anaerobically digested biomasses have been known to be a good feedstock to produce biochars possessing numerous physicochemical characters qualifying them to be used as a low-cost sorbent. Previous studies reported that anaerobic digestion of sugar beet tailings and bagasse enhanced pH, CEC and surface area of the digested biochar and hence, increased its sorption capacity towards heavy metals. Biochar produced from anaerobically digested sugarcane bagasse (DBC) has been found to be effective lead sorbent compared with the raw bagasse (BC) as well as commercial activated carbon (AC). It was found that maximum sorption capacity of DBC towards lead was 653.9 $mmol.kg^{-1}$ which was about twenty times higher than that of BC (31.3 $mmol.kg^{-1}$) and double of AC (395.3 $mmol.kg^{-1}$) [422]. Digested whole sugar beet biochar (DWSBC) and digested dairy waste biochar (DAWC) showed good abilities to eliminate a mixture of heavy metals from aqueous phase. DWSBC sorbent had removal efficiency higher than 97% for Cu^{2+}, Cd^{2+}, Pb^{2+} and Ni^{2+}. Whereas DAWC sorbent had high removal efficiency of 99% for Pb^{2+} and 98% for Cu^{2+} and

relatively low removal efficiency of 57% for Cd^{2+} and 26% for Ni^{2+}. From the same study, the estimated Langmuir sorption capacity of DWSBC towards Pb^{2+} was around 197mmol.kg^{-1} which is comparable to that of other biochar sorbents (11-680 kg^{-1}) in addition to commercial activated carbon (101-395 mmol.kg^{-1}) [423]. Transabdominal transformation is described as a typical digestion process in animal stomach, characterized by full utilization of amino acid, protein, sugar and other nutrients in straw and effectively realize straw utilization. Other studies showed that transabdominal transformation-based corn straw silage (TCB) had a significantly higher surface area, oxygen-containing functional groups and development of mineral components in comparison with the pristine biochar prepared from corn straw (CB). Additionally, involvement of different mechanisms such as (precipitation, ion exchange, adsorption and complexation) was explained for the sorption behaviour of Cd using TCB. It was reported that maximum sorption capacity obtained from Langmuir model for TCB700 (175.44 mg.g^{-1}) was 3 times of CB700 (56.82 mg.g^{-1}) [424]. This greatly confirms the importance of biological modification in amending the physicochemical properties of the native biosorbents.

3.2.10 Recyclability of spent biosorbents

Basically, Nanomaterials based adsorbents can achieve the requirements of a green circular economy as it characterizes by admirable physicochemical characteristics such as large surface area, numerous surface active sites, high sorption efficiency, low cost, low toxicity and recyclability. From economic and environmental perspectives, reusability of saturated (spent) sorbent is of great concern because it is considered as a true criterion for judging the sorbent quality and its applicability for large industrial scales through consecutive sorption/desorption cycles. A successful operational desorption process is not limited to reduce the overall cost of as-used process, but it also paves the recovery of extracted heavy metals captured from examined aqueous

solutions (i.e. electrolysis process) and hence using them as feedstocks for various industrial sectors [373]. Fundamentally, an effective regeneration (recovery) process depends on sorbent type, sorption mechanism, and appropriate desorption scenario. For example, and not as a limitation, different strategies were implemented to regenerate magnetic iron oxide nanocomposites such as thermal treatment, chemical treatment, irradiation treatment (microwave, gamma) and ultrasonic treatment [425]. Other studies revealed the successful regeneration of numerous as-fabricated nanomaterials-based adsorbents loaded with different heavy metals. Desorption of loaded Hg(II) from the as-designed Chitosan-poly(maleic acid) nanomaterial (PMACS) sorbent was successfully investigated after five cycles of sorption-desorption of 100%, 95.8%, 91.7%, 87.5% and 83.3%, respectively, using 0.05 $mol.L^{-1}$ of EDTA solution [426]. Remarkable regeneration results for the carbonaceous nanofiber/Ni-Al layered double hydroxide (CNF/LDH) loaded with Cu(II) and Cr(VI) were reported using 1 M of Na_2CO_3 solution. The sorption capacity of as-synthesized sorbent decreased from 219.6 to 205.8 $mg.g^{-1}$ for Cu(II) and declined from 341.2 to 323.1 $mg.g^{-1}$ for Cr(VI) after five working cycles, which make it be a promising candidate for manipulation of heavy metals [427]. Succeeding adsorption and desorption cycle up to six cycles to remove the loaded Ni(II) from the exhausted molecularly imprinted ferrite ($SiO_2@Fe_2O_3$) nanomaterials was also recorded by using 0.1 M HCl solution [428].

3.2.11 Analytical techniques in biosorption studies

A number of complementary characterization techniques have been employed as prerequisite tools to clarify the physicochemical characteristics of the as-synthesized biosorbent and hence, giving more insight into the biosorption mechanism. Plausible apprehension of the biosorption mechanism plays a crucial role in the successful design, optimization of biosorption processes and

modelling at large industrial scale. Taking into consideration the various analytical techniques, it should be noted that in most studies not an individual technique is used, but a combination of numerous characterization methods are being used. They perceptually provide valuable information characterized to biosorbent structure including specific surface area, particle size, pore (volume, diameter), morphology, porosity, heterogeneity, thermal and pyrolytic features. Other analyses help in identifying and quantifying functional groups present on the biosorbents surfaces, elemental composition, moisture content, ash content, fixed carbon and morphological and structural changes of biosorbent surface before and after the sorption process. Therefore, characterization techniques can be categorized into four main classes including:

- Assessing methods for evaluating the sorbate total content in the as-used biosorbent.
- X-ray based methods.
- Microscopic techniques.
- Other techniques.

ICP-OES (Inductively Coupled Plasma - Optical Emission Spectroscopy) is utilized to provide information about all constituent elements of the original samples [429]. On the other hand, ICP-MS (Inductively Coupled Plasma - Mass Spectroscopy) is an accurate characterization technique and substantially better than (ICP-OES) as the sorbates (s) content involved in the sorption process is almost high. However, there are some drawbacks such as analytical problems associated with double charged ionic species [409].

AAS (Atomic Absorption Spectroscopy) is performed to determine the concentration of sorbate (s) by atomic absorption spectra and hence, investigation regarding the sorption kinetics and isotherm. This highly sensitive technique is usually utilized for the determination of most metals and metalloids [412]. Generally, it is divided into Electrothermal Atomic Absorption Spectroscopy

(ETAAS) and Flame Atomic Absorption Spectroscopy (FAAS). The former is presented to directly elucidate the sorbate and organic matrices inside the graphite furnace. The electrothermal atomizer unit consists of two graphite-based components (cuvette and furnaces). The atomization process includes three stages: drying, incineration and atomization. Its advantages comprise low detection limits (ppt) ability as well as the possibility to analyze the examined solid samples [430]. While the FAAS is conducted to investigate the elemental analysis characterized to biosorbent after mineralization of samples by using mineral acids such as (HNO_3, HCl) to release organic matters. In spite of, ensuring good reproducibility by flame atomization, this technique requires great amount of sample and among different atomization methods, it has the lowest sensitivity (ppb). The limitation of this methodology is the process occurrence (i.e.) ionization or excitation in parallel with atomization [430]. HGAAS (Hydride Generation Atomic Absorption spectroscopy) is adopted for the generation of volatile hydrides contained in the tested samples. Once, released into a heated cuvette, they are broken down with free atoms discharge especially characterized to the examined element [431]. Ultraviolet-Visible Spectrophotometry (UV – Vis) detection is a cheap and simple measuring method, employed for metals analysis on the basis of metal ions capabilities to react with a ligand resulting in complex formation which can be measured by using UV-Vis [432]. X-ray based techniques such as XPS, XRD, XRF and EDX can be utilized (i.e. separate and/or in combination with other strategies) such as microscopy techniques to visualize chemical composition as well as topographical differences on the surface of biosorbent before and after sorption process. XPS is the non-destructive methodology used to clarify the functions involved in the sorption of water pollutants on the biosorbent and hence identify the binding mechanism. It clears the oxidation states of the bound pollutant, reveals the surface groups of biosorbent (i.e. amino, hydroxyl, carboxyl and sulfonate groups) and explains the interaction

between the active sites found on the biosorbent surface and the sorbed pollutant. Also, it provides information about surface layers of biosorbent or its thin film structures. Samples analysis before and after sorption process can be done to show and compare the free and interacted functional groups of biosorbent and target pollutants [433]. XRF is a useful methodology carried out for the determination of major constituents contained in the biosorbent (solid sample). This method characterizes by cheap, quick and non-destructive to biological samples. Also, it can be performed using a device (portable) which allows minimum sample processing in term of sieving and drying and the results can be obtained immediately [434]. XRD is a non-destructive methodology used to determine the crystalline components present in the examined composite [435]. While, XAS is used to identify and understand the materials local structure details as well as the elemental speciation in metal clusters, metalloproteins and organometallic compounds. The contribution of material x-ray absorption coefficient as an energy function was measured. The intensities of the incident and transmitted x-ray are recorded. An increment of incident x-ray energy occurs. Both XANES (X-ray Absorption Near-Edge Structure) [436] and EXAFS (Extended X-ray Absorption Fine Structure) are regions of the spectrum obtained from XAS [437]. EXAFS is a beneficial technique for the analysis of the solid-state material to give insights about the chemical and electronic structure of active sites found inside the materials and other information related to the neighbouring atoms such as their numbers, chemical nature and distance [438]. Energy-Dispersive X-ray (EDX) is also used to provide information about the chemical composition of the sample, where the detected peak height is proportional to the energy [439]. On the other hand, Particle-induced X-ray emission or proton-induced X-ray emission (PIXE) is a non-destructive, simultaneous trace-multi element characterization technique that presents information about the elemental composition of biosorbent. It has the ability to monitor the difference in the elemental

composition of biosorbent before and after sorption which may be referred to different mechanism (i.e. ion exchange mechanism) [440]. While PIXE-Rutherford backscattering **(**PIXE-RBS) is also a non-destructive and quantitative tool used to investigate the contribution of ion exchange mechanism during the sorption process by quantifying the replaced biosorbent sorbate with the new pollutant (molecules and/or ions) attached to the biosorbent surface. The energy and intensity of the backscattered beam is helpful to analyze the composition and depth profiling of elements on the biosorbent surface. It can be applied to determine the concentrations of light element which is not available by PIXE [441].

To investigate the morphology of the surface of the adsorbent, different microscopy techniques are used such as scanning electron microscopy [442], high-resolution transmission electron microscopy (HRTEM) [443] or atomic force microscopy (AFM). They are helpful in surface atoms identification, change in physical features and the atoms interaction together with the neighbouring atoms [444]. Fourier-transform infrared spectroscopy (FTIR) spectrum profiles are employed to study and identify the vibrational frequencies of chemical bonds and consequently active sites contained in the as-prepared biosorbent and hence clearly investigate their availability to chemically interact with the target sorbet (s). Their emission from the tested samples works over a wide range of spectra. Mathematical Fourier Transformation can convert the origin outcomes into the spectrum, studies surface chemistry and quantitatively as well as qualitatively examines different samples whether organic or inorganic present in different sample forms (i.e. solid, liquid, gas) [445]. Matrix-assisted laser desorption/ionization mass spectrometry (MALDI MS) is described as an ionization methodology in term of laser energy forms ions in the gas phase, normally utilized for the analysis of biomolecules [446]. Neutron Activation Analysis **(**NAA) is a qualitative and quantitative elemental analysis based on specific radiation of radionuclides which

is produced from the neutron irradiation of the tested sample. Its advantages including accuracy, high (selectivity, sensitivity), non-destructive and independence of matrix effects, ease of samples preparation and elemental analysis of biological samples [447].

3.2.12 Biosorption mechanism

Biosorption mechanistic studies of different water pollutants are critical for appraising their manipulation efficiency. This is beneficial for optimizing the removal process conditions. Up to now, numerous studies have focused on investigating the possible interaction mechanism of diverse water pollutants on the as-used biosorbents. High biosorption efficiency is an important aspect that should be characterized to the biosorbent for effective elimination of different water pollutants. Generally, the biosorption process is based on physicochemical features of the biosorbent (i.e. solubility, molecular size, surface charge, chemical composition, reactivity and hydrophobicity). The structural components vary based on the presence of numerous functional groups with varying degrees on its surface (i.e. amino, carboxyl, hydroxyl, phosphate, thiol, etc) facilitates the sorption of water pollutants onto biosorbent through multiple sorption mechanisms. Commonly, the interaction between contaminants and biosorbent surface can occur through aggregation, complexation/coordination, electrostatic interaction, ion exchange, microprecipitation, oxidation and reduction. Figure 7 shows different possible mechanisms for clarifying the biosorption process. The possibility of precipitation, as well as crystallization occurrence, cannot be ignored which simultaneously complicates with sorption and/or desorption processes.

To explore the main biosorption mechanism, variable characterization strategies and theoretical calculations related to the different models' assumptions in term of kinetics, isotherms and thermodynamics have been performed. The biosorption interaction between water pollutants and

various biosorbents mainly occurs in two opposite scenarios; surface sorption and interstitial sorption. During surface sorption, sorbate molecules migrate from the aqueous matrices to the biosorbent surface. Once the pollutant (molecules and/or ions) have outstripped the boundary layer surrounding to biosorbent, they are sorbed to the active sites found on its surface and subsequently, removed from aqueous solutions. Usually, this type of sorption is achieved by dipole interactions, hydrogen bonding or Van Der Waals forces [448]. Whereas, during interstitial sorption, pollutants (molecules and/or ions) diffuse towards the biosorbent in terms of entering the biosorbent pores (macro, meso and/or micropores) and finally, biosorbed to the interior surface of the biosorbent. Several sorption mechanisms have been proposed for water pollutants elimination [55].

Tackling of various pollutants from synthetic and/or real wastewater solutions by biosorbents can be explained through electrostatic interactions. They have been identified as a major contributor to the biosorption of water contaminants. Existence of abundant functional groups on the biosorbent surface makes them typical candidates for efficient pollutant capture from different water systems. The capability of these functional groups is greatly influenced by environmental pH. The biosorbent surface charge and pollutants speciation are significantly dependent on the pH of the medium. Lower pH values cause protonation of surface functional groups, which leads to developing a positive charge on the biosorbent surface. Consequently, electrostatic repulsion occurs, reducing and/or preventing the sorption of positively charged pollutants (i.e. metals cations). Conversely, electrostatic repulsion declines with raising the medium pH, leading to an increase in their biosorption in terms of electrostatic attraction phenomena. For example, the negatively functional moieties including carboxylate ($–COO^-$) and hydroxyl ($–OH^-$) on the biosorbent surface provides it with a negative charge and hence, facilitates the binding of positively charged pollutants (molecules and/or ions). Contrarily, holding of positively functional groups

such as amine sites (-NH_2) is considered as the main force responsible for sorption of negatively charged water pollutants.

Dissociation constant values (pK_a) of biosorbent functional groups and its (pH_{PZC}) value are relative to pH of the solution and hence, influence the biosorbent sorption capacity. (pK_a) values of numerous functional groups like carboxylic and phenol groups range from (3.5-5.5). This indicates that most of these groups deprotonate in these value working ranges and that enhancement of negatively charged sorption sites will be available for biosorption process [449]. Additionally, the biosorbent (pH_{PZC}) value greatly effects on the biosorption process. The charge of the biosorbent surface is positive when pH of solution < pH_{PZC}, whereas, it is negative in case of pH of solution > pH_{PZC}. As a result, the elimination of pollutants (molecules and/or ions), particularly those that possess positive charges (i.e. metals cations) is low when pH is lower than pH_{PZC} and increases when pH is greater than pH_{PZC}. This proposes significant involvement of electrostatic forces during the biosorption process. The biosorption process can be interpreted on the basis of ion exchange mechanism between the biosorbent and the studied pollutants. Its contribution is explained through the replacement (exchange) of protons from the exchangeable sites present on biosorbent surface with pollutant (i.e. metal ions). The proposed mechanism is facilitated by the existence of hydroxyl, carboxyl and phenols groups which can be occupied by pollutant ions (i.e. divalent heavy metal ions) via two electrons pairs associated with release of two H^+ and/or Na^+ into the solution [450]. The solution pH influencing on the ion exchange mechanism; in the acidic medium, the elevation in the H^+ ions leads to compete with positively charged pollutant (molecules and/or ions) to be sorbed onto the biosorbent, while, in the basic medium, the increase in the OH^- ions leads to competing with negatively charged pollutants (molecules and/or ions) to be sorbed on the sorption sites. For example, the possible ion-exchange

mechanism between pollutants such as metal cations and exchangeable protons from the biosorbent surface can be described as shown in the following equations:

Biosorbent surface--- H^+ + (metal ions)$^+$ ⟶ Biosorbent surface--- metal ion$^+$ + H^+.

Biosorbent surface--- Na^+ + (metal ions)$^+$ ⟶ Biosorbent surface--- metal ion$^+$ + Na^+.

Biosorbent surface ---Ca^{+2} + (metal ion)$^+$ ⟶ Biosorbent surface --- metal ion$^+$ + Ca^{+2}.

Biosorbent surface --- 2(-ROH) + (metal ion)$^{++}$ ⟶ Biosorbent surface $(-RO)_2$--metal ion^{++} +2H^+.

Formation of surface complexes (complexation) involves the interaction of pollutants (i.e. metal ions) with oxygen donor atoms from the oxygen-containing functional groups (coordination) associated with the release of protons and formation of surface complexes. Ligand tendency for metal complexes formation significantly depends on the metals classification based on their chemical characters including the hard-soft-acid-base principle (HSAB). Metal ions (cations) can bind with biosorbent surface through an inner-sphere or outer-sphere complex mechanisms by the covalent bond chemically established between the metal and the oxygen atom (electron donor) or by cations approaching to the negative groups present on the surface (critical distance) associated with presence of at least water molecule between the cation and base, respectively [338]. Table 8 presents sorption of different water pollutants on various low-cost biosorbents.

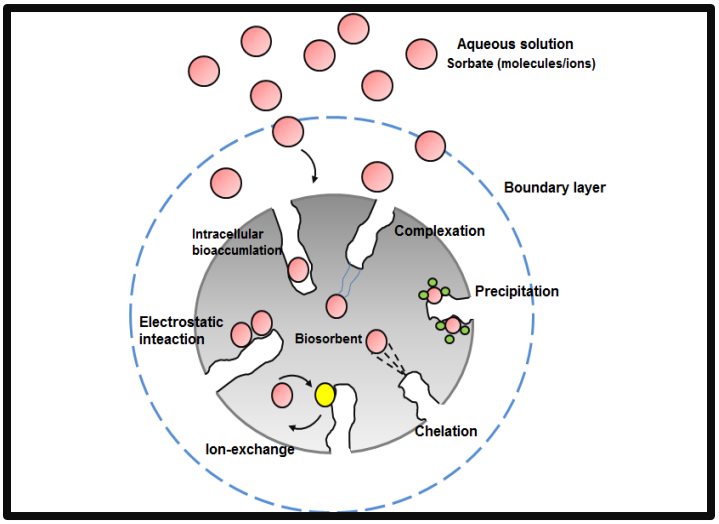

Figure 7: Different mechanisms involved in the biosorption process.

Table 8: Sorption of different water pollutants on various low-cost biosorbents.

Biosorbent	Pollutants (sorbate)	Biosorption capacity ($mg.g^{-1}$)	Biosorption mechanism	References
bacterium *Bacillus amyloliquefaciens*	U(VI)	179.5	Chemical interaction	[451]
Sulfur functionalized marine brown algae *Cystoseira indica*	La(III)	185.44	Internal and external diffusion mechanisms	[452]
Sulfur functionalized marine brown algae *Cystoseira indica*	Ce(III)	172.33	Internal and external diffusion mechanisms	[452]
yeast Saccharomyces cerevisiae	Cu (II)	4.73	Ion exchange	[453]
Sargassum glaucescens	As(III)	116.6	Electrostatic interaction	[454]
Sargassum glaucescens	As(V)	207.3	Electrostatic interaction	[454]
Phanerochaete chrysosporium	Cd(II)	71.43	Chemical interaction	[455]
Phanerochaete chrysosporium	Ni(II)	46.50	Chemical interaction	[455]
Gliricidia sepium leaf powder	Cr(VI)	35.71	Chelation, Ion exchange, Complexation, Physical adsorption and chemical adsorption	[404]
Ion-imprinted Tetraethylenepentamine modified chitosan beads	Pb (II)	259.68	Complexation	[456]
Renewable durian peels	Zn (II)	36.73	Electrostatic interaction	[457]
Formaldehyde modified green tomato husk	Fe (III)	19.83	Precipitation and ion exchange	[458]
Formaldehyde modified green tomato husk	Mn (II)	15.22	Ion exchange and complexation	[458]
Magnetized *C. micaceus*	Hg (II)	26.2	Complexation	[459]
Magnetized C. micaceus	Co(II)	24.7	Complexation	[459]
Chitin	Au	35	Complexation	[405]
Brown seaweed *Sargassum muticum*	Sb(III)	4 ± 1	Complexation and hydrogen bonding	[460]
Magnetic chitosan Glutaraldehyde composite	Crystal violet dye	105.467	Electrostatic interaction	[300]
Nerium oleander seed fibre	Methylene blue dye	280.2	Electrostatic interaction	[406]
IL modified AC (ILAC)	Congo red dye	150.0	Electrostatic interaction	[461]

IL modified AC (ILAC)	Reactive blue dye	364.4	Electrostatic interaction	[461]
Green microalgae *Chlorella pyrenoidosa*	Rhodamine B dye	63.14	Electrostatic interaction	[462]
Residual defatted biomass (RDB) of the fungus *Nigrospora sp.*	Procion red H–E7B dye	188.79	Electrostatic interaction	[297]
Carica papaya wood	Malachite green dye	52.63	Electrostatic interaction	[463]
Chemically modified masau stones	Orange (II) dye	136.8	Hydrogen bonding and electrostatic attraction	[464]
Ethylenediamine modified fibre	Acid Blue 25	67	Van Der Waals' forces, π-π stacking and hydrogen bond	[407]
Grape pomace	KROM KGT dye	180.2 ± 3.2	Electrostatic interaction	[465]
Pine fruit shells PFS (BC550)	Phenol	26.738	Dispersive interaction and π-π interaction	[296]
Modified biomass of green alga *Scenedesmus obliquus*	Tramadol (TRAM)	42	Hydrophilic interactions	[466]
Modified biomass of green alga *Scenedesmus obliquus*	Cefadroxil (CEFA)	68	Hydrophilic interactions	[466]
Modified biomass of green alga *Scenedesmus obliquus*	Paracetamol (PARA)	58	Hydrophilic interactions	[466]
Modified biomass of green alga *Scenedesmus obliquus*	Ciprofloxacin (CIP)	39	Hydrophilic interactions	[466]
Modified biomass of green alga *Scenedesmus obliquus*	Ibuprofen (IBU)	42	Hydrophilic interactions	[466]
Biochar derived from corn straw	Atrazine	11.566	Electrostatic interaction	[467]
Corn cob-derived porous carbons (PCs)	Naphthalene	592.97	Pore filling, hydrophobic effects and π-π stacking interactions	[408]
Corn cob-derived porous carbons (PCs)	Acenaphthene	480.27	Pore filling, hydrophobic effects and π-π stacking interactions	[408]
Corn cob-derived porous carbons (PCs)	Phenanthrene	692.27	Pore filling, hydrophobic effects and π-π stacking interactions	[408]

4. Conclusion

This review attempts to investigate a range of adsorbents; primarily focusing on magnetic nanoparticles and biosorbents. This is due to their effective, safe, eco-friendly, low cost and low-energy intensive properties. These properties aid the co-existing excellent adsorption characteristic of both techniques and the removal of pollutants from wastewater streams such as heavy metals, dyes, pesticides, phenols, radionuclides, pharmaceutical compounds and insecticides using these methods. Firstly, the use of these magnetic adsorbents for water purification gives a significant advantage over other adsorbents, such as their low-cost and ease of separation of suspending adsorbents to be used again to reduce cost, as well as the ease to synthesize. It is illustrated from this review that the incorporation of the recent nanoscale magnetic materials with the superior adsorbents such as WO_3, TiO_2, ZnO, and GO reduces the rapid recombination of photoinduced electron-holes and therefore, enhances the photocatalysis potential of these materials besides the ease of separation of suspending adsorbents. Furthermore, the mechanism and kinetics of the sorption approach depend on many factors such as surface morphology, magnetic behaviour of the adsorbent and the experimental conditions like pH, adsorbent concentration, irradiation time, temperature and the initial dosage of pollutant. Secondly, biosorbents have an advantage over other adsorbents in that they occur naturally in high abundance, associating next to no cost and can always be renewed. Utilizing this waste stream to combat another waste stream in the form of wastewater, means that the usage of biosorbents promotes the remediation of this stream and concepts like recycling, reuse and the circular economy. Nevertheless, both, magnetic adsorbents and biosorbents face many obstacles that require discussion and dissemination in the form of research and development, such as the commercialization of these adsorbents to estimate their

utility on a wider scale as well as a complete evaluation of the possibility of using these adsorbents to eliminate the multipollutant solutions.

This review aims to inform academics and policymakers alike in reporting and discussing the state-of-the-art of these two promising routes to adsorption to remove pollutants from wastewater streams in a synergistic way to help alleviate environmental and ecological impact whilst promoting reuse and sustainable development.

Acknowledgement: The corresponding author AO would like to acknowledge the support given by the EPSRC project "Advancing Creative Circular Economies for Plastics via Technological-Social Transitions" (ACCEPT Transitions, EP/S025545/1). The authors also wish to acknowledge the support of The Bryden Centre project (Project ID VA5048) which was awarded by The European Union's INTERREG VA Programme, managed by the Special EU Programmes Body (SEUPB), with match funding provided by the Department for the Economy in Northern Ireland and the Department of Business, Enterprise and Innovation in the Republic of Ireland. The authors would like to thank Charlie Farrell who assisted in the proof-reading of the manuscript.

Competing financial interests: The author declares no competing financial interests.

5. References:

[1] G.M. Geise, H.-S. Lee, D.J. Miller, B.D. Freeman, J.E. McGrath, D.R. Paul, Journal of Polymer Science Part B: Polymer Physics, 48 (2010) 1685-1718.

[2] S. Sharma, V. Dutta, P. Singh, P. Raizada, A. Rahmani-Sani, A. Hosseini-Bandegharaei, V.K. Thakur, Journal of Cleaner Production, 228 (2019) 755-769.

[3] N. Yahya, F. Aziz, N.A. Jamaludin, M. A. Mutalib, A.F. Ismail, W.N. W. Salleh, J. Jaafar, N. Yusof, N. A. Ludin, Journal of Environmental Chemical Engineering, 6 (2018) 7411-7425.

[4] M.A.P. Kelm, M.J. da Silva Júnior, S.H. de Barros Holanda, C.M.B. de Araujo, R.B. de Assis Filho, E.J. Freitas, D.R. dos Santos, M.A. da Motta Sobrinho, Environmental Science and Pollution Research, (2019).

[5] D.H.K. Reddy, Y.-S. Yun, Coordination Chemistry Reviews, 315 (2016) 90-111.

[6] J.S. Famiglietti, Nature Climate Change, 4 (2014) 945.

[7] A. Biewald, S. Rolinski, H. Lotze-Campen, C. Schmitz, J.P. Dietrich, Ecological Economics, 101 (2014) 43-53.

[8] P. T.C, S.K. Sharma, M. Kennedy, Separation and Purification Technology, 199 (2018) 260-270.

[9] R. Bhateria, R. Singh, Journal of Water Process Engineering, 31 (2019) 100845.

[10] H.T. Madsen, Chapter 6 - Membrane Filtration in Water Treatment – Removal of Micropollutants, in: E.G. Søgaard (Ed.) Chemistry of Advanced Environmental Purification Processes of Water, Elsevier, Amsterdam, 2014, pp. 199-248.

[11] W. Fu, W. Zhang, Journal of Membrane Science, 568 (2018) 97-104.

[12] L. Deng, H.-H. Ngo, W. Guo, H. Zhang, Water Research, 157 (2019) 155-166.

[13] C.V. Subban, A.J. Gadgil, Desalination, 465 (2019) 38-43.

[14] I. Levchuk, J.J. Rueda Márquez, M. Sillanpää, Chemosphere, 192 (2018) 90-104.

[15] J. Bratby, Coagulation and flocculation in water and wastewater treatment, IWA publishing, 2016.

[16] H. Wei, B. Gao, J. Ren, A. Li, H. Yang, Water Research, 143 (2018) 608-631.

[17] K.-W. Kim, W.-J. Shon, M.-K. Oh, D. Yang, R.I. Foster, K.-Y. Lee, Nuclear Engineering and Technology, 51 (2019) 738-745.

[18] V. Yargeau, 17 - Water and wastewater treatment: chemical processes, in: F. Zeman (Ed.) Metropolitan Sustainability, Woodhead Publishing, 2012, pp. 390-405.

[19] F. Ruiz-Beviá, M.J. Fernández-Torres, Journal of Cleaner Production, 217 (2019) 398-408.

[20] V.K. Gupta, I. Ali, Chapter 2 - Water Treatment for Inorganic Pollutants by Adsorption Technology, in: V.K. Gupta, I. Ali (Eds.) Environmental Water, Elsevier, 2013, pp. 29-91.

[21] A. Bonilla-Petriciolet, D.I. Mendoza-Castillo, G.L. Dotto, C.J. Duran-Valle, Adsorption in Water Treatment, in: Reference Module in Chemistry, Molecular Sciences and Chemical Engineering, Elsevier, 2019.

[22] M. Kraus, U. Trommler, F. Holzer, F.-D. Kopinke, U. Roland, Chemical Engineering Journal, 351 (2018) 356-363.

[23] X. Yu, W. Cui, F. Zhang, Y. Guo, T. Deng, Desalination, 458 (2019) 76-83.

[24] Y. Xie, L. Ren, X. Zhu, X. Gou, S. Chen, Process Safety and Environmental Protection, 116 (2018) 180-198.

[25] S.S. Fiyadh, M.A. AlSaadi, W.Z. Binti Jaafar, M.K. AlOmar, S.S. Fayaed, N.S. Binti Mohd, L.S. Hin, A. El-Shafie, Journal of Cleaner Production, (2019).

[26] C. Shen, Y. Zhao, W. Li, Y. Yang, R. Liu, D. Morgen, Chemical Engineering Journal, 372 (2019) 1019-1027.

[27] J. Singh, S. Basu, H. Bhunia, Microporous and Mesoporous Materials, 280 (2019) 357-366.

[28] M.E. de Oliveira Ferreira, B.G. Vaz, C.E. Borba, C.G. Alonso, I.C. Ostroski, Microporous and Mesoporous Materials, 277 (2019) 208-216.

[29] A.I. Osman, E. O'Connor, G. McSpadden, J.K. Abu-Dahrieh, C. Farrell, A.a.H. Al-Muhtaseb, J. Harrison, D.W. Rooney, Journal of Chemical Technology & Biotechnology, 0.

[30] S. Vyazovkin, K. Chrissafis, M.L. Di Lorenzo, N. Koga, M. Pijolat, B. Roduit, N. Sbirrazzuoli, J.J. Suñol, Thermochimica Acta, 590 (2014) 1-23.
[31] Z. Yin, Duoni, H. Chen, J. Wang, W. Qian, M. Han, F. Wei, Carbon, 132 (2018) 329-334.
[32] J. Zhang, Y. Hong, M. Liu, Y. Yue, Q. Xiong, G. Lorenzini, International Journal of Heat and Mass Transfer, 104 (2017) 871-877.
[33] X. Niu, Q. Xiong, J. Pan, X. Li, W. Zhang, F. Qiu, Y. Yan, Fuel, 190 (2017) 174-181.
[34] J. Zhang, F. Xu, Y. Hong, Q. Xiong, J. Pan, RSC Advances, 5 (2015) 89415-89426.
[35] A. Chafidz, F. Hamdan Latief, A.S. Al-Fatesh, M. Kaavessina, Philosophical Magazine Letters, 96 (2016) 367-374.
[36] A.I. Osman, A.T. Ahmed, C.R. Johnston, D.W. Rooney, Environmental Progress & Sustainable Energy, 37 (2018) 1058-1067.
[37] A.I. Osman, A. Abdelkader, C.R. Johnston, K. Morgan, D.W. Rooney, Industrial & Engineering Chemistry Research, 56 (2017) 12119-12130.
[38] A.I. Osman, A. Abdelkader, C. Farrell, D. Rooney, K. Morgan, Fuel Processing Technology, 192 (2019) 179-202.
[39] A.I. Osman, Renewable Energy, 146 (2020) 484-496.
[40] M. Kumita, N. Yamawaki, K. Shinohara, H. Higashi, A. Kodama, N. Kobayashi, T. Seto, Y. Otani, International Journal of Refrigeration, 94 (2018) 127-135.
[41] T.H. Tu, P.T.N. Cam, L.V.T. Huy, M.T. Phong, H.M. Nam, N.H. Hieu, Materials Letters, 238 (2019) 134-137.
[42] A. Zeraatkar Moghaddam, E. Esmaeilkhanian, M. Shakourian-Fard, International Journal of Biological Macromolecules, 128 (2019) 61-73.
[43] M.-p. Wei, H. Chai, Y.-l. Cao, D.-z. Jia, Journal of Colloid and Interface Science, 524 (2018) 297-305.
[44] E. Chmielewská, Chapter 4 - Natural zeolite: Alternative adsorbent in purification or post-treatment of waters, in: M. Mercurio, B. Sarkar, A. Langella (Eds.) Modified Clay and Zeolite Nanocomposite Materials, Elsevier, 2019, pp. 87-112.
[45] R. Soni, D.P. Shukla, Chemosphere, 219 (2019) 504-509.
[46] N.M. Mahmoodi, M.H. Saffar-Dastgerdi, Microchemical Journal, 145 (2019) 74-83.
[47] H. Hassan, A. Salama, A.K. El-ziaty, M. El-Sakhawy, International Journal of Biological Macromolecules, 131 (2019) 520-526.
[48] A. Abolghasemi Mahani, S. Motahari, A. Mohebbi, Marine Pollution Bulletin, 129 (2018) 438-447.
[49] T.L. Rodrigues Mota, A.P. Marques de Oliveira, E.H.M. Nunes, M. Houmard, Microporous and Mesoporous Materials, 253 (2017) 177-182.
[50] V.B. Yadav, R. Gadi, S. Kalra, Journal of Environmental Management, 232 (2019) 803-817.
[51] K. Buruga, H. Song, S. Jin, N. Bolan, T.K. Jagannathan, K.-H. Kim, Journal of Hazardous Materials, (2019).
[52] J. Gogoi, A.D. Choudhury, D. Chowdhury, Materials Chemistry and Physics, 232 (2019) 438-445.
[53] D. Mehta, S. Mazumdar, S.K. Singh, Journal of Water Process Engineering, 7 (2015) 244-265.
[54] X. Xu, B. Gao, B. Jin, Q. Yue, Journal of Molecular Liquids, 215 (2016) 565-595.
[55] L. Joseph, B.-M. Jun, J.R.V. Flora, C.M. Park, Y. Yoon, Chemosphere, 229 (2019) 142-159.
[56] T. Hou, N. Chen, S. Tong, B. Li, Q. He, C. Feng, Biochemical Engineering Journal, (2018).
[57] K. Kaya, E. Pehlivan, C. Schmidt, M. Bahadir, Food Chemistry, 158 (2014) 112-117.
[58] H. Alidadi, M. Dolatabadi, M. Davoudi, F. Barjasteh-Askari, F. Jamali-Behnam, A. Hosseinzadeh, Process Safety and Environmental Protection, 117 (2018) 51-60.
[59] R. Ahmad, S. Haseeb, Groundwater for Sustainable Development, 1 (2015) 41-49.
[60] S.J. Segovia-Sandoval, R. Ocampo-Pérez, M.S. Berber-Mendoza, R. Leyva-Ramos, A. Jacobo-Azuara, N.A. Medellín-Castillo, Journal of Water Process Engineering, 25 (2018) 45-53.

[61] M.A. Hossain, H.H. Ngo, W.S. Guo, T. Setiadi, Bioresource Technology, 121 (2012) 386-395.
[62] R.M. Kulkarni, K.V. Shetty, G. Srinikethan, Journal of the Taiwan Institute of Chemical Engineers, 45 (2014) 1628-1635.
[63] L. Semerjian, Environmental Technology & Innovation, 12 (2018) 91-103.
[64] M. Adibmehr, H. Faghihian, Comptes Rendus Chimie, 21 (2018) 840-853.
[65] I.L.A. Ouma, E.B. Naidoo, A.E. Ofomaja, Journal of Environmental Chemical Engineering, 6 (2018) 5409-5419.
[66] S. Liu, C. Ma, M.-G. Ma, F. Xu, 12 - Magnetic Nanocomposite Adsorbents, in: G.Z. Kyzas, A.C. Mitropoulos (Eds.) Composite Nanoadsorbents, Elsevier, 2019, pp. 295-316.
[67] K.H.J. Buschow, F.R. Boer, Physics of magnetism and magnetic materials, Springer, 2003.
[68] M. Getzlaff, Fundamentals of magnetism, Springer Science & Business Media, 2007.
[69] C. Martinez-Boubeta, K. Simeonidis, Chapter 20 - Magnetic Nanoparticles for Water Purification, in: S. Thomas, D. Pasquini, S.-Y. Leu, D.A. Gopakumar (Eds.) Nanoscale Materials in Water Purification, Elsevier, 2019, pp. 521-552.
[70] K. Zhu, C. Chen, Chapter 6 - Application of nZVI and its composites into the treatment of toxic/radioactive metal ions, in: C. Chen (Ed.) Interface Science and Technology, Elsevier, 2019, pp. 281-330.
[71] F. Fu, D.D. Dionysiou, H. Liu, Journal of Hazardous Materials, 267 (2014) 194-205.
[72] A. Fujishima, X. Zhang, D.A. Tryk, Surface Science Reports, 63 (2008) 515-582.
[73] S. Jokar Baloochi, A.R. Solaimany Nazar, M. Farhadian, Environmental Nanotechnology, Monitoring & Management, 10 (2018) 212-222.
[74] K. Sravanthi, D. Ayodhya, P.Y. Swamy, Materials Science for Energy Technologies, 2 (2019) 298-307.
[75] R. Foroutan, R. Mohammadi, B. Ramavandi, Environmental Science and Pollution Research, (2019).
[76] W. Wang, Y. Cheng, T. Kong, G. Cheng, Journal of Hazardous Materials, 299 (2015) 50-58.
[77] R. Zhao, Z. Zhou, X. Zhao, G. Jing, Chemosphere, 218 (2019) 458-467.
[78] S. Yu, X. Wang, Y. Liu, Z. Chen, Y. Wu, Y. Liu, H. Pang, G. Song, J. Chen, X. Wang, Chemical Engineering Journal, 365 (2019) 51-59.
[79] B. Kakavandi, A. Takdastan, S. Pourfadakari, M. Ahmadmoazzam, S. Jorfi, Journal of the Taiwan Institute of Chemical Engineers, 96 (2019) 329-340.
[80] J. Cao, L. Lai, B. Lai, G. Yao, X. Chen, L. Song, Chemical Engineering Journal, 364 (2019) 45-56.
[81] P. Xie, L. Zhang, J. Chen, J. Ding, Y. Wan, S. Wang, Z. Wang, A. Zhou, J. Ma, Water Research, 149 (2019) 169-178.
[82] A. Mossmann, G.L. Dotto, D. Hotza, S.L. Jahn, E.L. Foletto, Journal of Environmental Chemical Engineering, 7 (2019) 102963.
[83] J. Yao, M. Gao, X. Guo, F. Ai, Z. Wang, Chemosphere, 221 (2019) 314-323.
[84] J. Wu, B. Wang, L. Blaney, G. Peng, P. Chen, Y. Cui, S. Deng, Y. Wang, J. Huang, G. Yu, Chemical Engineering Journal, 361 (2019) 99-108.
[85] Q. Jin, S. Zhang, T. Wen, J. Wang, P. Gu, G. Zhao, X. Wang, Z. Chen, T. Hayat, X. Wang, Environmental Pollution, 243 (2018) 218-227.
[86] A. Li, Z. Wu, T. Wang, S. Hou, B. Huang, X. Kong, X. Li, Y. Guan, R. Qiu, J. Fang, Journal of Hazardous Materials, 357 (2018) 207-216.
[87] K.-S. Lin, N.V. Mdlovu, C.-Y. Chen, C.-L. Chiang, K. Dehvari, Journal of Cleaner Production, 175 (2018) 456-466.
[88] S. Zha, Y. Cheng, Y. Gao, Z. Chen, M. Megharaj, R. Naidu, Chemical Engineering Journal, 255 (2014) 141-148.
[89] R.C. Pawar, D.-H. Choi, C.S. Lee, International Journal of Hydrogen Energy, 40 (2015) 767-778.

[90] E. Alp, H. Eşgin, M.K. Kazmanlı, A. Genç, Ceramics International, 45 (2019) 9174-9178.
[91] N.I. Mohd Razip, K.M. Lee, C.W. Lai, B.H. Ong, Materials Research Express, 6 (2019) 075517.
[92] M. Sumathi, A. Prakasam, P.M. Anbarasan, Journal of Materials Science: Materials in Electronics, (2019).
[93] A. Lassoued, M.S. Lassoued, S. García-Granda, B. Dkhil, S. Ammar, A. Gadri, Journal of Materials Science: Materials in Electronics, 29 (2018) 5726-5737.
[94] P. Rezai, S. Baniyaghoob, M.H. Sadr, Journal of Electronic Materials, 48 (2019) 3285-3296.
[95] H.B. Gasmalla, X. Lu, M.I. Shinger, L. Ni, A.N. Chishti, G. Diao, Journal of Nanobiotechnology, 17 (2019) 58.
[96] D. Adak, B. Show, A. Mondal, N. Mukherjee, Journal of Catalysis, 355 (2017) 63-72.
[97] J. Niu, Z. Zhang, P. Dai, B. Yao, X. Yu, Q. Zhang, R. Yang, Materials & Design, 150 (2018) 29-39.
[98] Z. Wei, X. Wei, S. Wang, D. He, Materials Letters, 118 (2014) 107-110.
[99] J. Liu, D. Zhang, X. Pu, D. Dong, P. Cai, H.J. Seo, Materials Letters, 130 (2014) 94-96.
[100] Y. Wen, Y. Zhao, M. Guo, Y. Xu, Journal of Materials Science, 54 (2019) 8236-8246.
[101] X. Li, H. Lin, X. Chen, H. Niu, J. Liu, T. Zhang, F. Qu, Physical Chemistry Chemical Physics, 18 (2016) 9176-9185.
[102] P. Wei, X. Yu, Y. Li, Journal of Electronic Materials, (2019).
[103] M.A. Ebrahimzadeh, S. Mortazavi-Derazkola, M.A. Zazouli, Journal of Materials Science: Materials in Electronics, (2019).
[104] Y. Areerob, J.Y. Cho, W.K. Jang, W.-C. Oh, Ultrasonics Sonochemistry, 41 (2018) 267-278.
[105] S.-H. Liu, J.-S. Lu, S.-W. Yang, Nanotechnology, 29 (2018) 305606.
[106] N. Abbas, G.N. Shao, S.M. Imran, M.S. Haider, H.T. Kim, Frontiers of Chemical Science and Engineering, 10 (2016) 405-416.
[107] Z. Zhao, Z. Cai, L. Yang, Z. Hu, Y. Zhang, X. Peng, Q. Wang, X. Yuan, G. Li, Journal of Materials Science: Materials in Electronics, 29 (2018) 17743-17749.
[108] B. Maddah, F. Jookar-Kashi, M. Akbari, Journal of Materials Science: Materials in Electronics, 29 (2018) 13723-13730.
[109] R.A. da Silva, M.J. Jacinto, V.C. Silva, D.C. Cabana, Journal of Sol-Gel Science and Technology, 86 (2018) 94-103.
[110] Z. Chen, M.-L. Fu, X.-D. Huang, B. Yuan, J.-C.E. Yang, Research on Chemical Intermediates, 44 (2018) 6369-6385.
[111] X. Lu, Y. Li, W. Jiang, Y. Huang, W. Zhang, G. Liang, S. Yang, Journal of Materials Science: Materials in Electronics, 29 (2018) 20856-20865.
[112] B. Cui, H. Peng, H. Xia, X. Guo, H. Guo, Separation and Purification Technology, 103 (2013) 251-257.
[113] B. Tian, T. Wang, R. Dong, S. Bao, F. Yang, J. Zhang, Applied Catalysis B: Environmental, 147 (2014) 22-28.
[114] A. Lassoued, M.S. Lassoued, B. Dkhil, S. Ammar, A. Gadri, Journal of Magnetism and Magnetic Materials, 476 (2019) 124-133.
[115] A.G. Abraham, A. Manikandan, E. Manikandan, S. Vadivel, S. Jaganathan, A. Baykal, P.S. Renganathan, Journal of Magnetism and Magnetic Materials, (2018).
[116] Y. Chen, Q. Wu, N. Bu, J. Wang, Y. Song, Chemical Engineering Journal, 373 (2019) 192-202.
[117] L. Bo, Y. Hu, Z. Zhang, J. Tong, Polyhedron, 168 (2019) 94-100.
[118] X.-T. Wang, Y. Li, X.-Q. Zhang, J.-F. Li, Y.-N. Luo, C.-W. Wang, Applied Surface Science, 479 (2019) 86-95.
[119] I. Ibrahim, C. Athanasekou, G. Manolis, A. Kaltzoglou, N.K. Nasikas, F. Katsaros, E. Devlin, A.G. Kontos, P. Falaras, Journal of Hazardous Materials, 372 (2019) 37-44.
[120] A. Hakimyfard, S. Mohammadi, Advanced Powder Technology, 30 (2019) 1257-1268.

[121] J. Kaur, M. Kaur, Ceramics International, 45 (2019) 8646-8659.
[122] V. Ramasamy Raja, A. Karthika, S. Lok Kirubahar, A. Suganthi, M. Rajarajan, Solid State Ionics, 332 (2019) 55-62.
[123] N. Khadgi, A.R. Upreti, Chemosphere, 221 (2019) 441-451.
[124] S. Samakchi, N. Chaibakhsh, Z. Moradi-Shoeili, Journal of Photochemistry and Photobiology A: Chemistry, 367 (2018) 420-428.
[125] Y. Xu, Q. Liu, M. Xie, S. Huang, M. He, L. Huang, H. Xu, H. Li, Journal of Colloid and Interface Science, 528 (2018) 70-81.
[126] Z. Liu, H. Feng, S. Xue, P. Xie, L. Li, X. Hou, J. Gong, X. Wei, J. Huang, D. Wu, Applied Surface Science, 458 (2018) 880-892.
[127] K. Shoueir, H. El-Sheshtawy, M. Misbah, H. El-Hosainy, I. El-Mehasseb, M. El-Kemary, Carbohydrate Polymers, 197 (2018) 17-28.
[128] X. Wang, A. Wang, J. Ma, Journal of Hazardous Materials, 336 (2017) 81-92.
[129] F. He, Y. Ji, Y. Wang, Y. Zhang, Journal of the Taiwan Institute of Chemical Engineers, 80 (2017) 553-562.
[130] P. Kharazi, R. Rahimi, M. Rabbani, Materials Research Bulletin, 103 (2018) 133-141.
[131] X.H. Vu, L.H. Phuoc, N.D. Dien, T.T.H. Pham, L.D. Thanh, Journal of Electronic Materials, 48 (2019) 2978-2985.
[132] M.A. Rehman, I. Yusoff, P. Ahmad, Y. Alias, Journal of Molecular Liquids, 224 (2016) 1256-1265.
[133] M.E. Mahmoud, M.S. Abdelwahab, International Journal of Biological Macromolecules, 128 (2019) 196-203.
[134] Y. Zhao, H. Chen, J. Li, C. Chen, Journal of Colloid and Interface Science, 450 (2015) 189-195.
[135] A. Liu, Z. Xia, W. Zhou, S. Huang, Journal of Environmental Chemical Engineering, 5 (2017) 6039-6044.
[136] L.A. Kafshgari, M. Ghorbani, A. Azizi, Applied Surface Science, 419 (2017) 70-83.
[137] M. Fayazi, M. Ghanei-Motlagh, M.A. Taher, Materials Science in Semiconductor Processing, 40 (2015) 35-43.
[138] D. Chen, Z. Zeng, Y. Zeng, F. Zhang, M. Wang, Water Resources and Industry, 15 (2016) 1-13.
[139] L. Lu, J. Li, J. Yu, P. Song, D.H.L. Ng, Chemical Engineering Journal, 283 (2016) 524-534.
[140] Q. Yang, H. Song, Y. Li, Z. Pan, M. Dong, F. Chen, Z. Chen, Journal of Molecular Liquids, 234 (2017) 18-23.
[141] S.-H. Huang, D.-H. Chen, Journal of Hazardous Materials, 163 (2009) 174-179.
[142] S. Nizamuddin, M.T.H. Siddiqui, N.M. Mubarak, H.A. Baloch, E.C. Abdullah, S.A. Mazari, G.J. Griffin, M.P. Srinivasan, A. Tanksale, Chapter 17 - Iron Oxide Nanomaterials for the Removal of Heavy Metals and Dyes From Wastewater, in: S. Thomas, D. Pasquini, S.-Y. Leu, D.A. Gopakumar (Eds.) Nanoscale Materials in Water Purification, Elsevier, 2019, pp. 447-472.
[143] R.M. Cornell, U. Schwertmann, The iron oxides: structure, properties, reactions, occurrences and uses, John Wiley & Sons, 2003.
[144] W. Wu, Z. Wu, T. Yu, C. Jiang, W.-S. Kim, Science and Technology of Advanced Materials, 16 (2015) 023501.
[145] G.K. Rozenberg, L.S. Dubrovinsky, M.P. Pasternak, O. Naaman, T. Le Bihan, R. Ahuja, Physical Review B, 65 (2002) 064112.
[146] S. Krehula, M. Ristić, M. Reissner, S. Kubuki, S. Musić, Journal of Alloys and Compounds, 695 (2017) 1900-1907.
[147] K.K. Kefeni, T.A.M. Msagati, T.T.I. Nkambule, B.B. Mamba, Journal of Environmental Chemical Engineering, 6 (2018) 1865-1874.
[148] Y.H. Chen, C.C. Lin, Physics and Chemistry of Minerals, 41 (2014) 727-736.

[149] A.S. Teja, P.-Y. Koh, Progress in Crystal Growth and Characterization of Materials, 55 (2009) 22-45.
[150] M. Tadic, D. Trpkov, L. Kopanja, S. Vojnovic, M. Panjan, Journal of Alloys and Compounds, 792 (2019) 599-609.
[151] C. Santhosh, A. Malathi, E. Dhaneshvar, A. Bhatnagar, A.N. Grace, J. Madhavan, Chapter 16 - Iron Oxide Nanomaterials for Water Purification, in: S. Thomas, D. Pasquini, S.-Y. Leu, D.A. Gopakumar (Eds.) Nanoscale Materials in Water Purification, Elsevier, 2019, pp. 431-446.
[152] K. Zhang, Y. Liu, J. Deng, S. Xie, H. Lin, X. Zhao, J. Yang, Z. Han, H. Dai, Applied Catalysis B: Environmental, 202 (2017) 569-579.
[153] M.J. Kang, H. Yu, W. Lee, H.G. Cha, Journal of Physics and Chemistry of Solids, 130 (2019) 93-99.
[154] L. Chen, S. Yang, Y. Huang, B. Zhang, F. Kang, D. Ding, T. Cai, Journal of Hazardous Materials, 371 (2019) 566-575.
[155] H.H. Mohamed, Journal of Photochemistry and Photobiology A: Chemistry, 378 (2019) 74-84.
[156] X. Li, B. Jin, J. Huang, Q. Zhang, R. Peng, S. Chu, Solid State Sciences, 80 (2018) 6-14.
[157] B. Li, W. Yin, M. Xu, X. Tan, P. Li, J. Gu, P. Chiang, J. Wu, Chemosphere, 224 (2019) 220-227.
[158] S. Wang, M. Zhao, M. Zhou, Y. Zhao, Y.C. Li, B. Gao, K. Feng, W. Yin, Y.S. Ok, X. Wang, Environment International, 124 (2019) 473-481.
[159] R. Ravindranath, P. Roy, A.P. Periasamy, Y.-W. Chen, C.-T. Liang, H.-T. Chang, New Journal of Chemistry, 41 (2017) 7751-7757.
[160] M. Hashemzadeh, A. Nilchi, A.H. Hassani, R. Saberi, International Journal of Environmental Science and Technology, 16 (2019) 775-792.
[161] X. Shuibo, Z. Chun, Z. Xinghuo, Y. Jing, Z. Xiaojian, W. Jingsong, Journal of Environmental Radioactivity, 100 (2009) 162-166.
[162] Z. Dongsheng, G. Wenqiang, C. Guozhang, L. Shuai, J. Weizhou, L. Youzhi, Advanced Powder Technology, 30 (2019) 581-589.
[163] H. Yu, T. Zhang, Z. Jing, J. Xu, F. Qiu, D. Yang, L. Yu, Chemical Engineering Science, 205 (2019) 278-286.
[164] M.H. Park, S. Jeong, G. Lee, H. Park, J.Y. Kim, Waste Management, 92 (2019) 49-58.
[165] Q. Zhang, D. Zhao, S. Feng, Y. Wang, J. Jin, A. Alsaedi, T. Hayat, C. Chen, Journal of Colloid and Interface Science, (2019).
[166] S. Li, W. Wang, W. Yan, W.-x. Zhang, Environmental Science: Processes & Impacts, 16 (2014) 524-533.
[167] S. Luo, T. Lu, L. Peng, J. Shao, Q. Zeng, J.-D. Gu, Journal of Materials Chemistry A, 2 (2014) 15463-15472.
[168] S. Li, T. You, Y. Guo, S. Yao, S. Zang, M. Xiao, Z. Zhang, Y. Shen, RSC Advances, 9 (2019) 12428-12435.
[169] H. Lu, H. Xu, Y. Chen, J. Zhang, J. Zhuang, RSC Advances, 4 (2014) 5873-5879.
[170] W. Han, F. Fu, Z. Cheng, B. Tang, S. Wu, Journal of Hazardous Materials, 302 (2016) 437-446.
[171] V. Danila, S. Vasarevicius, V. Valskys, Energy Procedia, 147 (2018) 214-219.
[172] J. Liu, T. Mwamulima, Y. Wang, Y. Fang, S. Song, C. Peng, Journal of Molecular Liquids, 243 (2017) 205-211.
[173] L.-N. Shi, Y. Zhou, Z. Chen, M. Megharaj, R. Naidu, Environmental Science and Pollution Research, 20 (2013) 3639-3648.
[174] Z. Lv, S. Yang, L. Chen, A. Alsaedi, T. Hayat, C. Chen, Journal of Environmental Sciences, 76 (2019) 377-387.
[175] L. Chen, S. Feng, D. Zhao, S. Chen, F. Li, C. Chen, Journal of Colloid and Interface Science, 490 (2017) 197-206.

[176] X. Dou, R. Li, B. Zhao, W. Liang, Journal of Hazardous Materials, 182 (2010) 108-114.
[177] R. Darvishi Cheshmeh Soltani, M. Safari, A. Maleki, R. Rezaee, B. Shahmoradi, S. Shahmohammadi, E. Ghahramani, Environmental Science and Pollution Research, 24 (2017) 15157-15166.
[178] A. Mahapatra, B.G. Mishra, G. Hota, Journal of Hazardous Materials, 258-259 (2013) 116-123.
[179] X. Kong, G. Huang, Z. Han, Y. Xu, M. Zhu, Z. Zhang, Environmental Science and Pollution Research, 24 (2017) 13837-13844.
[180] J.K. Grewal, M. Kaur, Ceramics International, 43 (2017) 16611-16621.
[181] M. Ahmadi, M. Hazrati Niari, B. Kakavandi, Journal of Molecular Liquids, 248 (2017) 184-196.
[182] P. Bahmani, A. Maleki, H. Daraei, R. Rezaee, M. Khamforoush, S. Dehestani Athar, F. Gharibi, A.H. Ziaee, G. McKay, Environmental Science and Pollution Research, (2019).
[183] D. Chauhan, J. Dwivedi, N. Sankararamakrishnan, Environmental Science and Pollution Research, 21 (2014) 9430-9442.
[184] T.H. Bui, C. Kim, S.P. Hong, J. Yoon, Environmental Science and Pollution Research, 24 (2017) 24235-24242.
[185] V.I. Mikhaylov, T.P. Maslennikova, P.V. Krivoshapkin, Materials Chemistry and Physics, 186 (2017) 612-619.
[186] H.C. Vu, A.D. Dwivedi, T.T. Le, S.-H. Seo, E.-J. Kim, Y.-S. Chang, Chemical Engineering Journal, 307 (2017) 220-229.
[187] D.-W. Cho, B.-H. Jeon, C.-M. Chon, Y. Kim, F.W. Schwartz, E.-S. Lee, H. Song, Chemical Engineering Journal, 200-202 (2012) 654-662.
[188] D. Zhao, X. Gao, C. Wu, R. Xie, S. Feng, C. Chen, Applied Surface Science, 384 (2016) 1-9.
[189] M.E. Mahmoud, E.A. Saad, M.A. Soliman, M.S. Abdelwahab, Microchemical Journal, 145 (2019) 1102-1111.
[190] J. Shou, C. Jiang, F. Wang, M. Qiu, Q. Xu, Journal of Molecular Liquids, 207 (2015) 216-223.
[191] Z. Guo, Y. Li, S. Pan, J. Xu, Journal of Molecular Liquids, 206 (2015) 272-277.
[192] Z. Majidnia, A. Idris, M. Majid, R. Zin, M. Ponraj, Applied Radiation and Isotopes, 105 (2015) 105-113.
[193] X. Han, L. Gai, H. Jiang, L. Zhao, H. Liu, W. Zhang, Synthetic Metals, 171 (2013) 1-6.
[194] A. Ahmadi, S. Heidarzadeh, A.R. Mokhtari, E. Darezereshki, H.A. Harouni, Journal of Geochemical Exploration, 147 (2014) 151-158.
[195] A. Roy, J. Bhattacharya, Separation and Purification Technology, 115 (2013) 172-179.
[196] Z. Zhang, H. Liu, P. Lu, T. Chen, W. Ma, Applied Geochemistry, 96 (2018) 92-99.
[197] C. Santhosh, P. Kollu, S. Felix, V. Velmurugan, S.K. Jeong, A.N. Grace, RSC Advances, 5 (2015) 28965-28972.
[198] L.P. Lingamdinne, J.R. Koduru, Y.-L. Choi, Y.-Y. Chang, J.-K. Yang, Hydrometallurgy, 165 (2016) 64-72.
[199] M.S. Podder, C.B. Majumder, Biochemical Engineering Journal, 105 (2016) 114-135.
[200] P. Beigzadeh, F. Moeinpour, Transactions of Nonferrous Metals Society of China, 26 (2016) 2238-2246.
[201] M. Naushad, T. Ahamad, B.M. Al-Maswari, A. Abdullah Alqadami, S.M. Alshehri, Chemical Engineering Journal, 330 (2017) 1351-1360.
[202] W. Wang, K. Cai, X. Wu, X. Shao, X. Yang, Journal of Alloys and Compounds, 722 (2017) 532-543.
[203] K.-W. Jung, S. Lee, Y.J. Lee, Bioresource Technology, 245 (2017) 751-759.
[204] B. Xiang, D. Ling, H. Lou, H. Gu, Journal of Hazardous Materials, 325 (2017) 178-188.
[205] S. Duan, X. Liu, Y. Wang, D. Shao, N.S. Alharbi, A. Alsaedi, J. Li, Journal of the Taiwan Institute of Chemical Engineers, 65 (2016) 367-377.

[206] M.A. Attia, S.I. Moussa, R.R. Sheha, H.H. Someda, E.A. Saad, Applied Radiation and Isotopes, 145 (2019) 85-94.
[207] Y. Hu, C. Zhao, L. Yin, T. Wen, Y. Yang, Y. Ai, X. Wang, Chemical Engineering Journal, 349 (2018) 347-357.
[208] Y. Huang, W. Wang, Q. Feng, F. Dong, Journal of Saudi Chemical Society, 21 (2017) 58-66.
[209] X.-M. Zheng, J.-F. Dou, M. Xia, A.-Z. Ding, Carbohydrate Polymers, 167 (2017) 306-316.
[210] J. Ma, Y. Zeng, M. Sun, M. Zhang, W. Zheng, C. Zhang, Q. Wang, Y. Xiao, S. Zhang, Journal of Environmental Chemical Engineering, 7 (2019) 102874.
[211] A.I. Ivanets, V. Srivastava, M.Y. Roshchina, M. Sillanpää, V.G. Prozorovich, V.V. Pankov, Ceramics International, 44 (2018) 9097-9104.
[212] R. Nasiri, N. Arsalani, Y. Panahian, Journal of Cleaner Production, 201 (2018) 507-515.
[213] V. Javanbakht, S.M. Ghoreishi, Adsorption Science & Technology, 35 (2017) 241-260.
[214] M. Okube, T. Yasue, S. Sasaki, Journal of Synchrotron Radiation, 19 (2012) 759-767.
[215] J. Noh, O.I. Osman, S.G. Aziz, P. Winget, J.-L. Brédas, Science and Technology of Advanced Materials, 15 (2014) 044202.
[216] D. Tunega, The Journal of Physical Chemistry C, 116 (2012) 6703-6713.
[217] F. Farahbakhsh, M. Ahmadi, S.H. Hekmatara, M. Sabet, E. Heydari-Bafrooei, Materials Chemistry and Physics, 224 (2019) 279-285.
[218] S. Mahalingam, Y.-H. Ahn, New Journal of Chemistry, 42 (2018) 4372-4383.
[219] S.B. Atla, W.-R. Lin, T.-C. Chien, M.-J. Tseng, J.-C. Shu, C.-C. Chen, C.-Y. Chen, Materials Chemistry and Physics, 216 (2018) 380-386.
[220] N.D. Banić, B.F. Abramović, J.B. Krstić, D.V. Šojić Merkulov, N.L. Finčur, M.N. Mitrić, Journal of Industrial and Engineering Chemistry, 70 (2019) 264-275.
[221] H. Fan, X. Ma, S. Zhou, J. Huang, Y. Liu, Y. Liu, Carbohydrate Polymers, 213 (2019) 39-49.
[222] G. Feng, J. Ma, X. Zhang, Q. Zhang, Y. Xiao, Q. Ma, S. Wang, Journal of Colloid and Interface Science, 538 (2019) 132-141.
[223] H. Guo, H. Wang, N. Zhang, J. Li, J. Liu, A. Alsaedi, T. Hayat, Y. Li, Y. Sun, Chemical Engineering Journal, 369 (2019) 736-744.
[224] A. Khan, J. Xing, A.M. Elseman, P. Gu, K. Gul, Y. Ai, R. Jehan, A. Alsaedi, T. Hayat, X. Wang, Dalton Transactions, 47 (2018) 11327-11336.
[225] C. Ding, W. Cheng, Y. Sun, X. Wang, Journal of Hazardous Materials, 295 (2015) 127-137.
[226] V.O. Leone, M.C. Pereira, S.F. Aquino, L.C.A. Oliveira, S. Correa, T.C. Ramalho, L.V.A. Gurgel, A.C. Silva, New Journal of Chemistry, 42 (2018) 437-449.
[227] N. Boukhalfa, M. Boutahala, N. Djebri, A. Idris, Journal of Molecular Liquids, 275 (2019) 431-440.
[228] H. Dai, S. Xu, J. Chen, X. Miao, J. Zhu, Chemosphere, 199 (2018) 147-153.
[229] A.E. Chávez-Guajardo, J.C. Medina-Llamas, L. Maqueira, C.A.S. Andrade, K.G.B. Alves, C.P. de Melo, Chemical Engineering Journal, 281 (2015) 826-836.
[230] S. Rajput, L.P. Singh, C.U. Pittman, D. Mohan, Journal of Colloid and Interface Science, 492 (2017) 176-190.
[231] K.M. Lee, A.H. Abdullah, Materials Science in Semiconductor Processing, 30 (2015) 298-306.
[232] Y.L. Pang, S. Lim, H.C. Ong, W.T. Chong, Ultrasonics Sonochemistry, 29 (2016) 317-327.
[233] H. Hernández-Flores, N. Pariona, M. Herrera-Trejo, H.M. Hdz-García, A.I. Mtz-Enriquez, Journal of Molecular Structure, 1171 (2018) 9-16.
[234] H. Park, N.V. Myung, H. Jung, H. Choi, Journal of Nanoparticle Research, 11 (2008) 1981.
[235] M.T. Farid, I. Ahmad, M. Kanwal, G. Murtaza, I. Ali, M.N. Ashiq, S.A. Khan, Journal of Magnetism and Magnetic Materials, 422 (2017) 337-343.
[236] M. Dar, D. Varshney, Journal of Magnetism and Magnetic Materials, 436 (2017) 101-112.

[237] A. Amirabadizadeh, Z. Salighe, R. Sarhaddi, Z. Lotfollahi, Journal of Magnetism and Magnetic Materials, 434 (2017) 78-85.
[238] S.A. Pour, H.R. Shaterian, M. Afradi, A. Yazdani-Elah-Abadi, Journal of Magnetism and Magnetic Materials, 438 (2017) 85-94.
[239] O. Alcalá, S. Briceño, W. Brämer-Escamilla, P. Silva, Materials Chemistry and Physics, 192 (2017) 17-21.
[240] Z. Yan, J. Luo, Journal of Alloys and Compounds, 695 (2017) 1185-1195.
[241] R. Sharma, P. Thakur, P. Sharma, V. Sharma, Journal of Alloys and Compounds, 704 (2017) 7-17.
[242] S. Winder, Power supplies for LED driving, Newnes, 2016.
[243] P. Samoila, C. Cojocaru, L. Sacarescu, P.P. Dorneanu, A.-A. Domocos, A. Rotaru, Applied Catalysis B: Environmental, 202 (2017) 21-32.
[244] X. Niu, B. Zong, H. Hu, B. Wu, Optik-International Journal for Light and Electron Optics, 134 (2017) 135-139.
[245] M. Anupama, B. Rudraswamy, N. Dhananjaya, Journal of Alloys and Compounds, 706 (2017) 554-561.
[246] H. El Moussaoui, T. Mahfoud, S. Habouti, K. El Maalam, M.B. Ali, M. Hamedoun, O. Mounkachi, R. Masrour, E. Hlil, A. Benyoussef, Journal of Magnetism and Magnetic Materials, 405 (2016) 181-186.
[247] S. Patil, A. Pawar, S. Tilekar, B. Ladgaonkar, Sensors and Actuators A: Physical, 244 (2016) 35-43.
[248] A. Ghafoor, M.A. Khan, M. Islam, Z.A. Gilani, A. Manzoor, H.M. Khan, I. Ali, M.F. Warsi, Ceramics International, 42 (2016) 14252-14256.
[249] M.I.A. Abdel Maksoud, A. El-ghandour, G.S. El-Sayyad, A.S. Awed, A.H. Ashour, A.I. El-Batal, M. Gobara, E.K. Abdel-Khalek, M.M. El-Okr, Journal of Sol-Gel Science and Technology, 90 (2019) 631-642.
[250] M.I.A. Abdel Maksoud, G.S. El-Sayyad, A.H. Ashour, A.I. El-Batal, M.S. Abd-Elmonem, H.A.M. Hendawy, E.K. Abdel-Khalek, S. Labib, E. Abdeltwab, M.M. El-Okr, Materials Science and Engineering: C, 92 (2018) 644-656.
[251] M.I.A.A. Maksoud, A. El-ghandour, G.S. El-Sayyad, A.S. Awed, R.A. Fahim, M.M. Atta, A.H. Ashour, A.I. El-Batal, M. Gobara, E.K. Abdel-Khalek, M.M. El-Okr, Journal of Materials Science: Materials in Electronics, 30 (2019) 4908-4919.
[252] A.H. Ashour, A.I. El-Batal, M.I.A.A. Maksoud, G.S. El-Sayyad, S. Labib, E. Abdeltwab, M.M. El-Okr, Particuology, 40 (2018) 141-151.
[253] A. Ashour, O. Hemeda, Z. Heiba, S. Al-Zahrani, Journal of Magnetism and Magnetic Materials, 369 (2014) 260-267.
[254] M.S. Shah, K. Ali, I. Ali, A. Mahmood, S.M. Ramay, M.T. Farid, Materials Research Bulletin, 98 (2018) 77-82.
[255] R.S. Yadav, I. Kuřitka, J. Havlica, M. Hnatko, C. Alexander, J. Masilko, L. Kalina, M. Hajdúchová, J. Rusnak, V. Enev, Journal of Magnetism and Magnetic Materials, 447 (2018) 48-57.
[256] J. Venturini, A.M. Tonelli, T.B. Wermuth, R.Y.S. Zampiva, S. Arcaro, A. Da Cas Viegas, C.P. Bergmann, Journal of Magnetism and Magnetic Materials, 482 (2019) 1-8.
[257] A.A. Rodríguez-Rodríguez, M.B. Moreno-Trejo, M.J. Meléndez-Zaragoza, V. Collins-Martínez, A. López-Ortiz, E. Martínez-Guerra, M. Sánchez-Domínguez, International Journal of Hydrogen Energy, 44 (2019) 12421-12429.
[258] M.A. Almessiere, Y. Slimani, A.D. Korkmaz, S. Guner, M. Sertkol, S.E. Shirsath, A. Baykal, Ultrasonics Sonochemistry, 54 (2019) 1-10.
[259] C. Wu, Y. Xu, S. Xu, J. Tu, C. Tian, Z. Lin, Journal of Environmental Sciences, 79 (2019) 248-255.

[260] H. Javed, A. Rehman, S. Mussadiq, M. Shahid, M.A. Khan, I. Shakir, P.O. Agboola, M.F.A. Aboud, M.F. Warsi, Synthetic Metals, 254 (2019) 1-9.
[261] M.A. Yousuf, M.M. Baig, N.F. Al-Khalli, M.A. Khan, M.F. Aly Aboud, I. Shakir, M.F. Warsi, Ceramics International, 45 (2019) 10936-10942.
[262] M. Sun, X. Han, S. Chen, Materials Science in Semiconductor Processing, 91 (2019) 367-376.
[263] I. Ibrahim, I.O. Ali, T.M. Salama, A. Bahgat, M.M. Mohamed, Applied Catalysis B: Environmental, 181 (2016) 389-402.
[264] M.J. Sampaio, M.J. Lima, D.L. Baptista, A.M.T. Silva, C.G. Silva, J.L. Faria, Chemical Engineering Journal, 318 (2017) 95-102.
[265] R. Rahimi, J. Shokraiyan, M. Rabbani, F. Fayyaz, Water Science and Technology, 71 (2015) 1249-1254.
[266] M. Rabbani, M. Heidari-Golafzani, R. Rahimi, Materials Chemistry and Physics, 179 (2016) 35-41.
[267] R. Rahimi, M. Heidari-Golafzani, M. Rabbani, Superlattices and Microstructures, 85 (2015) 497-503.
[268] R. Bayat, P. Derakhshi, R. Rahimi, A.A. Safekordi, M. Rabbani, Solid State Sciences, 89 (2019) 167-171.
[269] M.R.D. Khaki, M.S. Shafeeyan, A.A.A. Raman, W.M.A.W. Daud, Journal of Environmental Management, 198 (2017) 78-94.
[270] Y. Li, D. Chen, S. Fan, T. Yang, Journal of the Taiwan Institute of Chemical Engineers, 96 (2019) 185-192.
[271] M.A. Maksoud, G.S. El-Sayyad, A. Ashour, A.I. El-Batal, M.A. Elsayed, M. Gobara, A.M. El-Khawaga, E. Abdel-Khalek, M. El-Okr, Microbial pathogenesis, 127 (2019) 144-158.
[272] N. Bi, H. Zheng, Y. Zhu, W. Jiang, B. Liang, Journal of Environmental Chemical Engineering, 6 (2018) 3150-3160.
[273] F. Sun, Q. Zeng, W. Tian, Y. Zhu, W. Jiang, Journal of Environmental Chemical Engineering, 7 (2019) 103011.
[274] A. Behera, S. Mansingh, K.K. Das, K. Parida, Journal of Colloid and Interface Science, 544 (2019) 96-111.
[275] F. Wang, F. Ren, D. Ma, P. Mu, H. Wei, C. Xiao, Z. Zhu, H. Sun, W. Liang, J. Chen, L. Chen, A. Li, Journal of Materials Chemistry A, 6 (2018) 266-274.
[276] K. Atacan, M. Özacar, M. Özacar, International Journal of Biological Macromolecules, 109 (2018) 720-731.
[277] C. Liang, C.-G. Niu, H. Guo, D.-W. Huang, X.-J. Wen, S.-F. Yang, G.-M. Zeng, Catalysis Science & Technology, 8 (2018) 1161-1175.
[278] Y. Xu, Q. Liu, C. Liu, Y. Zhai, M. Xie, L. Huang, H. Xu, H. Li, J. Jing, Journal of Colloid and Interface Science, 512 (2018) 555-566.
[279] X.-G. Zhang, D.-L. Guan, C.-G. Niu, Z. Cao, C. Liang, N. Tang, L. Zhang, X.-J. Wen, G.-M. Zeng, Science of The Total Environment, 668 (2019) 730-742.
[280] Y. Chen, P. Zhu, M. Duan, J. Li, Z. Ren, P. Wang, Applied Surface Science, 486 (2019) 198-211.
[281] M. Sundararajan, S.K. Ghosh, The Journal of Physical Chemistry A, 115 (2011) 6732-6737.
[282] L. Tan, Q. Liu, X. Jing, J. Liu, D. Song, S. Hu, L. Liu, J. Wang, Chemical Engineering Journal, 273 (2015) 307-315.
[283] R. Huang, L. Zhang, P. Hu, J. Wang, International Journal of Biological Macromolecules, 86 (2016) 496-504.
[284] Y. Fan, W. Ma, D. Han, S. Gan, X. Dong, L. Niu, Advanced Materials, 27 (2015) 3767-3773.
[285] X. Zhou, Y. Zhou, L. Zhou, J. Wei, J. Wu, D. Yao, Ceramics International, 45 (2019) 6236-6242.

[286] Y. Slimani, M.A. Almessiere, M. Sertkol, S.E. Shirsath, A. Baykal, M. Nawaz, S. Akhtar, B. Ozcelik, I. Ercan, Ultrasonics Sonochemistry, (2019).
[287] V.S. Bushkova, I.P. Yaremiy, Journal of Magnetism and Magnetic Materials, 461 (2018) 37-47.
[288] A. Ashok, L.J. Kennedy, J.J. Vijaya, Journal of Alloys and Compounds, 780 (2019) 816-828.
[289] M.A. Almessiere, Y. Slimani, S. Guner, M. Nawaz, A. Baykal, F. Alkhamis, A. Sadaqat, I. Ercan, Journal of Molecular Structure, (2019).
[290] Y. Slimani, H. Güngüneş, M. Nawaz, A. Manikandan, H.S. El Sayed, M.A. Almessiere, H. Sözeri, S.E. Shirsath, I. Ercan, A. Baykal, Ceramics International, 44 (2018) 14242-14250.
[291] M. Madhukara Naik, H.S. Bhojya Naik, G. Nagaraju, M. Vinuth, K. Vinu, R. Viswanath, Nano-Structures & Nano-Objects, 19 (2019) 100322.
[292] A.A. Al-Ghamdi, F.S. Al-Hazmi, L.S. Memesh, F.S. Shokr, L.M. Bronstein, Journal of Alloys and Compounds, 712 (2017) 82-89.
[293] A.B. Nawale, N.S. Kanhe, S.A. Raut, S.V. Bhoraskar, A.K. Das, V.L. Mathe, Ceramics International, 43 (2017) 6637-6647.
[294] M. Behloul, H. Lounici, N. Abdi, N. Drouiche, N. Mameri, International Biodeterioration & Biodegradation, 119 (2017) 687-695.
[295] C.R.M. de Lima, D.N. Gomes, J.R. de Morais Filho, M.R. Pereira, J.L.C. Fonseca, Colloids and Surfaces B: Biointerfaces, 170 (2018) 210-218.
[296] N.A.S. Mohammed, R.A. Abu-Zurayk, I. Hamadneh, A.H. Al-Dujaili, Journal of Environmental Management, 226 (2018) 377-385.
[297] D. Tonato, F.C. Drumm, P. Grassi, J. Georgin, A.E. Gerhardt, G.L. Dotto, M.A. Mazutti, Journal of Water Process Engineering, 31 (2019) 100818.
[298] S. Rangabhashiyam, P. Balasubramanian, Bioresource Technology Reports, 5 (2019) 261-279.
[299] K. Yin, Q. Wang, M. Lv, L. Chen, Chemical Engineering Journal, 360 (2019) 1553-1563.
[300] A. Azari, M. Noorisepehr, E. Dehghanifard, K. Karimyan, S.Y. Hashemi, E.M. Kalhori, R. Norouzi, S. Agarwal, V.K. Gupta, International Journal of Biological Macromolecules, 131 (2019) 633-645.
[301] A. Bhatnagar, M. Sillanpää, Chemical Engineering Journal, 157 (2010) 277-296.
[302] W.-N. Du, S.-T. Chen, Journal of Environmental Management, 206 (2018) 507-515.
[303] M. Napoli, S. Cecchi, C. Grassi, A. Baldi, C.A. Zanchi, S. Orlandini, Chemosphere, 219 (2019) 122-129.
[304] A. Doggaz, A. Attour, M. Le Page Mostefa, K. Côme, M. Tlili, F. Lapicque, Journal of Water Process Engineering, 29 (2019) 100796.
[305] M. Nemati, S.M. Hosseini, M. Shabanian, Journal of Hazardous Materials, 337 (2017) 90-104.
[306] M.M. Ghobashy, M.A. Elhady, Radiation Physics and Chemistry, 134 (2017) 47-55.
[307] S.A. Hosseini, M. Vossoughi, N.M. Mahmoodi, M. Sadrzadeh, Journal of Cleaner Production, 183 (2018) 1197-1206.
[308] E. Kavitha, A. Sowmya, S. Prabhakar, P. Jain, R. Surya, M.P. Rajesh, International Journal of Biological Macromolecules, 132 (2019) 278-288.
[309] M. Qiu, C. He, Journal of Hazardous Materials, 367 (2019) 339-347.
[310] Y. Feng, S. Yang, L. Xia, Z. Wang, N. Suo, H. Chen, Y. Long, B. Zhou, Y. Yu, Journal of Hazardous Materials, 364 (2019) 562-570.
[311] Q. Chen, Y. Yao, X. Li, J. Lu, J. Zhou, Z. Huang, Journal of Water Process Engineering, 26 (2018) 289-300.
[312] H. Issa Hamoud, G. Finqueneisel, B. Azambre, Journal of Environmental Management, 195 (2017) 195-207.
[313] W. Yao, J. Wang, P. Wang, X. Wang, S. Yu, Y. Zou, J. Hou, T. Hayat, A. Alsaedi, X. Wang, Environmental Pollution, 229 (2017) 827-836.

[314] J.M. Jacob, C. Karthik, R.G. Saratale, S.S. Kumar, D. Prabakar, K. Kadirvelu, A. Pugazhendhi, Journal of Environmental Management, 217 (2018) 56-70.
[315] Z. Huang, K. He, Z. Song, G. Zeng, A. Chen, L. Yuan, H. Li, G. Chen, Chemosphere, 224 (2019) 554-561.
[316] X. Zhao, J.C. Joo, J.-K. Lee, J.Y. Kim, Chemosphere, 220 (2019) 965-973.
[317] I.P.S. Fernando, K.K.A. Sanjeewa, S.-Y. Kim, J.-S. Lee, Y.-J. Jeon, International Journal of Biological Macromolecules, 106 (2018) 330-337.
[318] M.R. Hadiani, K. Khosravi-Darani, N. Rahimifard, Journal of Environmental Chemical Engineering, 7 (2019) 102949.
[319] L.J. Alvarez-Vázquez, A. Martínez, C. Rodríguez, M.E. Vázquez-Méndez, M.A. Vilar, Applied Mathematical Modelling, 73 (2019) 387-400.
[320] A.O. Ekperusi, F.D. Sikoki, E.O. Nwachukwu, Chemosphere, 223 (2019) 285-309.
[321] S. Jeevanantham, A. Saravanan, R.V. Hemavathy, P.S. Kumar, P.R. Yaashikaa, D. Yuvaraj, Environmental Technology & Innovation, 13 (2019) 264-276.
[322] S. Ashraf, Q. Ali, Z.A. Zahir, S. Ashraf, H.N. Asghar, Ecotoxicology and Environmental Safety, 174 (2019) 714-727.
[323] Y. Xu, Z. Yuan, B.-J. Ni, Science of The Total Environment, 566-567 (2016) 796-805.
[324] N. Sultana, Steroids, 136 (2018) 76-92.
[325] T. Alvarino, S. Suarez, J. Lema, F. Omil, Science of The Total Environment, 615 (2018) 297-306.
[326] M.T. Zumstein, D.E. Helbling, Water Research, 155 (2019) 115-123.
[327] A. Pérez-Huerta, I. Coronado, T.A. Hegna, Earth-Science Reviews, 179 (2018) 95-122.
[328] H.J. Khadim, S.H. Ammar, S.E. Ebrahim, Environmental Technology & Innovation, 14 (2019) 100315.
[329] V. Pasquale, S. Fiore, D. Hlayem, A. Lettino, F.J. Huertas, E. Chianese, S. Dumontet, International Biodeterioration & Biodegradation, 140 (2019) 57-66.
[330] P. Anbu, C.-H. Kang, Y.-j. Shin, J.U. So, SpringerPlus, Conference Proceedings

(2016).
[331] A.J. Phillips, R. Gerlach, E. Lauchnor, A.C. Mitchell, A.B. Cunningham, L. Spangler, Biofouling, 29 (2013) 715-733.
[332] A. Mishra, A. Malik, Critical Reviews in Environmental Science and Technology, 43 (2013) 1162-1222.
[333] P. Diep, R. Mahadevan, A.F. Yakunin, Frontiers in Bioengineering and Biotechnology, 6 (2018).
[334] V. Krstić, T. Urošević, B. Pešovski, Chemical Engineering Science, 192 (2018) 273-287.
[335] N.K. Gupta, A. Sengupta, A. Gupta, J.R. Sonawane, H. Sahoo, Journal of Environmental Chemical Engineering, 6 (2018) 2159-2175.
[336] A. Işıldar, E.D. van Hullebusch, M. Lenz, G. Du Laing, A. Marra, A. Cesaro, S. Panda, A. Akcil, M.A. Kucuker, K. Kuchta, Journal of Hazardous Materials, 362 (2019) 467-481.
[337] N.K. Gupta, A. Gupta, P. Ramteke, H. Sahoo, A. Sengupta, Journal of Molecular Liquids, 274 (2019) 148-164.
[338] M. Fomina, G.M. Gadd, Bioresource Technology, 160 (2014) 3-14.
[339] N.B. Singh, G. Nagpal, S. Agrawal, Rachna, Environmental Technology & Innovation, 11 (2018) 187-240.
[340] S. Sarode, P. Upadhyay, M.A. Khosa, T. Mak, A. Shakir, S. Song, A. Ullah, International Journal of Biological Macromolecules, 121 (2019) 1086-1100.
[341] V. Ghormade, E.K. Pathan, M.V. Deshpande, International Journal of Biological Macromolecules, 104 (2017) 1415-1421.
[342] S. Shahraki, H. Samareh Delarami, Carbohydrate Polymers, 200 (2018) 211-220.

[343] P.S. Anbinder, C. Macchi, J. Amalvy, A. Somoza, Carbohydrate Polymers, 222 (2019) 114987.
[344] C. Zheng, H. Zheng, Y. Wang, Y. Sun, Y. An, H. Liu, S. Liu, Journal of Hazardous Materials, 367 (2019) 492-503.
[345] K. Harini, K. Ramya, M. Sukumar, Carbohydrate Polymers, 201 (2018) 329-339.
[346] H.-J. Hong, H. Yu, M. Park, H.S. Jeong, Carbohydrate Polymers, 210 (2019) 167-174.
[347] C. Wang, H. Wang, G. Gu, Carbohydrate Polymers, 182 (2018) 21-28.
[348] Y. Pan, H. Xie, H. Liu, P. Cai, H. Xiao, Bioresource Technology, 286 (2019) 121366.
[349] N. Najib, C. Christodoulatos, Journal of Hazardous Materials, 367 (2019) 256-266.
[350] A.I. Osman, J.K. Abu-Dahrieh, M. McLaren, F. Laffir, D.W. Rooney, ChemistrySelect, 3 (2018) 1545-1550.
[351] A.I. Osman, J.K. Abu-Dahrieh, M. McLaren, F. Laffir, P. Nockemann, D. Rooney, Scientific Reports, 7 (2017) 1-11.
[352] J. Yan, Y. Li, H. Li, Y. Zhou, H. Xiao, B. Li, X. Ma, Microchemical Journal, 145 (2019) 287-294.
[353] L. Cao, Z. Li, S. Xiang, Z. Huang, R. Ruan, Y. Liu, Bioresource Technology, 284 (2019) 448-455.
[354] Y. Dai, Q. Sun, W. Wang, L. Lu, M. Liu, J. Li, S. Yang, Y. Sun, K. Zhang, J. Xu, W. Zheng, Z. Hu, Y. Yang, Y. Gao, Y. Chen, X. Zhang, F. Gao, Y. Zhang, Chemosphere, 211 (2018) 235-253.
[355] J. Mo, Q. Yang, N. Zhang, W. Zhang, Y. Zheng, Z. Zhang, Journal of Environmental Management, 227 (2018) 395-405.
[356] R.R. Karri, N.S. Jayakumar, J.N. Sahu, Journal of Molecular Liquids, 231 (2017) 249-262.
[357] A.K. Nayak, A. Pal, Journal of Environmental Management, 200 (2017) 145-159.
[358] T. Ai, X. Jiang, Q. Liu, L. Lv, H. Wu, Bioresource Technology, 273 (2019) 8-15.
[359] L. Karimzadeh, R. Barthen, M. Stockmann, M. Gruendig, K. Franke, J. Lippmann-Pipke, Chemosphere, 178 (2017) 277-281.
[360] O. Williams, I. Clark, R.L. Gomes, T. Perehinec, J.L. Hobman, D.J. Stekel, R. Hyde, C. Dodds, E. Lester, Science of The Total Environment, 655 (2019) 1139-1149.
[361] A. Ghazali, M. Shirani, A. Semnani, V. Zare-Shahabadi, M. Nekoeinia, Journal of Environmental Chemical Engineering, 6 (2018) 3942-3950.
[362] Y. Yan, G. Yuvaraja, C. Liu, L. Kong, K. Guo, G.M. Reddy, G.V. Zyryanov, International Journal of Biological Macromolecules, 117 (2018) 1305-1313.
[363] M. Shaban, M.R. Abukhadra, A.A.P. Khan, B.M. Jibali, Journal of the Taiwan Institute of Chemical Engineers, 82 (2018) 102-116.
[364] H. Guo, C. Bi, C. Zeng, W. Ma, L. Yan, K. Li, K. Wei, Journal of Molecular Liquids, 249 (2018) 629-636.
[365] Z. Shang, L. Zhang, X. Zhao, S. Liu, D. Li, Journal of Environmental Management, 231 (2019) 391-396.
[366] B.M. Ibrahim, N.A. Fakhre, International Journal of Biological Macromolecules, 123 (2019) 70-80.
[367] I. Sargin, G. Arslan, M. Kaya, Carbohydrate Polymers, 207 (2019) 200-210.
[368] M.N. Sahmoune, Microchemical Journal, 141 (2018) 87-95.
[369] A.A. Inyinbor, F.A. Adekola, G.A. Olatunji, Applied Water Science, 7 (2017) 2297-2307.
[370] V.K. Gupta, I. Ali, T.A. Saleh, M.N. Siddiqui, S. Agarwal, Environmental Science and Pollution Research, 20 (2013) 1261-1268.
[371] S. Wierzba, A. Kłos, Journal of Cleaner Production, 225 (2019) 112-120.
[372] F. Li, Z. Yang, H. Weng, G. Chen, M. Lin, C. Zhao, Chemical Engineering Journal, 332 (2018) 340-350.
[373] Y. Huang, X. Lee, F.C. Macazo, M. Grattieri, R. Cai, S.D. Minteer, Chemical Engineering Journal, 339 (2018) 259-267.

[374] A.M. Elgarahy, K.Z. Elwakeel, G.A. Elshoubaky, S.H. Mohammad, Environmental Science and Pollution Research, 26 (2019) 22704-22722.
[375] R. Miandad, R. Kumar, M.A. Barakat, C. Basheer, A.S. Aburiazaiza, A.S. Nizami, M. Rehan, Journal of Colloid and Interface Science, 511 (2018) 402-410.
[376] N. Maaloul, P. Oulego, M. Rendueles, A. Ghorbal, M. Díaz, Journal of Environmental Chemical Engineering, 5 (2017) 2944-2954.
[377] S. Lagergren, Kungliga Svenska Vetenskapsakademiens Handlingar, 24 (1898) 1-39.
[378] Y.S. Ho, G. McKay, Process Biochemistry, 34 (1999) 451-465.
[379] W.J.a.M. Weber, J.C. , Journal Sanitary Engeering Division Proceedings.American Society of Civil Engineers,, 89 (1963) 31-60.
[380] A.O. Okewale, K.A. Babayemi, A.P. and Olalekan, International Journal of Applied Science and Technology 3(2013) 35-42.
[381] M.A. Malana, R.B. Qureshi, M.N. Ashiq, Chemical Engineering Journal, 172 (2011) 721-727.
[382] J. Zeldowitsch, Acta. Physicochim. URS, 1 (1934) 364-449.
[383] B. Chen, H. Zhao, S. Chen, F. Long, B. Huang, B. Yang, X. Pan, Chemical Engineering Journal, 356 (2019) 69-80.
[384] F. Arshad, M. Selvaraj, J. Zain, F. Banat, M.A. Haija, Separation and Purification Technology, 209 (2019) 870-880.
[385] A.L. Arim, K. Neves, M.J. Quina, L.M. Gando-Ferreira, Journal of Cleaner Production, 183 (2018) 272-281.
[386] V.J. Inglezakis, M.M. Fyrillas, M.A. Stylianou, Microporous and Mesoporous Materials, 266 (2018) 164-176.
[387] D. Guimarães, V.A. Leão, Journal of Environmental Management, 145 (2014) 106-112.
[388] M. Ch, S.S. P.M, A.B. C, R. K, R. K.K, Journal of Environmental Chemical Engineering, 3 (2015) 1546-1554.
[389] S. Chatterjee, S. Mondal, S. De, Journal of Cleaner Production, 177 (2018) 760-774.
[390] H.A. Alalwan, M.N. Abbas, Z.N. Abudi, A.H. Alminshid, Environmental Technology & Innovation, 12 (2018) 1-13.
[391] P.S. Boeris, A.S. Liffourrena, G.I. Lucchesi, Environmental Technology & Innovation, 11 (2018) 105-115.
[392] E. Oguz, M. Ersoy, Ecotoxicology and Environmental Safety, 99 (2014) 54-60.
[393] M. Riazi, A.R. Keshtkar, M.A. Moosavian, Journal of Environmental Chemical Engineering, 4 (2016) 1890-1898.
[394] Y. Shen, H. Li, W. Zhu, S.-H. Ho, W. Yuan, J. Chen, Y. Xie, Bioresource Technology, 244 (2017) 1031-1038.
[395] C.E.R. Barquilha, E.S. Cossich, C.R.G. Tavares, E.A. Silva, Journal of Cleaner Production, 150 (2017) 58-64.
[396] J.V. Milojković, Z.R. Lopičić, I.P. Anastopoulos, J.T. Petrović, S.Z. Milićević, M.S. Petrović, M.D. Stojanović, Journal of Environmental Management, 232 (2019) 97-109.
[397] H. Ding, X. Luo, X. Zhang, H. Yang, Colloids and Surfaces A: Physicochemical and Engineering Aspects, 562 (2019) 186-195.
[398] C. Li, X. Wang, D. Meng, L. Zhou, International Journal of Biological Macromolecules, 107 (2018) 1871-1878.
[399] A.H. El-Sheikh, A.M. Shudayfat, I.I. Fasfous, Industrial Crops and Products, 129 (2019) 105-113.
[400] J. Liao, H. Huang, Carbohydrate Polymers, 220 (2019) 191-201.
[401] A.C. Khorasani, S.A. Shojaosadati, Journal of Environmental Chemical Engineering, 7 (2019) 103062.
[402] M.N. Zafar, I. Aslam, R. Nadeem, S. Munir, U.A. Rana, S.U.-D. Khan, Journal of the Taiwan Institute of Chemical Engineers, 46 (2015) 82-88.

[403] Z. Ding, X. Hu, A.R. Zimmerman, B. Gao, Bioresource Technology, 167 (2014) 569-573.
[404] S. E, S. N, C. Patra, L.A. Varghese, S. N, Journal of Environmental Chemical Engineering, 7 (2019) 103112.
[405] L.N. Côrtes, E.H. Tanabe, D.A. Bertuol, G.L. Dotto, Waste Management, 45 (2015) 272-279.
[406] N. Sebeia, M. Jabli, A. Ghith, Y. El Ghoul, F.M. Alminderej, International Journal of Biological Macromolecules, 121 (2019) 655-665.
[407] N. Tka, M. Jabli, T.A. Saleh, G.A. Salman, Journal of Molecular Liquids, 250 (2018) 423-432.
[408] H. Cheng, Y. Bian, F. Wang, X. Jiang, R. Ji, C. Gu, X. Yang, Y. Song, Bioresource Technology, 284 (2019) 1-8.
[409] E.P. Pérez-Álvarez, R. Garcia, P. Barrulas, C. Dias, M.J. Cabrita, T. Garde-Cerdán, Food Chemistry, 270 (2019) 273-280.
[410] M.S. Podder, C.B. Majumder, Spectrochimica Acta Part A: Molecular and Biomolecular Spectroscopy, 168 (2016) 159-179.
[411] K.L.B. Solis, Y.-H. Kwon, M.-H. Kim, H.-R. An, C. Jeon, Y. Hong, Chemosphere, 238 (2020) 124656.
[412] S.J. Hill, A.S. Fisher, Atomic Absorption, Methods and Instrumentation, in: J.C. Lindon, G.E. Tranter, D.W. Koppenaal (Eds.) Encyclopedia of Spectroscopy and Spectrometry (Third Edition), Academic Press, Oxford, 2017, pp. 37-43.
[413] L. Zhang, W. Li, H. Cao, D. Hu, X. Chen, Y. Guan, J. Tang, H. Gao, Bioresource Technology, 291 (2019) 121818.
[414] D. Kołodyńska, J. Krukowska, P. Thomas, Chemical Engineering Journal, 307 (2017) 353-363.
[415] F.H.M. Luzardo, F.G. Velasco, I.K.S. Correia, P.M.S. Silva, L.C. Salay, Environmental Technology & Innovation, 7 (2017) 219-228.
[416] L. Chen, N. Chen, H. Wu, W. Li, Z. Fang, Z. Xu, X. Qian, Separation and Purification Technology, 207 (2018) 406-415.
[417] O. Pezoti, A.L. Cazetta, K.C. Bedin, L.S. Souza, R.P. Souza, S.R. Melo, V.C. Almeida, Chemical Engineering Journal, 283 (2016) 1305-1314.
[418] F.L. Braghiroli, H. Bouafif, A. Koubaa, Industrial Crops and Products, 138 (2019) 111456.
[419] G.M. Brito, D.F. Cipriano, M.Â. Schettino, A.G. Cunha, E.R.C. Coelho, J.C. Checon Freitas, Journal of Environmental Chemical Engineering, 7 (2019) 103113.
[420] A. Trubetskaya, J. Kling, O. Ershag, T.M. Attard, E. Schröder, Journal of Hazardous Materials, 365 (2019) 846-856.
[421] Y. Yao, Y. Zhang, B. Gao, R. Chen, F. Wu, Environmental Science and Pollution Research, 25 (2018) 25659-25667.
[422] M. Inyang, B. Gao, W. Ding, P. Pullammanappallil, A.R. Zimmerman, X. Cao, Separation Science and Technology, 46 (2011) 1950-1956.
[423] M. Inyang, B. Gao, Y. Yao, Y. Xue, A.R. Zimmerman, P. Pullammanappallil, X. Cao, Bioresource Technology, 110 (2012) 50-56.
[424] Q. Tao, Y. Chen, J. Zhao, B. Li, Y. Li, S. Tao, M. Li, Q. Li, Q. Xu, Y. Li, H. Li, B. Li, Y. Chen, C. Wang, Science of The Total Environment, 674 (2019) 213-222.
[425] N.H. Abdullah, K. Shameli, E.C. Abdullah, L.C. Abdullah, Composites Part B: Engineering, 162 (2019) 538-568.
[426] H. Ge, T. Hua, Carbohydrate Polymers, 153 (2016) 246-252.
[427] S. Yu, Y. Liu, Y. Ai, X. Wang, R. Zhang, Z. Chen, Z. Chen, G. Zhao, X. Wang, Environmental Pollution, 242 (2018) 1-11.
[428] I. Ahmad, W.A. Siddiqui, T. Ahmad, V.U. Siddiqui, Journal of Materials Research and Technology, 8 (2019) 1400-1411.
[429] I. Michalak, K. Chojnacka, K. Marycz, Microchimica Acta, 172 (2011) 65-74.

[430] L.B. Escudero, M.Á. Maniero, E. Agostini, P.N. Smichowski, TrAC Trends in Analytical Chemistry, 80 (2016) 531-546.
[431] S. Maity, S. Chakravarty, P. Thakur, K.K. Gupta, S. Bhattacharjee, B.C. Roy, Chemosphere, 54 (2004) 1199-1206.
[432] A.I.O. Barba, M.C. Hurtado, M.C.S. Mata, V.F. Ruiz, M.L.S.d. Tejada, Food Chemistry, 95 (2006) 328-336.
[433] C.S.D. Costa, B.G.M. Queiroz, R. Landers, M.G.C. da Silva, M.G.A. Vieira, Environmental Science and Pollution Research, (2018).
[434] A. Turner, A. Taylor, Talanta, 190 (2018) 498-506.
[435] Å. Kvick, X-Ray Diffraction, Materials Science Applications, in: J.C. Lindon, G.E. Tranter, D.W. Koppenaal (Eds.) Encyclopedia of Spectroscopy and Spectrometry (Third Edition), Academic Press, Oxford, 2017, pp. 648-655.
[436] S.N. Ehrlich, J.C. Hanson, A. Lopez Camara, L. Barrio, M. Estrella, G. Zhou, R. Si, S. Khalid, Q. Wang, Nuclear Instruments and Methods in Physics Research Section A: Accelerators, Spectrometers, Detectors and Associated Equipment, 649 (2011) 213-215.
[437] J.J. Rehr, A.L. Ankudinov, Coordination Chemistry Reviews, 249 (2005) 131-140.
[438] Ormerod, Buschow, K.H.J, et al. (Editors), Encyclopedia of Materials, Science and Technology (Second Edition)., Elsevier. 9008-9012., (2001).
[439] V.S. Joshi, S.R. Vasant, J.G. Bhatt, M.J. Joshi, Indian J Biochem Biophys, 51 (2014) 237-243.
[440] A. Subercaze, C. Koumeir, V. Métivier, N. Servagent, A. Guertin, F. Haddad, Nuclear Instruments and Methods in Physics Research Section B: Beam Interactions with Materials and Atoms, 417 (2018) 41-45.
[441] I. Llorente, M. Castellote, R. Gonzalez-Arrabal, M.D. Ynsa, A. Muñoz-Martin, P.G. de Viedma, A. Castillo, I. Martínez, C. Andrade, P. Zuloaga, M. Ordoñez, Nuclear Instruments and Methods in Physics Research Section B: Beam Interactions with Materials and Atoms, 267 (2009) 3670-3674.
[442] X.Y. Zheng, Y.H. Shen, X.Y. Wang, T.S. Wang, Chemosphere, 203 (2018) 109-116.
[443] S.D. House, C.S. Bonifacio, R.V. Grieshaber, L. Li, Z. Zhang, J. Ciston, E.A. Stach, J.C. Yang, Ultramicroscopy, 169 (2016) 22-29.
[444] U. Maver, T. Velnar, M. Gaberšček, O. Planinšek, M. Finšgar, TrAC Trends in Analytical Chemistry, 80 (2016) 96-111.
[445] M.A. Mohamed, J. Jaafar, A.F. Ismail, M.H.D. Othman, M.A. Rahman, Fourier Transform Infrared (FTIR) Spectroscopy, in: Membrane Characterization, 2017, pp. 3-29.
[446] X. Wang, N. Li, D. Xu, X. Yang, Q. Zhu, D. Xiao, N. Lu, Talanta, 190 (2018) 23-29.
[447] S. Waheed, I. Fatima, Applied Radiation and Isotopes, 77 (2013) 139-144.
[448] M. Sulyman, J. Namiesnik, A. Gierak, Polish Journal of Environmental Studies, 26 (2017) 479-510.
[449] M. Torab-Mostaedi, M. Asadollahzadeh, A. Hemmati, A. Khosravi, Journal of the Taiwan Institute of Chemical Engineers, 44 (2013) 295-302.
[450] V.R. Moreira, Y.A.R. Lebron, S.J. Freire, L.V.S. Santos, F. Palladino, R.S. Jacob, Microchemical Journal, 145 (2019) 119-129.
[451] L. Liu, J. Liu, X. Liu, C. Dai, Z. Zhang, W. Song, Y. Chu, Journal of Environmental Radioactivity, 203 (2019) 117-124.
[452] A.R. Keshtkar, M.A. Moosavian, H. Sohbatzadeh, M. Mofras, Groundwater for Sustainable Development, 8 (2019) 144-155.
[453] J.M. do Nascimento, J.D. de Oliveira, A.C.L. Rizzo, S.G.F. Leite, Biotechnology Reports, 21 (2019) e00315.
[454] R. Tabaraki, E. Heidarizadi, Ecotoxicology and Environmental Safety, 166 (2018) 35-41.
[455] H.R. Noormohamadi, M.R. Fat'hi, M. Ghaedi, G.R. Ghezelbash, Chemosphere, 216 (2019) 124-130.

[456] B. Liu, W. Chen, X. Peng, Q. Cao, Q. Wang, D. Wang, X. Meng, G. Yu, International Journal of Biological Macromolecules, 86 (2016) 562-569.
[457] M. Ngabura, S.A. Hussain, W.A.W.A. Ghani, M.S. Jami, Y.P. Tan, Journal of Environmental Chemical Engineering, 6 (2018) 2528-2539.
[458] A. García-Mendieta, M.T. Olguín, M. Solache-Ríos, Desalination, 284 (2012) 167-174.
[459] S. Özdemir, S.A. Mohamedsaid, E. Kılınç, M. Soylak, Food Chemistry, 271 (2019) 232-238.
[460] G. Ungureanu, S.C.R. Santos, I. Volf, R.A.R. Boaventura, C.M.S. Botelho, Journal of Environmental Chemical Engineering, 5 (2017) 3463-3471.
[461] I.A. Lawal, D. Chetty, S.O. Akpotu, B. Moodley, Environmental Nanotechnology, Monitoring & Management, 8 (2017) 83-91.
[462] A.L.D. da Rosa, E. Carissimi, G.L. Dotto, H. Sander, L.A. Feris, Journal of Cleaner Production, 198 (2018) 1302-1310.
[463] R. S, S. Lata, B. P, Surfaces and Interfaces, 10 (2018) 197-215.
[464] A.B. Albadarin, S. Solomon, T.A. Kurniawan, C. Mangwandi, G. Walker, Journal of Environmental Management, 204 (2017) 365-374.
[465] A.P.d. Oliveira, A.N. Módenes, M.E. Bragião, C.L. Hinterholz, D.E.G. Trigueros, I.G. de O. Bezerra, Bioresource Technology Reports, 2 (2018) 92-99.
[466] M.E.M. Ali, A.M. Abd El-Aty, M.I. Badawy, R.K. Ali, Ecotoxicology and Environmental Safety, 151 (2018) 144-152.
[467] X. Zhao, W. Ouyang, F. Hao, C. Lin, F. Wang, S. Han, X. Geng, Bioresource Technology, 147 (2013) 338-344.